Titre: Title:	A Microfluidic Platform for Culture and Drug Screening of Ex Vivo Tumour Explants
Auteur: Author:	Dina Dorrigiv
Date:	2022
Type:	Mémoire ou thèse / Dissertation or Thesis
Référence: Citation:	Dorrigiv, D. (2022). A Microfluidic Platform for Culture and Drug Screening of Ex Vivo Tumour Explants [Thèse de doctorat, Polytechnique Montréal]. PolyPublie. https://publications.polymtl.ca/10686/

POLYTECHNIQUE MONTRÉAL

affiliée à l'Université de Montréal

A Microfluidic Platform for Culture and Drug Screening of Ex Vivo Tumour Explants

DINA DORRIGIV

Institut de génie biomédical

Thèse présentée en vue de l'obtention du diplôme de *Philosophiæ Doctor*

Génie biomédical

Novembre 2022

POLYTECHNIQUE MONTRÉAL

affiliée à l'Université de Montréal

Cette thèse intitulée :

A Microfluidic Platform for Culture and Drug Screening of Ex Vivo Tumour Explants

présentée par **Dina DORRIGIV**

en vue de l'obtention du diplôme de *philosophiæ Doctor*

a été dûment acceptée par le jury d'examen constitué de :

Géraldine MERLE, présidente

Thomas GERVAIS, membre et directeur de recherche

Anne-Marie MES-MASSON, membre et codirectrice de recherche

Dominic ROY, membre

Rebecca POMPANO, membre externe

ACKNOWLEDGEMENTS

Thomas and Anne Marie, Thanks for trusting me and being patient with me. I learned a lot from the two of you, in many ways besides science and research. Thank you for forming such a great work culture where each of us felt we belong.

Amélie, your dedication, patience, and organisational skills always inspire me! Thanks for always being there to answer my questions and thanks for making my manuscripts and presentations look smarter.

P-A and Kayla, thanks for sharing your knowledge (and the secret recipes of your projects) with me. You help was one of the key ingredients in mine ;)

I like to thank all the amazing people in Anne Marie's group. All of you help to shape the perfect work environment. Laudine, thanks for always being kind and open to my questions! Manon, thanks for always cheering me up at work! And thanks for being my personal French tutor! You and Lise are the best French teachers I could have wished for <3 Jennifer, thanks for all the great baking and outdoor ideas you shared with me over the years. I learned a lot from you, in many aspects ☺ Véronique and Liliane, you're amazing work sisters. Thanks so much for being helpful all the time!

Thanks to my favourite Asian gang, Wenying, Su, and Rose (and the not-so-Asian Kevin, Patricia, Fay, and Max :p) for making the last few months so fun and memorable. I will miss our group outings so much!

I would also like to thank all members of the µFO laboratory, especially Elena, Rodin, Maryam, Gabriel, Étienne, Samuel, Lucas, Clementine, and Marie. Thanks for patiently listening to my long presentations in lab meetings over the years and giving useful insights to move the project forward.

Thanks to my friends outside of work for letting me go on and on about my research over dinner parties and showing (even if made-up) interest! This was what kept me going when nothing seemed to work in the lab

I have met and worked with so many wonderful people over the past four and a half years that the acknowledgement can go on for a hundred pages. I know it is limited, and so are my words.

I am forever grateful to my parents for initiating the passion and motivation for science in me, for pushing me forward, and for always supporting me. I am lucky to be your daughter!

And Moein, I am truly grateful for having you in my life. You always help me be a better version of myself. Thanks for bearing with me through these not-always-fun PhD years! And sorry about the many hours you had to wait for me in front of the CRCHUM because I was never done in the 15 minutes that I told you I would.

RÉSUMÉ

Un défi majeur en oncologie clinique et pharmaceutique est de prédire les réponses des patients aux médicaments anticancéreux. Pour cette raison, les chercheurs ont développé des modèles précliniques prédictifs dans l'espoir qu'ils pourront fournir aux patients un plan de traitement qui sera très probablement efficace pour leur cancer. Plusieurs modèles de tumeurs précliniques sont à la disposition des chercheurs, notamment 1) la culture de cellules cancéreuses en 2D, 2) les modèles de tumeurs *in vivo* et 3) les modèles de tumeurs 3D. Les cultures de cellules en 2D sont faciles à reproduire mais négligent la tridimensionalité de la structure tumorale et des interactions entre les cellules cancéreuses et le microenvironnement tumoral. La production des modèles *in vivo* prend du temps et demande beaucoup de travail, et ils échouent souvent à prédire l'efficacité clinique des médicaments en raison des différences entre les espèces. Des modèles de tumeurs 3D ont été développés pour combler le fossé entre les modèles 2D et *in vivo*: contrairement aux modèles 2D, les modèles de tumeurs 3D imitent l'architecture tumorale, sont d'origine humaine, et sont plus faciles à utiliser que les modèles *in vivo*. Les modèles de tumeurs 3D sont divisés en trois sous-groupes: 1) sphéroïdes (c.-à-d. culture 3D de lignées cellulaires cancéreuses), 2) organoïdes (c.-à-d. culture 3D de cellules cancéreuses primaires) et 3) explants de tissus tumoraux cultivés *ex vivo*. Parmi les trois sous-groupes, les explants de tissu tumoral sont le seul modèle qui ne nécessite pas la désintégration du tissu tumoral. Les tissus tumoraux intacts sont facilement disponibles après la chirurgie et conservent les informations spatiales et reflètent l'hétérogénéité inhérente de la tumeur.

Avec ces informations, cette thèse se concentre sur les explants tumoraux *ex vivo* comme modèle préclinique prédictif. Les deux principaux défis liés au travail avec ces explants de tissus tumoraux sont la viabilité *ex vivo* à court terme du tissu tumoral et le faible débit de ce système modèle. L'objectif principal de mon projet est de résoudre ces problèmes en explorant les facteurs qui contribuent à la viabilité des tissus et de développer un système qui prendrait en charge le dépistage de médicaments à haut débit sur les explants de tissus tumoraux. Pour caractériser les plateformes de culture de tumeurs *ex vivo*, j'ai comparé la survie *ex vivo* d'explants de tissus tumoraux appariés qui étaient différents en termes de tailles de tissu et de types de récipient de culture. Des tissus tumoraux microdisséqués (MDT) cultivés sur des puces microfluidiques ont été comparés à des tranches de tissu tumoral cultivées sur des puces microfluidiques ou dans des plaques à puits en plastique conventionnelles. Les résultats de ces travaux publiés dans l'article 1 (Chapitre 4)

démontrent que les MDT cultivées dans des puces microfluidiques survivent dans des conditions de culture *ex vivo* jusqu'à 15 jours, tandis que les tranches de tissu sont associées à la mort cellulaire, à la perte de prolifération et à l'hypoxie dès 5 jours de culture.

Malgré les profils de viabilité rassurants des MDT cultivés sur des puces microfluidiques, la méthodologie actuelle basée sur les puces microfluidiques pour gérer les MDT est encore lourde et a un débit relativement faible. Pour automatiser le système et augmenter son débit, j'ai intégré une technologie récemment développée, les écrans chimiques pixelisés microfluidiques (PCD), à la plate-forme MDT. Les PCD sont des processeurs fluidiques sans contact qui délivrent des réactifs à l'interface d'un substrat immergé, tels que les MDT, basés sur le concept de microfluidique en espace ouvert. Les réactifs sont localisés sur le substrat par la recirculation des flux de réactifs et leur confinement hydrodynamique dans le fluide d'immersion. Des «pixels» fluidiques sont créés lorsqu'un flux de fluide injecté au-dessus du substrat est confiné par des flux de fluide identiques voisins, formant une unité d'écoulement répétable. Les pompes fluidiques utilisées pour faire fonctionner le PCD sont contrôlées par ordinateur et peuvent être programmées. Malgré les diverses applications du PCD sur des surfaces planes 2D, celui-ci n'avait pas été utilisé sur des spécimens biologiques 3D avant les travaux de cette thèse. Ici, j'ai conçu et utilisé pour la première fois un PCD pour diffuser des composés biochimiques, tels que des colorants cellulaires et des cytokines sur les MDT. Les composés biochimiques traversent ensuite les tissus par diffusion. Le PCD dans ce travail comportait neuf pixels fluidiques, permettant la diffusion en continu de jusqu'à 9 réactifs différents sur les MDT. Pour maximiser le débit, j'ai conçu un réseau de 144 micropuits pour organiser et contenir les MDT pendant le fonctionnement du PCD, ce qui rend la plate-forme de dépistage des médicaments PCD nettement plus élevée que les puces microfluidiques (c'est-à-dire 32 MDT et une condition de traitement par puce). L'article 2 (Chapitre 5) présente la plate-forme de dépistage de médicaments PCD et présente quelques applications de preuve de concept. Tout d'abord, le PCD a été utilisé pour colorer les MDT avec divers colorants cellulaires en créant des pixels fluidiques distincts et sans diaphonie de colorants sur les MDT. Ensuite, les MDT ont été soumis à un stimulus pendant différentes durées à l'aide du PCD. Des expériences de stimulation biologique appariées ont été réalisées sur puce. Les résultats démontrent qu'une évaluation de la réponse médicamenteuse similaire et comparable est réalisable en utilisant le PCD par rapport à la puce microfluidique conventionnelle. Enfin, des sphéroïdes ont

été formés et colorés à l'aide de la plate-forme PCD pour montrer qu’elle se prête à divers modèles de tumeurs 3D.

La plateforme de criblage de médicaments PCD est un outil idéal pour évaluer la réponse d'un grand nombre de modèles de tumeurs 3D à plusieurs conditions de traitement en une seule expérience. En plus de l'augmentation du débit, la plate-forme automatise la plupart des parties de la procédure de dépistage de culture et de drogue, en minimisant l'intervention de l'utilisateur. La plate-forme de criblage de médicaments PCD est compatible avec différents modèles de tumeurs 3D et peut être mise à l'échelle pour des débits et un nombre de pixels encore plus élevés.

ABSTRACT

A major challenge in clinical and pharmaceutical oncology is predicting patients' responses to anti-cancer drugs. For this, researchers have developed predictive preclinical models with the hope that they will be able to provide patients with a treatment plan that will most likely be effective for their cancer. Multiple preclinical tumour models are available to researchers, including 1) monolayer culture of cancer cells, 2) *in vivo* tumour models, and 3) 3D tumour models. Monolayer cell cultures are easy to replicate but lack the 3D tumour structure and the interactions between the cancer cells and the tumour microenvironment. *In vivo* models are the gold standard of preclinical models, yet their production is time-consuming and labour intensive and they sometimes fail to predict the clinical efficacy of drugs due to species differences. 3D tumour models were developed to bridge the gap between 2D and *in vivo* models: unlike 2D monolayers, 3D tumour models mimic the tumoral architecture and are human-derived and easier to work with than *in vivo* models. 3D tumour models are divided into three subgroups: 1) spheroids (i.e., 3D culture of cancer cell lines), 2) organoids (i.e., the 3D culture of primary cancer cells), and 3) tumour tissue explants cultured *ex vivo*. Among the three subgroups, tumour tissue explants are the only model that does not require the disintegration of the tumour tissue. Intact tumour tissues are readily available following surgery and maintain spatial information and reflect inherent tumour heterogeneity.

With this information, this dissertation focuses on *ex vivo* tumour explants as a predictive preclinical model. The two key challenges in working with these tumour tissue explants are the short-term *ex vivo* viability of the tumour tissue and the low throughput of this model system. The main goal of my project was to address these issues by exploring factors that contribute to tissue viability and to develop a system that would support high throughput drug screening on tumour tissue explants. To characterize *ex vivo* tumour culture platforms, I compared the *ex vivo* survival of matched tumour tissue explants that were different in terms of tissue size and culture vessel type. Microdissected tumour tissues (MDTs) cultured on microfluidic chips were compared with tumour tissue slices cultured on microfluidic chips or in conventional plastic well plates. The results of this work published in article 1 (Chapter 4) demonstrate that MDTs cultured in microfluidic chips survive *ex vivo* culture conditions for up to 15 days, while tissue slices are associated with cell death, loss of proliferation, and hypoxia after more than 5 days in culture.

Despite the reassuring viability profiles of MDTs cultured on microfluidic chips, the current microfluidic chip-based methodology to handle the MDTs is still cumbersome and has relatively low throughput. To automate the system and increase its throughput, I integrated a recently developed technology, the microfluidic pixelated chemical displays (PCD), with the MDT platform. PCDs are contactless fluidic processors that deliver reagents to the interface of an immersed substrate, such as MDTs, based on the concept of open-space microfluidics. Reagents are localized over the substrate by the recirculation of reagent streams and hydrodynamically confining them in the immersion fluid. Fluidic "pixels" are created when a fluid stream injected above the substrate is confined by neighbouring identical fluid streams, forming a repeatable flow unit. The fluidic pumps used to operate the PCD are computer-controlled and can be programmed. Despite the diverse applications of the PCD over 2D flat surfaces, it had not been used on 3D biological specimens before the work of this dissertation. Here, I utilized the PCD to stream biochemical compounds, such as cellular dyes and cytokines over MDTs. Biochemical compounds then travel through the tissue by diffusion. The PCD in this work featured nine fluidic pixels, enabling streaming of up to 9 different reagents on MDTs. To maximize the throughput, I designed a 144-microwell array to arrange and contain MDTs during the operation of the PCD, rendering the PCD drug screening platform distinctly higher throughput than microfluidic chips (i.e., 32 MDTs and one treatment condition per chip). Article 2 (Chapter 5) introduces the PCD drug screening platform and demonstrates a few proof-of-concept applications. First, the PCD was used to stain MDTs with various cellular dyes by creating distinct and crosstalk-free fluidic pixels of dyes over MDTs. Next, MDTs were subjected to a stimulus for different durations using the PCD. Matched biological stimulation experiments were performed on-chip. The results demonstrate that a similar and comparable drug response assessment is achievable using the PCD as compared to the conventional microfluidic chip. Finally, spheroids were formed and stained using the PCD drug screening platform to showcase that the platform is amenable to various 3D tumour models.

The PCD drug screening platform is an ideal tool to assess the response of a large number of 3D tumour models to multiple treatment conditions in a single experiment. In addition to the increased throughput, the platform automates most parts of the culture and drug screening procedure, keeping user intervention at a minimum. The PCD drug screening platform is compatible with different 3D tumour models and can be scaled up for even higher throughputs.

Table OF CONTENTS

LIST OF TABLES

LIST OF FIGURES

LIST OF SYMBOLS AND ABBREVIATIONS

2D Two-dimensional

3D Three-dimensional

CHUM Centre hospitalier de l'Université de Montréal, University of Montreal Health Centre

CNC Computer numerical control

CRCHUM Centre de recherche du CHUM, CHUM research centre

CTG CellTrackerTM Green

CTO CellTrackerTM Orange

DMSO Dimethyl sulfoxide

DNA Deoxyribonucleic acid

DU145 prostate cancer cell line

ETE Ex vivo tumour tissue explant

FBS Fetal bovine serum

FI Fluorescent intensity

HBSS Hank's balanced salt solution

HER2 human epidermal growth factor receptor 2

IC50 Concentration at which 50% of colony formation is inhibited

IF Immunofluorescent

IHC Immunohistochemistry

MDT Microdissected tumour tissue

MFM Microfluidic multipole

OSE Name of culture medium for ovarian cancer cells

PBS Phosphate-buffered saline

PCD Pixelated chemical display

PDX Patient-derived xenograft

PDMS Polydimethylsiloxane

PMMA Poly (methyl methacrylate)

ROI Region of interest

TOV112D ovarian cancer cell line

TOV21G ovarian cancer cell line

LIST OF APPENDICES

CHAPTER 1 INTRODUCTION

1.1 Motivation

One in two Canadians will be diagnosed with cancer throughout their lifetimes. [1] More than $50 billion is invested in oncology R&D, and the number of active anticancer drugs has doubled since 2008. [2] However, a substantial challenge, which is predicting the response of patients to anticancer drugs, is often overlooked. [3, 4] To address this, researchers have developed predictive preclinical tumour models that mimic the clinical response of patients to drugs, and in the longer run, can offer patients a treatment plan that will most likely be beneficial for their cancer, reduce toxicities, accelerate the drug development process, and reduce costs. [5, 6] Multiple predictive preclinical tumour models, varying in terms of realism and complexity, are available to researchers, including 1) monolayer culture of cancer cells, 2) *in vivo* tumour models (modelling human cancer in animals), and 3) 3D tumour models (i.e., culture of cancer cells in 3D, and *ex vivo* culture of tumour specimens). 3D tumour models outrank monolayer cultures of cells and *in vivo* tumour models in many aspects; For example, unlike monolayer cell cultures that lack the 3D tumour structure, 3D models represent the tumour architecture and can mimic cell-matrix interactions. [7, 8] Moreover, contrary to *in vivo* models that suffer from species differences, and are ethically and economically challenging to work with, 3D tumour models can be readily and quickly produced from human samples. [9] Among the various 3D tumour models, the *ex vivo* culture of tumour tissue is the most realistic approach. Tumour tissue explants are more patient-relevant than tumour spheroids (i.e., 3D tumour models formed from the culture of immortalized cancer cell lines). [10] Furthermore, unlike tumour organoids (i.e., 3D tumour models formed from the culture of primary tumour cells) that require tedious and extensive manipulation of the primary tumours, tumour tissue explants are readily available from the surgery and can undergo experimentation directly. [11, 12]

With this information in mind**,** this project focuses on tumour tissue explants as the preclinical model of interest. **My effort throughout this project was to investigate, characterize, and improve the current state of *ex vivo* tumour explants as a predictive preclinical model**. The two major bottlenecks in working with tumour tissue explants are the short-term viability of tumours *ex vivo* and the low throughput of this model system due to the constraints in sample replication. Various techniques are used to increase the viability and the throughput of tumour

explant culture platforms, such as the use of shaker incubators, [13] fortified culture mediums, [14] perfusion-based culture, [15], and dissecting tumour tissues to sub-millimetre-sized fragments. [16] However, these methodologies had not been characterized and feature multiple varying parameters which might affect the *ex vivo* survival of tumour tissues. To address this and **characterize** *ex vivo* culture methods, I examined the impact of two of these varying parameters, tissue explant size and culture vessel type, on the survival of tumour tissue explants in tumour tissue slices and microdissected tumour tissues (MDTs) cultured in plastic well plates or on microfluidic chips. The results demonstrated that larger tumour tissue slices cultured for an extended time face hypoxia and cell death due to inherent diffusion limitations, while MDTs cultured in microfluidic chips survive. [17] Having shown the superior *ex vivo* survival of MDTs, I carried on the project with MDTs as the model of interest. The next step was to improve and facilitate the current MDT handling approach. The methodology developed in our laboratory for drug screening on MDTs consists of entrapping the MDTs on PDMS microfluidic chips and subjecting them to a culture medium and drugs through manual administration of the biochemical reagents in microchannels. Although this method has proven useful in preserving the viability of MDTs and providing the possibility of testing various treatments, the chip-based methodology has low throughput and is labour-intensive. To address this, I implemented tools and techniques to **improve** the efficiency and throughput of the chip-based MDT drug screening platform. One option available to me was to adopt a new technology developed in the laboratory of Professor Gervais, the microfluidic multipole, for drug screening on MDTs. Microfluidic multipoles are open-space fluidic processors that delivers fluids above a surface without using any channels bonded to the surface. The method is also contact-free and can be easily interfaced with large open surfaces such as glass slides or even petri dishes. Microfluidic multipoles use hydraulic confinement principles to localize biochemical reagents over a nearby immersed substrate by continuous recirculation of streams of fluid. [18, 19] Our laboratory has developed an advanced class of microfluidic multipole, the pixelated chemical display (PCD), that enables the localized delivery of a large number of reagents to a nearby substrate by forming repeatable “fluidic pixels”. Despite various applications over 2D substrates, the PCD has never been used over 3D samples. [20] In this project, for the first time, the PCD was adapted for processing 3D tissue models. The PCD in this work delivers biochemical reagents (e.g., culture medium, stimuli, cellular dyes) to tumour models deposited in a custom-

made array of microwells. The design of the PCD is reconfigurable to generate varying numbers, sizes, and patterns of fluidic pixels. For this work, I used a PCD with nine square-shaped 6 mm* 6 mm fluidic pixels, which enables testing up to 9 different treatment conditions. A custom-made microwell array was designed to accommodate tumour models subjected to the PCD. The microwell array has 144 microwells, which, when integrated with the PCD, makes the drug screening platform significantly higher throughput than the chip-based approach (i.e., 32 MDTs and one treatment condition per chip). I performed experiments with various types of reagents and different 3D tumour models to demonstrate the PCD's diverse applications. First, the PCD was used to stain MDTs with various cellular dyes. Three cellular dyes were administered at the nine pixels of the PCD, every 3 pixels streaming the same condition to have triplicates. The result was an array of MDTs stained thoroughly and without crosstalk between pixels. Subsequently, the PCD was used to subject MDTs produced from a cell line xenograft to a biological stimulus (a cytokine) for different durations at different fluidic pixels to assess its potential for dynamic drug screening. The response of matched MDTs cultured on-chip to the same stimulus was also assessed, which showed the consistency of the responses obtained using the PCD drug screening platform with the previously established methodology. Finally, spheroid formation and staining were also performed using the PCD to showcase that the platform is amenable to various 3D tumour models.

1.2 Research objectives

This dissertation aims to provide a versatile and robust drug screening platform for culture and drug response assessment on 3D tumour models and more specifically, tumour tissue explants. The first objective was to characterize the factors that impact the viability of tumour tissue explants *ex vivo*. Tissue size and culture vessel type were selected as variables in otherwise matched *ex vivo* tissue explants, and cell death, cell proliferation, and hypoxia that occur in tissue explants were examined over time.

Objective 1: Characterize the impact of tissue size and culture vessel type on the *ex vivo* survival of tumour tissue explants

---

Hypothesis 1.1: The size of the tissue and culture vessel type affect the viability of tumour tissue explants cultured *ex vivo*: MDTs cultured in microfluidic chips will maintain the baseline

proliferation and cell death levels, while tumour tissue slices will be deprived of nutrients due to the inherent diffusion limitations, resulting in hypoxia and cell death.

Impact: If the hypothesis turns true, this objective will highlight the impact of the previously neglected variables on the survival of tumour cells and, ultimately, the reliability of the drug response assessment using tumour tissue explants. The results of this part will provide tumour model selection criteria and experiment planning guidelines for other researchers working in the *ex vivo* tissue explant field.

The second objective was to evaluate the operation of the PCD on tumour tissue explants and adapt it for reagent screening over 3D tumour models. The properties of the substrate that the PCD operates over (e.g., 2D vs. 3D environment, surface imperfections, varying gaps between the PCD tip and the surface, and the porosity and permeability of the substrate) impact the operation of the PCD. Preliminary tests and simulations were performed to investigate the potential of the PCD in locally perfusing 3D microtissue structures. It was also essential to optimize the shape and number of the fluidic pixels and the number of microtissues to achieve higher throughputs while keeping the fabrication restrictions (e.g., limited frame size and resolution of the 3D printer) in mind. Then, with lessons learnt from the simulations and preliminary experiments, the PCD was adapted for reagent screening on tissue explants. These changes include modifications in the PCD, designing a 144-microwell array compartment to organize and accommodate microtissues, and extra parts to stabilize the system for the duration of experiments.

Objective 2: Evaluate the operation of the PCD over tissue explants and adapt the system for drug screening application.

Hypothesis 2.1: Numerical simulations to assess the operation of the PCD over 3D tissue substrates suggest that the quality of the fluidic pixels is comparable to when the PCD operates over flat 2D surfaces, and it can locally perfuse microtissues with several reagents. However, a few hardware additions are required to adapt the PCD for reagent screening over tumour tissues.

Impact: Should the hypothesis turns true, and the simulations show that the PCD can operate precisely over 3D tumour models, the platform will be modified to facilitate its use over tumour

models. The outcome of this objective will be a robust multiplexed reagent streaming system capable of operating over tumour tissue explants. The product of this objective will pave the way for further applications of the PCD on microtissues and using appropriate biochemical compounds.

The third and final objective was to validate the operation of the PCD platform for drug screening over 3D tumour models, specifically MDTs. MDTs were stained with multiple cellular dyes using the PCD to validate that the PCD can form crosstalk-free pixels over tumour models. A treatment response assessment test with a stimulus was performed using the PCD and compared to the results of matched experiments in microfluidic chips to measure the reliability of the PCD platform compared to previously established methods. Finally, to assess the applicability of the PCD for other 3D tumour models, tumour spheroids were formed in the microwell array and subjected to the PCD for further manipulations.

Objective 3: Validate the potential of the PCD as a drug screening tool for 3D tumour models.

Hypothesis 3.1: The PCD can form crosstalk-free fluidic pixels over MDTs deposited in a microwell array.

Hypothesis 3.2: The PCD drug screening platform can reproduce the response to biological stimulation obtained in microfluidic chips.

Hypothesis 3.3: The formation and drug screening of other 3D tumour models such as tumour spheroids is possible using the PCD drug screening platform

---

Impact: Shall the hypotheses turn true; this objective will provide proof of evidence for PCD's various applications and its potential as a preclinical drug screening platform. The experiments with MDTs will demonstrate the strength of the PCD platform for multiplexed and high throughput drug screening on tumour tissue explants. The spheroid experiments will showcase an all-in-one spheroid formation and drug screening assay. Moreover, the amenability of the system to various 3D tumour models enables researchers to perform experiments on and merge or compare drug response assessments in different tumour models and correlate the results with the clinical response to choose the most appropriate tumour model.

1.3 The dissertation organization

The first (current) chapter of this dissertation includes the motivation of the project, research objectives, the dissertation organization, and the contributions of the thesis. The literature review is presented in Chapter 2 and delineates what tumour models are and how they are used for drug screening in cancer, how microfluidics can be used for tumour model research, what open-space microfluidics are, and why and how new microfluidic systems can improve the current state of tumour models. Chapter 3 presents the general methodology of the work. The first article written on work from this dissertation is presented in Chapter 4. It is published in *Cancers* and talks about the effect of tissue size and culture vessel type on the *ex vivo* survival of tumour models. The second article is presented in Chapter 5. This article is submitted to *biorxiv.org* and showcases the applicability of the PCD for drug screening on 3D tumour model systems. Chapter 6 entails a general discussion of the methodologies developed in this work and their limitations. Chapter 6 also discusses significant unpublished observations that ultimately resulted in this dissertation and the two articles presented here. Chapter 7 is the conclusion. Appendix A is a summary of the image analysis workflow used to quantify immunofluorescent staining of tumour tissues. Appendix B lists my contributions in terms of articles, oral presentations, and scientific posters based on this work. The following chart demonstrates the organization of this dissertation.

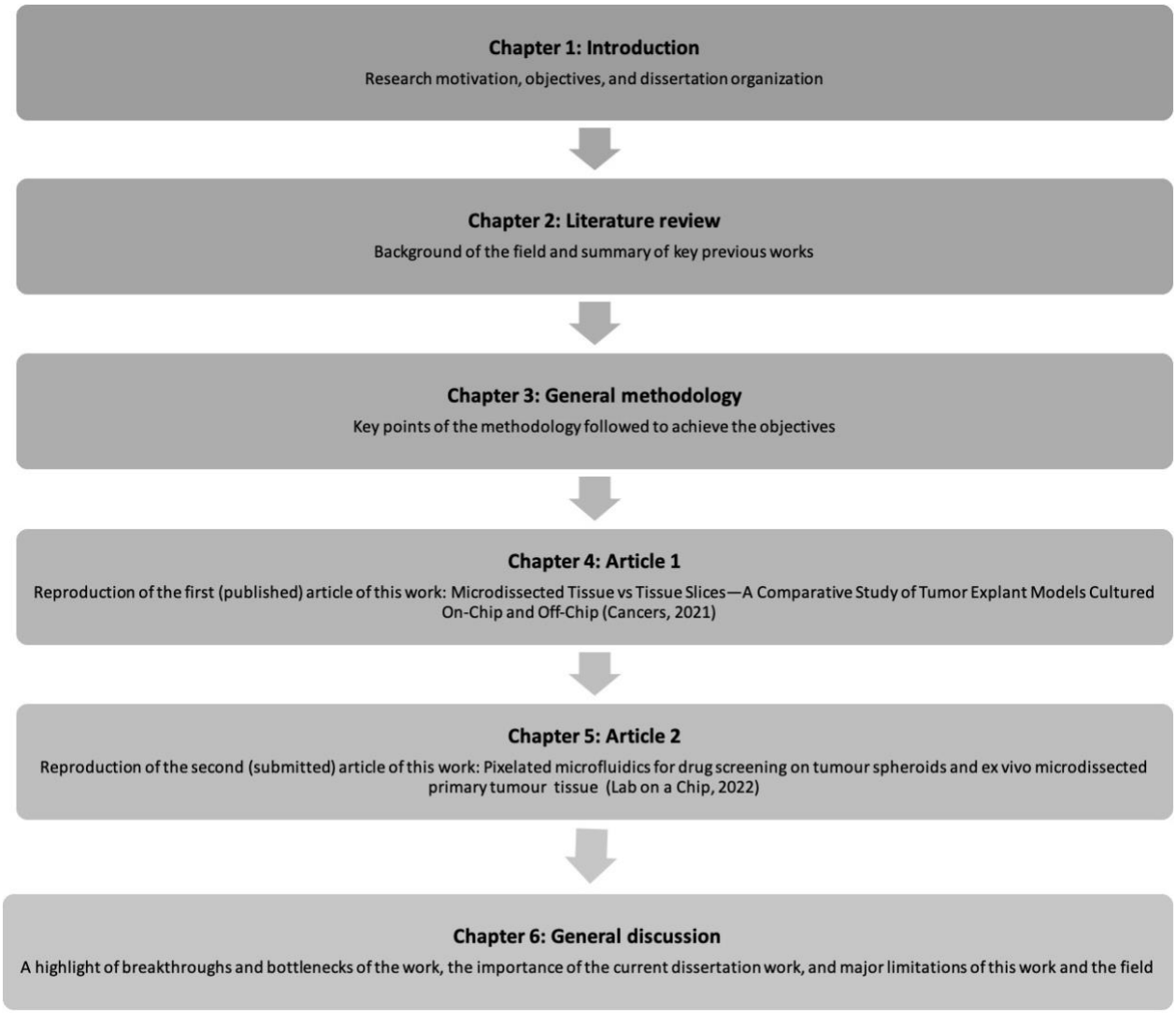

1.4 Thesis contributions

The work of my PhD has led to three articles, presented in chapters 4, 5 and of this dissertation. The detailed contributions of each article are provided at the beginning of the corresponding chapter.

The biological experiments for all of the articles were performed at the CRCHUM with great support from Prof. Mes-Masson's team members. The animal works were done by Kim Leclerc-Desaulniers at the animal facility of the CRCHUM. Tissue processes to produce MDTs and tissue slices were performed at the microfluidic core facility of the CRCHUM, with the help of Jennifer Kendal Dupont, Benjamin Péant, and Amélie St-Georges Robillard. Histopathology processes

were performed at the molecular pathology platform of the CRCHUM with the help of Véronique Barrès and Liliane Meunier. The licence for the image analysis software was provided by the cellular and molecular imaging platform of the CRCHUM. Isabelle Clement and Aurélie Cleret-Buhot provided training and technical support for image analysis. The fabrication of microfluidic devices was performed at Prof. Gervais's laboratory at Polytechnique of Montréal and at the Microfluidic core facility of the CRCHUM. Polytechnique Montréal provided licences for Catia and Fusion 360, CAD programs used to design microfluidic devices. CMC microsystems provided licences for COMSOL, the software used for numerical simulations.

CHAPTER 2 LITERATURE REVIEW

2.1 Drug screening in cancer

It is estimated that one in two Canadians will be diagnosed with cancer throughout their lifetimes. [1] Along with surgery and radiotherapy, the use of anti-cancer drugs, such as cytotoxic chemotherapy, immunotherapy, and molecularly targeted therapy are common treatment approaches to combat cancer. Since the discovery of the first anti-cancer compounds in the early 1940s, they have significantly contributed to increasing life expectancy and quality of life of cancer patients. [21] However, anti-cancer drugs often have many side effects and restrictions that limit their use. For example, cytotoxic anti-cancer compounds kill healthy proliferative cells such as immune cells, bone marrow cells, and hair cells along with cancer cells. [22] Novel anti-cancer drugs, such as immunotherapeutics and molecularly targeted drugs are designed to be more cancer cell-specific when delivered correctly. Targeted therapies target specific genomic alterations and are only effective in the proper molecular context and for a small subpopulation of patients. Immunotherapeutics are often expensive and their therapeutic benefits vary between patients. [23, 24] The toxicity of drugs, high costs, and inter- and intra-patient heterogeneity in response to drugs highlight the need for predictive preclinical assays that can estimate the response of patients to treatments and help with clinical decision-making. [25, 26] Moreover, tumour drug resistance, a known cause of treatment failure, can be predicted and managed using predictive preclinical assays. [27] Various tools and techniques have been developed for predictive preclinical assays. Much attention for predictive preclinical assays has focused on the identification and detection of biomarkers. Multiple biomarkers are available for various cancer types and guide personalized treatment approaches. A more comprehensive approach to predictive preclinical assays is developing model systems to mimic the different aspects of a tumour in a controlled setting. This chapter briefly touches on biomarkers and their applications, but the main focus remains on tumour model systems. It is also noteworthy that while some of the tools discussed here are used for solid and liquid tumours (i.e., blood cancers), solid tumours and preclinical tools associated with them were the focus of this study.

2.2 Cancer biomarkers

Biomarkers are measurable characteristics of the human body that can be used as indicators in susceptibility assessment, disease prevention, diagnostics, prognostics and prediction.[28] In oncology research, different types of biomarkers, such as molecular and genetic (e.g., proteins, genes, nucleic acids, antibodies, and peptides), histological (e.g., microscopic anatomy and morphology of tumour and normal tissues), physiological (e.g., blood pressure and heart rate), and radiographical (e.g. x-ray of tumours and other organs) are used for diagnosis, treatment outcome prediction, and prognosis. [3, 29] Diagnostic biomarkers help differentiate specific disease states, like distinguishing different subtypes of cancer. Prognostic biomarkers provide information on the evolution of the disease, (e.g., aggressive versus indolent). Predictive biomarkers give information about the effect of a therapeutic intervention. In targeted therapies, drugs are often coupled with predictive biomarkers to predict which patients will respond to a specific form of treatment. [30] For example, the status of a signalling receptor, called human epidermal growth factor receptor 2 (HER2), was initially identified as a prognostic biomarker identifying breast cancer patients with poor outcomes. [31, 32] Overtime it was possible to develop a monoclonal antibody drug, Herceptin®, that specifically target HER2 overexpressing tumour cells. Thus, breast cancer patients whose tumours have many HER2 overexpressing tumour cells will generally benefit from this targeted therapy, while other breast cancer patients do not show a positive response to this drug. [33] HER2 amplification is now routinely tested as a predictive biomarker for response to Herceptin®. Prognostic biomarkers are vital to drug discovery and drug development because they sometimes point to a targetable alteration or vulnerability within the tumour cell. Alternatively, predictive biomarkers are useful in the overall strategy of personalized medicine, where each patient is offered the treatment most likely to affect a positive outcome.

2.3 Tumour model systems

Tumour model systems are cells, tissues, or animals that recapitulate certain aspects of the human tumour. Tumour model systems vary in terms of complexity and relevance to human tumours (Figure 2-1). In preclinical research, the model is selected based on the purpose of the study and the availability of resources. In what follows, various tumour models and their application in predictive preclinical models are introduced. In this document, tumour models are classified into

two general sub-groups: 1) *in vitro* tumour models refer to a group of tools and techniques developed to manipulate tumour cells or tissues in a laboratory; 2) *in vivo* tumour models refer to using animal surrogates by inoculating cancer cells or tissue in animals or inducing gene mutations to cause human-like cancers in animals.

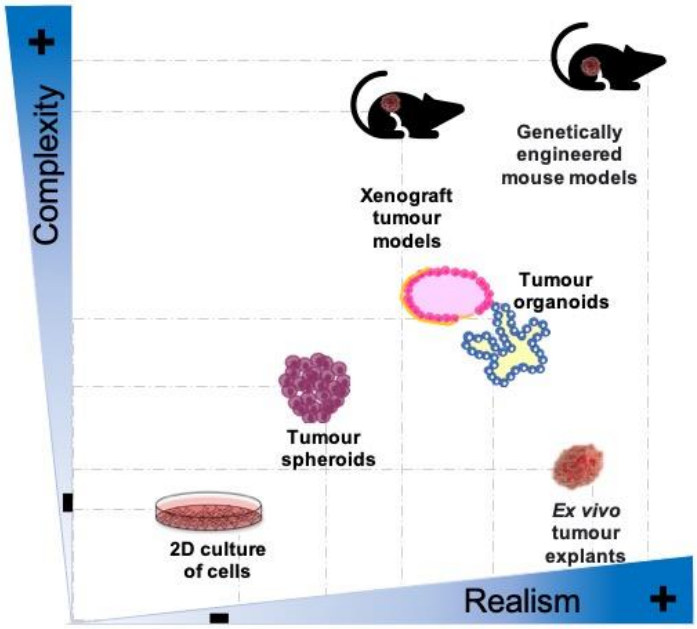

Figure 2-1 the various tumour models used as preclinical drug screening tools. Tumour models vary in terms of complexity and realism.

2.3.1 *In vitro* tumour models

2.3.1.1 2D culture of cells

2D cell cultures have been widely used to study the molecular and genetic mechanisms underlying cancer. [30] To produce 2D cell cultures, cells are cultured in culture flasks or Petri dishes. These cells are then propagated to reproduce several batches of cells (Figure 2-2-b). Researchers then store these cells in biobanks and use them for various purposes such as DNA and RNA extractions and drug response assessment. Two main types of cell sources are used to produce 2D tumour models: primary tumour cells and cancer cell lines. Primary tumour cells are cells isolated from biological specimens such as blood or tumour tissue that directly undergo experimentation. Working with primary tumour cells can be challenging because many samples die quickly in

culture. Cancer cell lines are primary cells that have been immortalized through multiple subsequent passages and adapted for *in vitro* culture conditions. [34] Cancer cell lines can be replicated infinitely and enable repeatable experimentation. Multiple cancer cell lines for various types of cancers have been established and used by researchers worldwide. Even though 2D cell cultures have shaped our current understanding of cancer progression and treatment and offer many benefits such as the simplicity of manipulation, replication, and analysis, these models have certain drawbacks. The main drawback of cancer cell lines is that cells may lose the native genomic and transcriptomic characteristics of the primary tumour and acquire new qualities during subsequent passages. More importantly, 2D cell cultures do not reflect the features related to the 3D architecture of the tumour, such as cell-matrix interactions. [35]

2.3.1.2 3D tumour models

3D tumour models are developed to overcome the spatial limitations of 2D cultures and provide a better understanding of human tumours. 3D tumour models refer to culture of cancer cells in 3D and *ex vivo* culture of tumour explants. 3D cultures of cancer cells are divided into two sub-groups based on cells from which tumour models are produced: cancer cell lines are used to form tumour spheroids and scaffold-based cultures, and primary tumour cells are used to form tumour organoids. The following sub-sections describe the various 3D tumour model models.

2.3.1.2.1 Cancer cell line spheroid

Cancer cell line spheroids are self-formed spherical cell aggregates formed from one or more cancer cell lines. [36] The commonly used technique to form spheroids is to seed a high-density suspension of cells on a non-adherent surface. If the cell-cell adhesion forces are greater than the cell-surface adhesion forces, spheroids will form. Several techniques are used for spheroid formation such as hanging droplets, bioreactors, synthetic 3D matrices and microfabrication techniques (Figure 2-2-c). Spheroids maintain similar features to the human tumour such as the 3D spatial resolution, cell-cell interactions in 3D, and possibility of forming hypoxic and nutrient-deprived cores. [37] Several studies have shown that cells' sensitivity and resistance to anti-cancer drugs are different and more similar to patients' responses in spheroids compared to 2D cell cultures. [7, 38, 39],[40] The main drawback of working with spheroids is the use of cancer cell lines instead of primary tumour cells, and the lack of the tumour microenvironment.

2.3.1.2.2 Scaffold-based culture of cancer cell lines

It is reported that some cell lines do not naturally form spheroids in culture. [36] To address this, tissue engineering techniques, such as the use of scaffolds, have been applied. Scaffolds are supporting matrices that hold the cells in a specific pattern. For the formation of 3D tumour structure, scaffolds are enriched with components of the tumour microenvironment to promote the growth of cancer cells. A suspension of cancer cell lines is then seeded on the scaffold, where they form 3D structures. Natural substances such as Matrigel, fibroblast-driven matrices and collagen-enriched hydrogels are often used to host cancer cells (Figure 2-2-c). [41] Moreover, scaffold-based cultures provide the potential to vary the biochemical or mechanical properties of the biomaterials-based scaffolds to test mechanistic questions for scaffold-based cultures. While scaffold-based models are compliant with many cell lines and allow for precise control over the structure, the fact that they are formed from established cancer cell lines makes them less relevant for personalized studies. Moreover, the design and modification of the scaffold is a time-consuming and expensive process.

2.3.1.2.3 Tumour organoids

Organoids are self-organizing 3D structures of stem cells. Organoids were conventionally used for modelling healthy organs. [42] More recently, gene editing techniques have been used to mutate normal tissue organoids and transform them into tumour organoids (Figure 2-2-e). [43]. Patient-derived tumour organoids are formed from primary human tumour specimens. To do so, tumour tissue is disintegrated mechanically and chemically into micro-sized fragments. These tumour fragments are then cultured on a supporting matrix such as Matrigel™, where they aggregate to form 3D structures (Figure 2-2-d). [44] It is possible to passage and replicate organoids several times and store them over a long period. [45] It has been shown that tumour organoids recapitulate the genetic features of the primary tumours, and reflect the clinical drug response of the corresponding patients. [9, 46] The applicability of tumour organoids as a tumour model has been verified in various types of cancers, such as ovarian [45], colorectal [9], breast [46], and lung [47] cancers. Although tumour organoids provide a versatile drug screening platform, the establishment of organoids is cumbersome and time-consuming (3-6 weeks) and may exceed the clinical decision-making time frame. [48] Besides, establishment of organoids for some specimens is

challenging and may limit their clinical utility. For example, it has been shown that lung cancer organoids from patients are rapidly repopulated by normal cells with loss of the tumour component. [49]

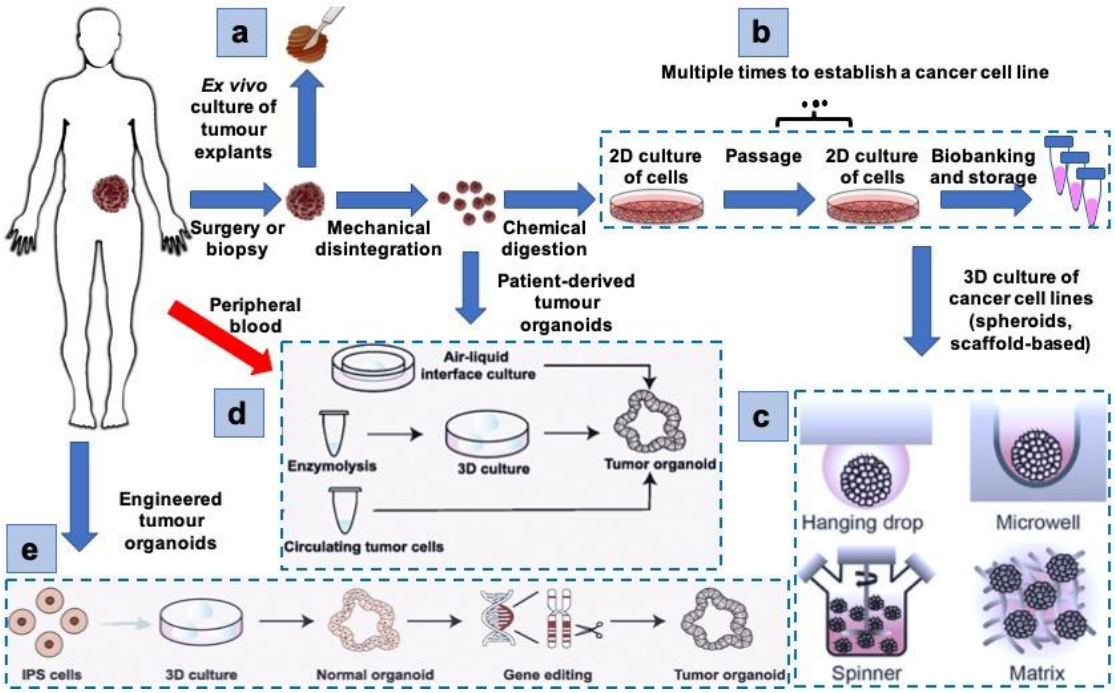

Figure 2-2 tumour models. Tumour tissue harvested through surgery or biopsy can be used to produce a variety of tumour models: a) Tumour tissue explants: tumour tissue is dissected, and tumour explants are cultured *in vitro* for different tests; b) Cancer cells cultured in 2D: tumour tissue is disintegrated and digested, and tumour cells are cultured in a monolayer. Primary cells can be used directly or undergo immortalization processes to establish cancer cell lines.; c) Tumour spheroids: many of the established cancer cell lines can form tumour spheroids in the appropriate culture condition. A few techniques to form spheroids are shown. Reproduced from reference [50], CC BY 4.0.; d) Tumour organoids: disintegrated tumour tissue is cultured with peripheral blood and normal cells to form tumour organoids. Reproduced from [43] with permission; e) Engineered tumour organoids: pluripotent human stem cells are used to form normal organoids. These normal organoids undergo mutations to transform into tumour organoids. Reproduced with permission from [43]

2.3.1.2.4 Tumour tissue explants

Ex vivo tumour tissue explants are fragments of solid tumours that are cultured and studied for various tests such as drug response assessment (Figure 2-2. a). [12] *Ex vivo* tumour tissue explants maintain the histological features and gene expression profiles of corresponding primary tumours and reflect the clinical responses of patients. [14, 51] *Ex vivo* tumour tissue explants provide an

excellent tumour model since they are readily available from biopsy or surgery, do not require disintegration, and mirror the individual's tumour features. Substantial challenges in working with tumour explants are 1) the short-term survival of tumour tissue out of its natural environment and 2) the impossibility to replicating and expanding tumour tissue explants. Short-term *ex vivo* survival is due to the interruption of the vasculature that is tumour cells' means of nutrient delivery and waste removal. Blood and lymph capillaries in tumours are bifurcated all over the tumour and deliver oxygen and nutrients to cells. Capillaries are close and inter-connected with the maximum intercapillary distance at 200 µm, which is also the passive diffusion length of oxygen. [52] The interruption of the vascular system in ex vivo cultured tumour tissues deprives tumour cells of oxygen and nutrients, especially cells in the tissue core and far from the tissue-culture medium interface. The lack of nutrients leads to phenomena such as hypoxia (i.e., lack of sufficient levels of oxygen available to cells), necrosis (i.e., irreversible cell death usually due to the lack of nutrients and oxygen), and accumulation of cellular byproducts, and results in poor viability of tumour explants. Several methodologies have been developed to improve *ex vivo* survival by increasing the accessibility of nutrients to tumour explants. For example, to increase the accessibility of nutrients to tumour cells, tumour tissue is sectioned into thin slices. Thin tumour tissue slices are then cultured in a shaker incubator to make nutrient delivery more efficient by stirring. [13, 53] Another technique is culturing tumour tissue slices on porous membrane lifts installed in well plates to mount the tissue closer to the air interface and expose both sides of the tissue slice to the medium. [6, 11] These studies have reported varying survival times of 2 to 5 days (i.e., the maximum time that tumour tissue slices maintain the baseline viability levels of the native tumour). Other methods, such as fortified culture medium [14] and perfusion chambers [15], have also been employed to increase the longevity of tumour explants. Our group has developed a methodology in which tumour tissues are dissected into micron-sized fragments to compensate for the lack of vasculature. [16] These microdissected tissues (MDTs) are small enough that passive diffusion of nutrients is possible throughout the tumour tissue. [54] In addition to the different techniques to keep tumour tissues alive, the readout and endpoint analysis varies between approaches. Table 2-1summarizes the varying parameters in *ex vivo* tumour culture methods.

Table 2-1 The various methodologies used for (non-perfused) culture of tumour explants *ex vivo*. There are many variations in the experimental parameters, and the assessment of tissue survival. N/S not stated

Cancer type and tumour source	**Explant diameter thickness**	**Culture method**	**Max days in culture**	**Readout**
Breast/human [13]	5 mm, 200 µm	Shaking incubator	4	live/dead assay, CC3, BrdU, ATP assay
Head and Neck/human [53]	N/S, 350 µm	Membrane lifts	4-7	Ki67, CC3, H&E
Pancreatic/ human [6]	N/S, 350 µm	Membrane lifts	4	H&E, ki67, (MTOR activity marker), CaIX
Pancreatic/ human [10]	N/S, 250 µm	Membrane lifts	5	H&E, Ki67, CC3
Breast/human [55]	N/S, 300 µm	Rotary shaker	6	H&E, CC3
Multiple/PDX [14]	N/S, 300 µm	Fortified medium	4	H&E, Ki67, CC3, ATP assay, RPPA profiling
Multiple/human [11]	N/S, 300-500 µm	Membrane lifts	5	H&E, Ki67, CC3, MTT
Breast/human [56]	4 mm, 300 µm	Shaking incubator	3	AlamarBlue assay, H&E, Ki67
Multiple/cell line xenografts [57]	N/S, 200-300 µm	Membrane lifts	1-4	Ki67, CC3, CICK18
Gastric cancers/ human [58]	400 µm	Membrane lifts	6	Ki67,CC3, cytokeratines, H&E

2.3.2 *In vivo* tumour models

In vivo tumour models refer to inoculating human tumours in living animals, such as rodents, that share a similar genetic homology with humans. *In vivo* tumour models are generated as xenografts or genetically engineered animals. For the preparation of xenografts, a suspension of a cancer cell line (i.e., cell line xenograft) or a fragment or cells of a primary tumour [i.e., patient-derived xenograft (PDX)] are introduced into a surrogate animal. Often immunocompromised animals are used for xenotransplantation to reduce the risk of tumour rejection. [59] More complex xenografts are produced using humanized animals that recapitulate immune responses. [60] Genetically engineered *in vivo* tumour models are formed by modifying cancer-promoting genes in an animal's genome and inducing cancer. Genetically engineered animals mimic the genetic and biological evolution of human cancers more faithfully. [61] *In vivo* tumour models have shed light on the mechanisms related to the growth and development of a tumour and its sensitivity and resistance to therapeutics in a natural environment. *In vivo* models remain indispensable for certain studies such as pharmacodynamics and pharmacokinetics modelling. [62] However, *in vivo* tumour models are challenging to monitor, lack a relevant immune system, and have crucial genetic and microenvironmental species differences from humans. [63, 64] Moreover, the preparation of *in vivo* tumour models is time-consuming (several months for some PDX) and labour-intensive (<10 % engraftment rate for some cancer types). [65, 66].

2.4 Companion diagnostics

An increasing number of therapeutic compounds are being discovered and developed to treat cancer. With advances in biomarkers field and tumour model systems, FDA has recently put a policy in place naming the co-approval program, which requires a diagnostic tool along with each new therapeutic product. The goal is to ensure the safety and effectiveness of the product. [33] These diagnostic tools, known as companion diagnostics, are tests and devices used to match patients to a specific drug or to discover new biomarkers. By FDA's definition, *"A companion diagnostic device can be in vitro diagnostic (IVD) device or an imaging tool that provides information that is essential for the safe and effective use of a corresponding therapeutic product".* [67] Imaging companion diagnostics refer to various imaging tools that capture cellular processes in living subjects at the molecular or genomic level. [68] The term "*in vitro* companion diagnostic

device" was used for biomarker detection tools only. The concept of companion diagnostics is continuously growing to be more than biomarker detection devices and imaging tools. The progress in tumour model systems makes it possible to introduce complex preclinical models, such as an organoid assay as a companion diagnostic for a new therapeutic compound.

2.5 Microfluidics in cancer research

Microfluidics is the science and technology of manipulating small amounts of samples on micro and nano scales. Microfluidic systems provide researchers with many benefits, such as parallelization of experiments, reduced cost of equipment and reagents, and precise control of the system in time and space. [69] Most microfluidic systems are fabricated using biocompatible and transparent or translucent materials, such as Poly Dimethyl Siloxane (PDMS), which create appropriate surfaces for cell and tissue culture, and allow for visualization using various imaging techniques. Due to these reasons, many conventional tumour model systems have been miniaturized using microfluidic tools. For example, it is possible to culture cancer cells on microfluidic chips and subject them to several types and concentrations of drugs for multiplexed drug screening. [70] Multi-compartment chips housing cells of different organs are used to model multi-organ communications. For example, a group of researchers developed a drug screening chip to measure the off-target toxicity of anti-cancer drugs. The microfluidic chip accommodated cancer cells, cardiomyocytes, and hepatocytes. Cells were subjected to various treatments in an *in vivo*-like fashion (i.e., drugs passed through liver cells initially), and the effect of treatment on various cells was measured. [71] It is also possible to make the surface of microfluidic devices low attachment for spheroid formation assays. [72] Various patterns and designs of microfluidic chips have been developed for high throughput spheroid formation. Spheroids formed on microfluidic chips can later be used for various purposes such as assessing the response to anti-cancer drugs [73] and radiotherapy [74], and the development of new drug delivery approaches. [75] Varying microfluidic chip designs also allow for controlling the sizes of spheroids. [76] Large spheroids (above 500 μm in diameter) have been formed on microfluidic chips to model tumour hypoxia. [77] Tumour-stroma interactions have been modelled on microfluidic chips by forming spheroids in which tumour cells are encapsulated in stromal fibroblasts. Furthermore, microfluidic devices have been used for long-term static culture of microtissues, resulting in significantly longer survival

of tumour tissue compared to non-microfluidic setups. [78] Perfusion-based culture of tumour tissue explants on microfluidic chips has also been a topic of interest over the past decade. The following sub-section explains perfusion-based *ex vivo* culture setups.

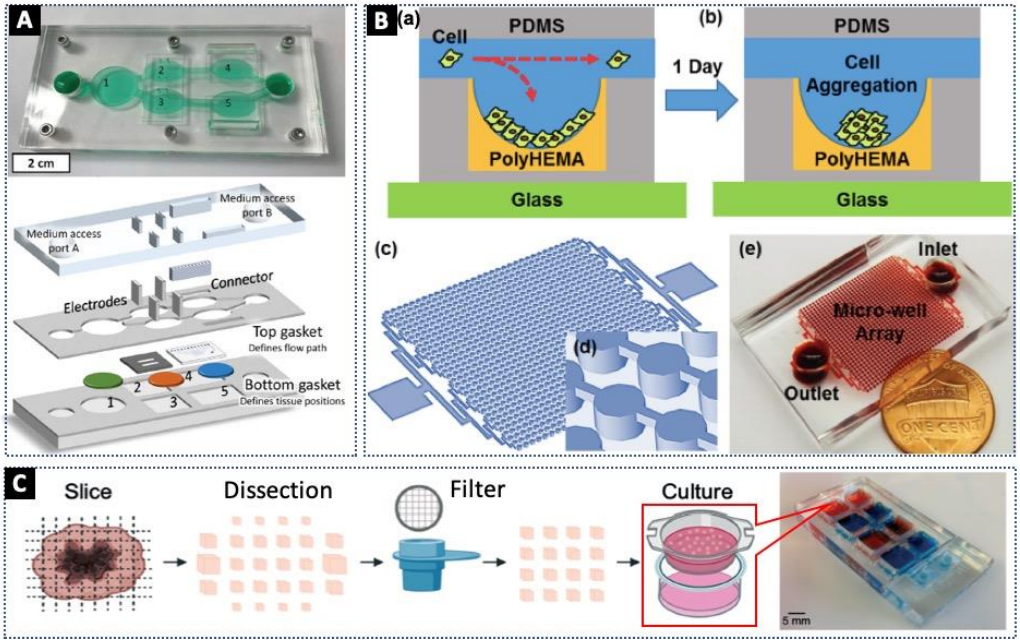

Figure 2-3 Applications of microfluidics in oncology A) A multi-compartment microfluidic chip, housing cancer and normal cells allow for assessment of the off-target toxicity of anti-cancer drugs on normal heart and liver cells, reproduced from [71] and reprinted with permission from AAAS; B) High throughput spheroid formation is possible on microfluidic chips. The surface of PDMS is coated with another polymer, poly HEMA, to render the surfaces low attachment. 1024 spheroids are formed on-chip and subjected to novel photodynamic therapy, reproduced from [79] with permission granted under CC BY 4.0; C) Drug response assessment of ex vivo tumour explants on-chip. Tumour tissue slices are dissected into micro-sized cuboids and cultured on-chip, where they are subjected to various treatments., reproduced from [78] and reprinted with permission from the Royal Society of Chemistry

2.5.1 Microfluidics for *ex vivo* culture of tissue explants

Maintaining the viability and *in vivo* features of tissue explants out of their native environment requires elaborate precautions. Microfluidic tools can improve the *ex vivo* culture by using perfusion to mimic a physiological environment by recreating *in vivo*-like fluid flows. For example, to model the gastrointestinal tract on-chip, Richardson and colleagues designed a multi-compartment microfluidic chip that accommodated a gut tissue explant and streamed media with differential oxygen concentrations across the two opposite faces of the tissue, and have shown that

oxygen gradients impact the bacterial composition present in the gut tissue. [80] It has also been shown that tumour tissue explants cultured in perfusion-based microfluidic devices maintain their viability over multiple days in culture. [81],[82] More interestingly, modelling immunity and organ-organ interactions *in vitro* is possible with microfluidics. [83] For example, to model tumour immunity on chip, a microfluidic device was designed to study the tumour-lymph node interactions using *ex vivo* tissue explants. A tumour explant and a lymph node explant were deposited on a chip, and lymph drainage from the lymph node to the tumour and blood flow in the reverse direction was applied. The results confirmed that lymph nodes co-cultured with tumour cells are immunosuppressed. [84] Perfusion-based microfluidic *ex vivo* culture devices offer many benefits over non-perfused conventional methods. The main drawback of working with these devices remains the fact that the throughput of these systems is extremely low: perfusion-based devices can accommodate a very limited number of tissue explants per device and enable testing a limited number of conditions in each experiment.

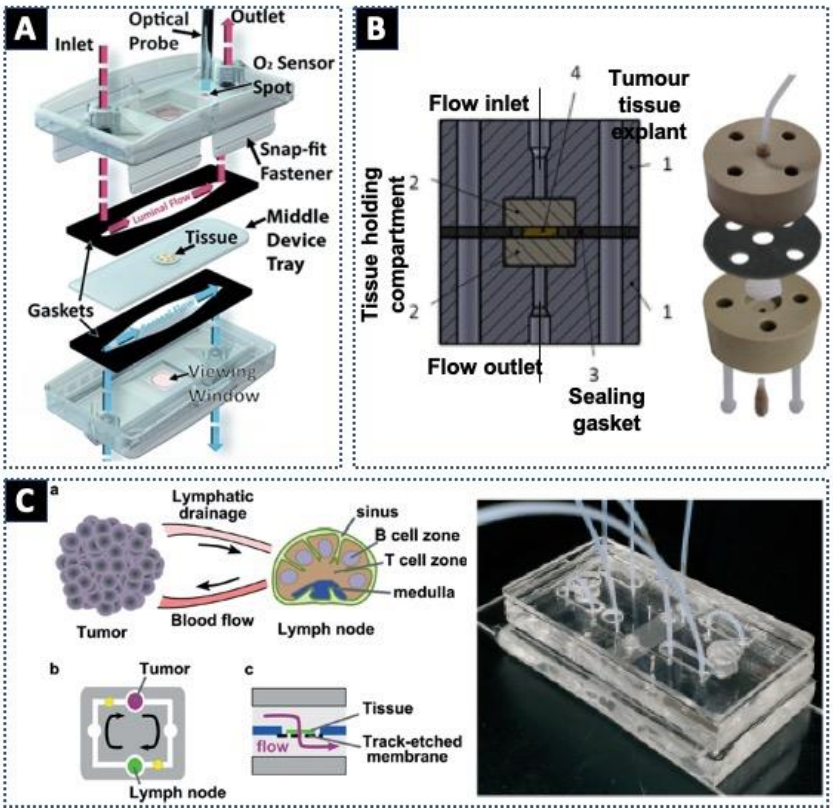

Figure 2-4 Perfusion-based *ex vivo* tissue culture systems A) Physiologically relevant environment for the culture of gut tissue on-chip. A gut tissue slice is exposed to media with different concentrations of oxygen to investigate the impact of in vitro oxygenation on the bacterial population in gut tissue explants. Reproduced from [80] with permission from the Royal Society of Chemistry; B) Microfluidic device maintains the functionality of thyroid carcinoma specimens ex vivo by perfusion. Reproduced from [81] with permission granted under CC BY 4.0; C) Model of inter-organ communications on a chip. A microfluidic chip holding tumour tissue and lymph node tissue explants is used to investigate the suppressive effect of tumour cells on lymph node immunity. Reprinted from [84] with permission from the Royal Society of Chemistry

2.5.2 Open microfluidics

Channel-based microfluidic systems are used for various cell and tissue tumour model systems. However, closed microchannels have inherent limitations that make them less appropriate for some biological applications, such as processing large surfaces (e.g., tissue slices, Petri-dishes and well plates) and/or large (above the millimeter scale) samples. [19] In addition, most devices with closed microchannels require pre-processing of the specimen (e.g., dissecting the tissue) and trapping them into channels. The pre-processing can impose large shear stress (several tens of Pascals),

orders of magnitude higher than what most sensitive tissue can tolerate. The stress of the insertion into the microchannels followed by long-term culture inside a spatially confined environment may cause secondary changes in the characteristics of samples. For this, researchers have developed microfluidic systems with partly open microchannels and channel-less microfluidic devices. For example, it is possible to inject multiple miscible fluid streams at low velocities in one channel and control the mixing of the reagents by adjusting the injection flow rates (Figure 2-5-A). [85] The parallel flow of unmixed reagents enables multiplexed and dynamic delivery of reagents to samples deposited in the channel. [86] Roofless microfluidic channels have been developed for easy manipulation of samples during experiments. For example, cells were cultured in microchannels of a roofless microfluidic chip. The chip design allowed micropipette insertion and patch-clamp electrophysiological recording of cells (Figure 2-5-B). [87] In another work for parallel drug testing on tumour tissue slices, a tumour tissue slice was placed over a network of roofless microchannels and subjected to multiple reagents streaming through the microchannels underneath (Figure 2-5-C). [88]

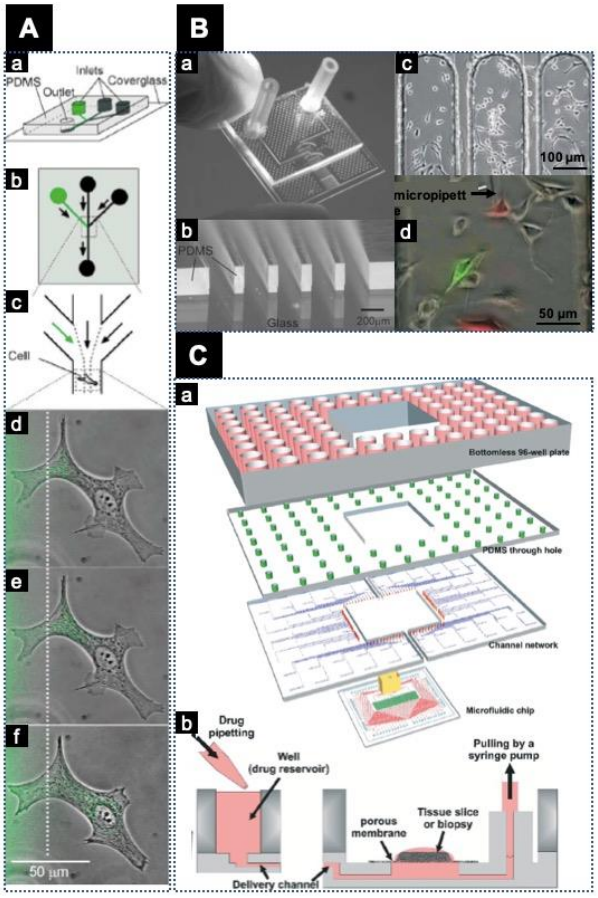

Figure 2-5 Open microfluidic systems used for cell and tissue culture and manipulation. A) Localized perturbation of single cells: multiple laminar flows deliver membrane permeable molecules to selected subcellular microdomains. (a-c) schematics of the microfluidic device, (d-f) micrographs of localized fluorescent labelling of the mitochondria of a bovine capillary endothelial cell over time Reproduced with permission from [86]; B) Micropipette access to single cells in roofless microchannels. (a-b) images of the microfluidic device, (c-d) micrographs of cells cultured in the channels, showing a few selected cells microinjected with fluorescent dyes in (d). reproduced from reference [87] with permission from the Royal Society of Chemistry; C) Multiplexed chemosensitivity testing on tumour tissue slices. Streams of drugs flow parallelly underneath the tissue slice. (a) Layer-by-layer schematic view of the device, (b) Cross-sectional schematic of the device showing that the device is operated by gravity flow and the total flow rate is driven by a syringe pump. Reproduced from [88] with permission from the Royal Society of Chemistry.

2.5.3 Microfluidics in the open space

Partially open microchannels offer more flexibility compared to closed microchannels. However, they still require sample entrapment inside a device, and the working area is limited to the dimensions of the microchannels. In response, researchers have developed channel-free

microfluidic systems that operate in the open space, otherwise known as open-space microfluidic systems. Open-space microfluidic systems are fluidic processors that deliver localized streams of reagents to the sample interface without enclosing the sample in a device. [19] Open-space microfluidic systems are capable of working over immersed planar surfaces, such as Petri dishes and culture flasks. The pioneering open-space microfluidic systems were inspired by commonly used experimental tools such as pipettes, microelectrodes, and microscopy techniques. For example, micro- and nano-pipettes were developed for localized delivery of reagents to cells [89], and for the deposition of biological molecules on surfaces. [90] These pipettes generally use ionic gradients between the pipette tip and the surface to control the delivery rates. Another open-space microfluidic system, inspired by microelectrodes, chemically stimulates a sample of interest. This system, called the Chemistrode, disperses a droplet of a biological stimulus over a substrate, allowing the stimulation to happen, and recollects the reacted species to measure the molecular response. [91] The integration of microfluidics with atomic force microscopy (i.e., very-high-resolution scanning probe microscopy developed for the localized measurement of surface forces, imaging, or sample manipulation) resulted in an open-space microfluidic system for single-cell processing. In this system, with the help of atomic force microscopy, a microfluidic cantilever was designed to deliver biochemical reagents over the surface or into single cells. Atomic force microscopy's force feedback also allowed for measurement of the intensity of the probe's contact with the cells (e.g., to discriminate between gentle cell touch or cell perforation). [92-94]

The main limitation common between primary open-space microfluidic systems is the precise control of the distance between the microfluidic device and the sample, often resulting in the invasiveness of the method. To tackle this issue, contactless open-space microfluidic systems have been developed. The first examples of contactless microfluidic systems are microfluidic probes, mobile microfluidic devices featuring two apertures to inject and aspirate reagents to a nearby substrate (Figure 2-6 a,b). [95] The tip of the microfluidic probe scans a sub-millimetre area of the surface and needs to be serially moved over the surface to cover larger areas (Figure 2-6 c). Due to their design flexibility, researchers have developed microfluidic probes for various single cells and tissue processing applications such as selective staining of adherent cells, [96] and immunohistochemistry on frozen tissue slices. [19] Microfluidic probes have also been integrated with other analysis techniques. For example, a microfluidic probe featuring an add-on fluorometric

assay scanned a plate of adherent cells. The microfluidic probe injected a cell lysis buffer and collected cell lysates, which were then analyzed for kinase activity using the fluorometric assay incorporated inside the microfluidic probe. [97] The pitfall of microfluidic probes is that the scanning speed is limited by the reaction kinetics between the delivered reagent and the substrate, which can be very slow for biological reactions. The low scanning speed caused by the duration of biological reactions and the serial nature of the scanning process renders microfluidic probes tedious to operate for cell-based assays. [18] For example, the microfluidic probe for cell lysis incubates the cells with the lysis buffer for a few minutes, followed by several minutes for the fluorometric assay to produce readouts. The microfluidic probe repeats the process many times to cover a whole substrate.

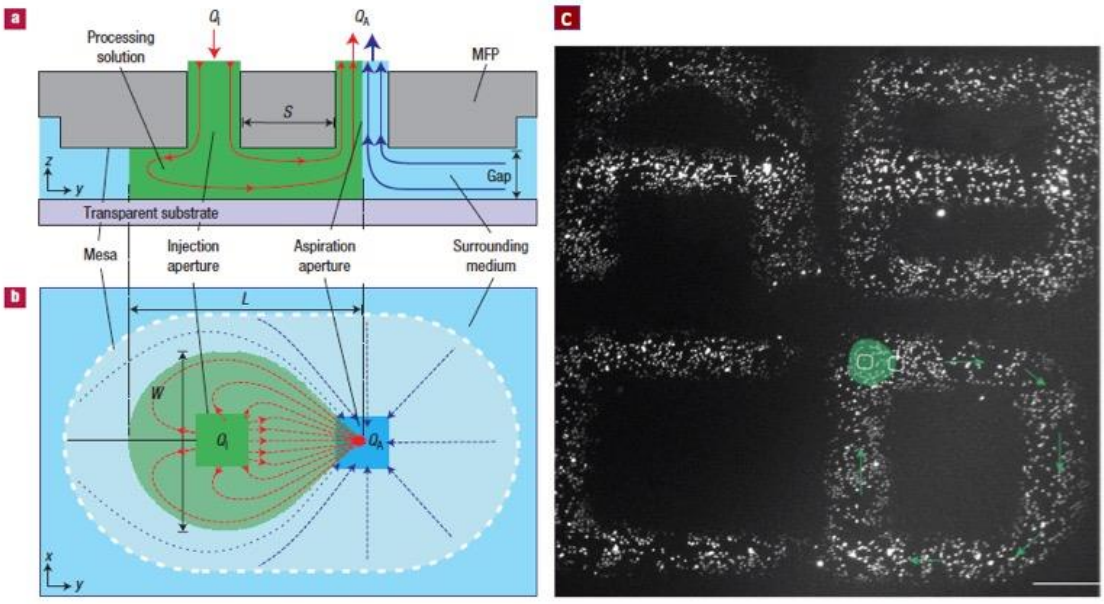

Figure 2-6 Microfluidic probe working principle. The microfluidic probe is held close to a substrate to process. By keeping the aspiration flow rates higher than the injection flow rates, flow streams can be confined over the substrate to create precise patterns. (a) side view. (b) bottom view. Reprinted with permission from [96] The device can be scanned over the surface to generate patterns. (c) shows selective staining of live adherent HeLa cells using the microflruidic probe. Reproduced with permission from [98]

2.5.3.1 Microfluidic multipoles

To multiplex and speed up the reagent delivery of microfluidic probes, microfluidic multipoles (MFM), a generalization of microfluidic probes with a larger number of apertures, have been

developed. MFMs feature different numbers of injections and aspiration apertures. A two-aperture microfluidic multipole previously referred to as a microfluidic probe can be construed as a microfluidic dipole. (Figure 2-7 A,D). MFMs feature a blunt tip installed close to a substrate immersed in a liquid (Figure 2-7 B,D). The tip of the MFM, the substrate, and the liquid that fills the gap between the two form a Hele-Shaw cell (i.e., two parallel flat surfaces separated by an infinitesimally small gap). [99] At sufficiently small gap sizes, the flow between the MFM tip and the substrate can be considered quasi-two-dimensional, and the flow ejected from point source openings (apertures) can be analyzed using the analogy between 2D flow fields and electrostatic fields. Qasaimeh et al., [100] have shown that at usual operational injection and aspiration flowrates (10-1000 nL/s), the flow under an MFM is viscous (Re <<1), and hydraulic confinement of injected flow can be controlled by modifying the ratio of aspiration to injection flowrates. If the net aspiration rate is higher than the total injection rate under the device, streams of reagents can be confined over the substrate, forming addressable fluidic patterns. [99] By modulating the flow ratio between injection and aspiration apertures, fluidic patterns with high spatial resolution, low shear stress, and low reagent consumption can be formed over the substrate. [100, 101] In the interior of fluidic patterns created by the MFM, advection is higher than diffusion (high Péclet number), owing to the injection and aspiration flow velocities. [18, 101] Under such circumstances, the concentration of injected streams remains constant in the interior of the fluidic patterns. Thus, an MFM can create several adjacent fluidic patterns of different reagents with minimal cross-talk. There is also no limit to the number of pixels that can be operated in parallel, making it a highly promising format for highly multiplexed surface processing. With this in mind, our group has recently introduced highly multiplexed MFMs, which we refer to as the pixelated chemical display (PCD). Fluidic “pixels” are formed when a fluid stream injected above a surface is confined by neighbouring identical fluid streams, forming a repeatable flow unit that can be used to tesselate a surface. Highly parallel and reconfigurable PCDs have been produced that enable the formation of up to 144×1 mm^2 pixels with successive reagent changes as fast as 1 change/30s (Figure 2-7-C,D). [20] The fact that the PCD can stream many reagents over a surface simultaneously, and switch between reagents quickly renders it more appropriate than microfluidic probes for processing planar biological surfaces. Table 2-2 compares the various microfluidic approaches for processing tumour models.

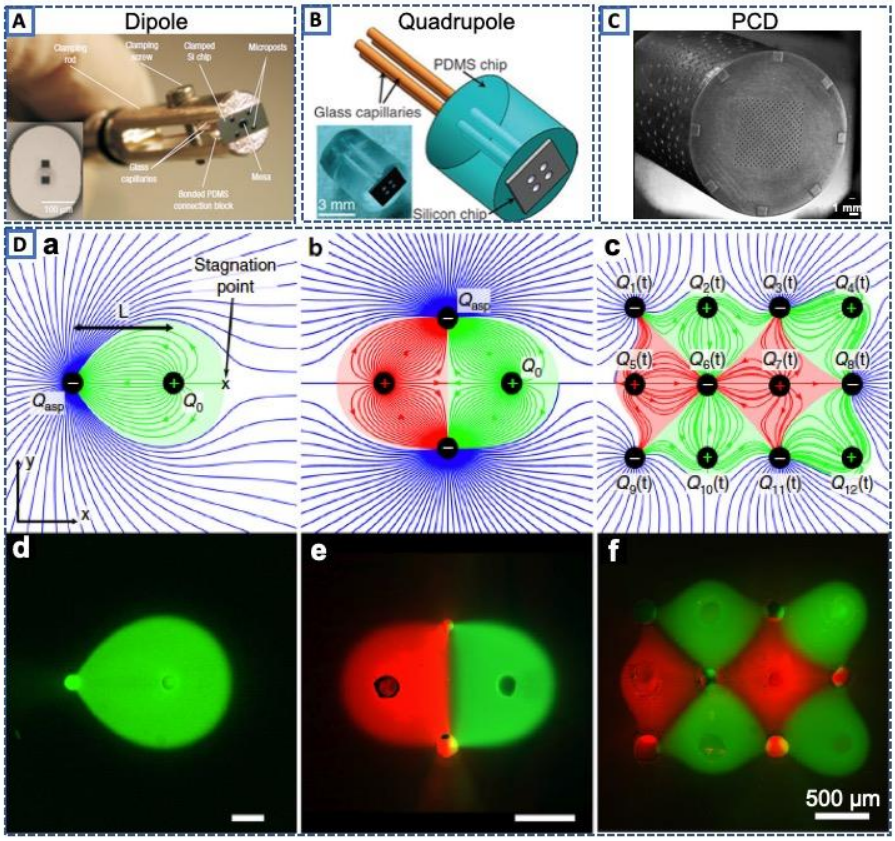

Figure 2-7 From dipoles to quadrupoles and PCDs. A) Close-up view of a microfluidic probe composed of microfabricated parts, reproduced with permission from [96]; B) A 3D illustration of a quadrupole MFM. The MFM is an assembly of several micromachined parts. Reproduced with permission from [100]; C) Micrograph of a 3D-printed 144-pixel PCD reproduced from [20] with permission granted under CC-BY NC-ND; D) theoretical streamlines (a-c) and fluorescence micrograph (d-f). Positive and negative signs, respectively, represent injection and aspiration apertures. a, d Microfluidic probe (dipole). b, e Microfluidic quadrupole. c, f 12 pixels of a PCD. reproduced from [18] with permission granted under CC BY 4.0.

Table 2-2 the comparison of various microfluidic tools for tumour model processing

	Conventional (closed) microfluidic chips	**Open microfluidics (open channels)**	**Open-space microfluidics (nanopipettes, etc.)**	**Microfluidic probe**	**MFM and PCD**
Compatibility with 2D and 3D models	yes	yes	Only 2D	Only 2D	yes
Invasiveness to the sample	Moderate (due to sample entrapment)	low	high	low	low
Access to sample/surface processing	no	yes	yes	yes	yes
Processing time	moderate	moderate	long	long	fast
Cost	$	$	$$$$	$$$	$$

Reviewing the literature and comparing various tumour models to one another has made it clear that 3D tumour model systems, especially *ex vivo* tumour explants, are an excellent choice for preclinical drug screening. Also, the PCD has the potential to perform multiplexed reagent screening over tumour models. Accordingly, I have adapted the PCD for drug screening over 3D tumour model systems.

2.6 The special case of ovarian cancer

Epithelial ovarian cancer (EOC) is the leading cause of death among gynaecological malignancies. [102] The net 5-years survival rate of ovarian cancer in Canada (44%) remains significantly lower than the five-year net survival for all female cancers (66%) combined. [1] The current gold-standard first-line chemotherapy for EOC, meaning the first chemotherapy treatment that the majority of patients receive after diagnosis, is a combination of a platinum agent (carboplatin) with a taxane drug (paclitaxel). [103, 104] Despite the initially favourable response to this treatment, 75% of patients relapse with resistance or lower sensitivity to treatments. [105] There are few

options, such as secondary surgery, or new class drugs (e.g., Poly-ADP-ribose polymerase inhibitors) available to refractory or relapsed patients. [106] Hence, the successful identification of effective anti-cancer drugs is essential and largely depends on appropriate preclinical models. [107] Various microfluidic approaches have been used to develop tumour models for ovarian cancer. The frequently used technique is to use microfluidic chips for culture and treatment response assessment of ovarian cancer cell line spheroids. [108]Also, to take the tumour microenvironment into account in the metastasis model of ovarian cancer, co-cultures of ovarian cancer cell line spheroids with peritoneal mesothelial cells subjected to physiologically relevant shear stress are developed on microfluidic chips. [109] In a more complex omentum-on-a-chip system, a vascularized model of the human peritoneal omentum and ovarian tumour microenvironment was developed to study stromal cell effects on tumour cell attachment and growth. [110]Furthermore, to highlight the role of tumour structure and the tumour microenvironment in treatment response, microfluidic chips have been used to culture and treatment of ovarian cancer MDTs and spheroids which are then compared with 2D cultures and *in vivo* models in terms of treatment response. This study has shown that there is a close correlation between 3D and *in vivo* responses while 2D cultures' responses to treatment differ in some cell lines. [111] To continue these efforts and to address the urgent need for ovarian cancer models, tissue explants were mostly produced from ovarian cancer patient specimens or ovarian cancer cell line xenografts throughout this work. However, the technologies developed here are not cancer-specific and are applicable to most solid tumours.

CHAPTER 3 GENERAL METHODOLOGY

This chapter presents the general methodology applied to fulfil the theoretical work and experiments resulting in this dissertation. The methodology chapter is divided into 3 parts, correlating with the research objectives. The relation between the articles and each research objective is also stated.

3.1 Characterization of culture conditions for the *ex vivo* culture of tumour explants

Objective 1: Characterize the impact of tissue size and culture vessel type on the *ex vivo* survival of tumour tissue explants.

There is ample literature on tool and techniques designed to increase the survival of *ex vivo* cultured tumour explants. Previous studies on *ex vivo* tumour models feature multiple varying parameters between the culture conditions, such as the size of the explant, endpoint analyses, tissue type, and the culture vessel type, and these factors had not been characterized. The goal of sub-objective 1 was to characterize *ex vivo* tumour models. To do so, I investigated the effect of two of these factors, namely the size of the explant and culture vessel type on otherwise matched tumour explants in culture. Matched MDTs and tissue slices (the two different tissue sizes) were cultured on microfluidic chips and plastic well plates (the different culture vessel types). I performed numerical simulations and experiments to compare the *ex vivo* survival of these tumour models. The details of the work are presented in Article 1, Chapter 4. Briefly, numerical simulations were performed in COMSOL Multiphysics® using the diffusion and Michaelis-Menten uptake kinetics parameters of oxygen and glucose for cancer cells to model the availability of nutrients to tumour explants. For the experimental part, MDTs were cultured on a microfluidic chip previously developed by our group. [51] I designed a new chip for tumour tissue slices that recreated the MDT culture conditions for tumour tissue slices (Figure 4-2). The details of the chip developed for the culture of tumour tissue slices are presented in Chapter 4, section 4.4.1. Briefly, similar to the microfluidic chip for the culture of MDTs, on the chip to culture tissue slices, the volume of the culture medium was 100 times the volume of the tissue. The thickness of PDMS on the top and

bottom of the tissue, and the height of the liquid over the tissue slices, which determine the tissue's access to oxygen, were equal to the parameters for the MDT chip. Tumour tissue slices were also cultured on plastic well plates to represent conventional culture conditions. Microfluidic devices were fabricated using soft lithography. Briefly, moulds were designed in CATIA (3DEXPERIENCE® platform) and fabricated by 3D printing or micromachining. PDMS replications were made using the moulds. To produce tumour models, tumour tissue slices (3 mm in diameter) and MDTs (500 µm in diameter) of the same thickness (350 µm) were produced from xenografted tumours as described in section 4.4.4. The diameter of the MDTs is chosen based on previous work to determine the maximum diameter of an explant that survives in a passive *ex vivo* culture setting. [16] The volume of each tissue slice is approximately 32 times the volume of an MDT, thus the same volume of tumour tissue is used in each system. Besides, the diameter of tissue slices represents the size generally used in the literature, even though there are variations in terms of tissue size in previous works.Tumour tissue slices and MDTs were cultured on-chip in a CO_2 incubator for up to 15 days. At different time points, tumour models were removed from the culture and underwent formalin fixation and paraffin embedding protocol for further analyses. The detailed histopathology protocol for MDTs and tissue slices is presented in section 4.4.6. Biomarkers for the epithelial compartment (cytokeratin), cell proliferation (Ki67), apoptotic cell death (cleaved caspase 3), and cell hypoxia (carbonic anhydrase IX) were used to measure tissue survival. These biomarkers are the most commonly used biomarkers to study the survival and treatment responses of tissue explants found in the literature as presented in Table 2-1. Immunofluorescent (IF) staining was used to allow for multiplexed staining of paraffin sections of tissue. The detailed methodology for immunostaining of tissue explants is given in section 4.4.7. To quantify the immunostaining, an image analysis software was used that allowed for quantifying the expression of biomarkers. The details of the image analysis protocol used to quantify immunofluorescent staining are presented in Appendix C.

3.2 Preparation of the PCD for 3D tissue manipulation

Objective 2: Evaluate the operation of the PCD over tissue explants and prepare the system for culture and drug screening on MDTs.

After demonstrating that MDTs survive *ex vivo* culture conditions for 15 days, MDTs were selected as the tumour model of interest. The next step was to enhance the chip-based MDT drug screening platform. The major complications of the chip-based MDT drug screening platform are low throughput (32 MDTs and one treatment condition per chip) and labour intensiveness. The goal of sub-objective 2 was to address these issues by increasing the throughput and automating drug screening on MDTs. For this, I adapted an open-space microfluidic technology developed by our laboratory for computer-controlled reagent streaming (automation) over a large number MDTs (increased throughput). To integrate the PCD with the MDT drug screening platform, I first performed numerical simulations to investigate the operation of the PCD over MDTs. Several parameters which may challenge the operation of the PCD on MDTs compared to flat 2D surfaces, such as surface imperfections, inhomogeneous porosity of the material, and the presence of walls between MDTs were modelled in COMSOL Multiphysics®. The details of the numerical work are presented in the second article (Chapter 5) in section 5.4.3. After observing the promising operation of the PCD over MDTs in the simulations, changes were made to the PCD to adapt its application over MDTs. These changes include increasing the size of fluidic pixels from 1 mm^2 to 6 mm^2 to cover a larger number of MDTs under each fluidic pixel and increasing the size of the spacers on the PCD to increase the gap between the PCD tip and the tissue and making sure the PCD does not squash MDTs. PCDs and manifolds were designed and modified using script-assisted CAD previously developed by the group [98], and 3D printed. Tubes were connected to the PCD using the protocol developed by our group. [98] Switch valves were incorporated on the fluidic lines to enable rotating between two reagent flasks without interrupting the system. Then, a microwell array was fabricated to house and arrange the MDTs underneath the PCD. The microwell array also served to keep the MDTs in groups corresponding to each fluidic pixel. The microwell array was designed in Fusion 360 (Autodesk©), and micromachined in poly methyl methacrylate (PMMA), a rigid and gas-impermeable polymer as explained in section 5.5.1. Pierre Alexandre Goyette and I designed and fabricated a few other parts such as a holder and a bracket to ensure the correct alignment and stability of the PCD over the microwell array. As a final addition to automating the system, fluidic sensors were added and a PID controller was developed by Pierre Alexandre Goyette to measure the flow rates of injection and aspiration of the PCD. These sensors and the PID controller served to diagnose unexpected flow rate fluctuations and prevent the system rupture

by reversing the fluctuations. The final setup referred to as the PCD platform is composed of the PCD, the microwell array, holder and bracket, fluidic pumps, the computer that controls the pumps, and flasks of reagents.

3.3 Verifying the capability of the PCD platform for multiplexed reagent screening

Objective 3: Validate the potential of the PCD as a drug screening tool for 3D tumour models.

The outcome of sub-objective 2 is a functional reagent screening platform with the potential to perform various drug screening assays on 3D tumour models. The goal of sub-objective 3 was to validate several operational parameters of the PCD such as the precision of fluidic pixels and crosstalk between them, and the ability to perform dynamic reagent screening over tumour models. For this, first I used the PCD to stream cellular dyes over 3D tumour models. My goal was to visualize pixels and trace any possible crosstalk between pixels or pixel bleeding. Next, to investigate the potential of the PCD to perform dynamic reagent screening, I performed dynamic treatment of MDTs with a cytokine to track the time-dependent response of MDTs to biological stimulation. Finally, I used the PCD drug screening platform for spheroid formation and reagent screening on them. Details of tests and experiments performed to validate the operation of the PCD over MDTs are presented in Chapter 5. Briefly, Numerical simulations using COMSOL Multiphysics to model reagent dispersion in microwells and MDTs showed that the fluid in wells is replenished after 20 minutes of streaming (section 5.4.3). For this, upon each change of reagents, 20 minutes was considered as the baseline for the concentration in the tissue and the microwells to reach the steady state, and the incubation time with biochemical reagents started 20 minutes after the change of the injected reagent. For the experimental part, MDTs were produced from xenografted tumours as explained in section 0. Depending on the experiment, formalin-fixed or fresh MDTs were deposited in the microwell array and subjected to different cellular dyes streaming at different fluidic pixels by the PCD. Every 3 pixels streamed the same reagent to provide experimental triplicates. At the end of the experiment, MDTs were rinsed and removed from the microwells and embedded in OCT. OCT blocks were sectioned following the protocol explained in section 5.5.8 to investigate the diffusion of dyes throughout the MDTs. MDTs were

subjected to dyes for different durations ranging from 1 to 3 hours in different experiments, resulting in a differential dispersion of dyes inside MDTs. Subsequently, MDTs produced from an ovarian cancer cell line xenograft were treated for different time courses with Tumour Necrosis Factor-alpha (TNF-a) as explained in sections 5.5.8 and 5.4.7. TNF-a induces the activation of the NF-kB group of proteins in a reversible manner: TNF-a exposure causes an instantaneous nuclear translocation of proteins, but the nuclear signal is reversed after a while. For this experiment, freshly produced MDTs were first subjected to the culture medium for 20 minutes to replenish the nutrients. At 20 minutes, the reagent flask for the 4-hour treatment group was switched to a solution of 20 ng/ml TNF-a in the complete culture medium, while the other pixel groups still received the complete medium. At 230 minutes, the reagent flask for the 30-minute treatment group was switched to the TNF-a solution (20 ng/ml TNF in complete medium), and the experiment continued for 50 minutes (counting for 20 minutes to replenish the wells followed by 30 minutes incubation). At 280 minutes all the injection reagent flasks were replaced with PBS 1X, which was injected for 20 minutes. The PCD was removed and MDTs were formalin-fixed and taken out of the well. MDTs underwent IF staining with p65, a sub-unit of the NF-kB group of proteins. The nuclear signal of p65 was quantified using the Visiomorph™ software.

I was also interested in testing the operation of the PCD over other 3D tumour models, for example, spheroids. To verify if the PCD operates uniformly over a whole spectrum of 3D tumour models ranging from tumour spheroids to MDTs, I performed spheroid formation and staining in the PCD drug screening platform. First, I prepared the microwell array and used it for the formation of cancer cell line spheroids as detailed in section 5.5.7. I the subjected spheroids to cellular dyes dynamically using the PCD. For this experiment, spheroids were treated with cellular dyes for 2 hours, then the dyes were swiped, subjecting fluidic groups to a different colour than they were exposed to in the first round. In the second round, spheroids were treated with the dyes for 3 hours, and perfused with PBS afterwards to purge the dyes. Fluorescent intensity of tumour models for each channel was measured using Image J software as detailed in section 5.5.11, and pixels treated for 2 vs. 3 hours were compared. To do this, for each channel, I selected at least 3 random spheroids in each fluidic pixel and the corrected total fluorescence intensity of spheroids was calculated by subtracting out the background signal.

CHAPTER 4 ARTICLE 1: MICRODISSECTED TISSUE VS TISSUE SLICES—A COMPARATIVE STUDY OF TUMOR EXPLANT MODELS CULTURED ON-CHIP AND OFF-CHIP

Dina Dorrigiv [1,2], Kayla Simeone [1,3], Laudine Communal [1], Jennifer Kendall-Dupont [1], Amélie St-Georges-Robillard [1,4], Benjamin Péant [1], Euridice Carmona [1], Anne-Marie Mes-Masson [1,3,*] and Thomas Gervais [1,2,4,*]

[1] Centre de recherche du Centre hospitalier de l'Université de Montréal, (CRCHUM) and Institut du cancer de Montréal, Montreal, QC H2X 0A9, Canada; dina.dorrigiv@polymtl.ca (D.D.); kayla.simeone@umontreal.ca (K.S.); laudine.eve.desreumaux@umontreal.ca (L.C.); jennifer.kendall-dupont.chum@ssss.gouv.qc.ca (J.K.-D.); amelie.st-georges-robillard@polymtl.ca (A.S.R.); benjamin.peant.chum@ssss.gouv.qc.ca (B.P.); euridice.carmona.chum@ssss.gouv.qc.ca (E.C.); anne-marie.mes-masson@umontreal.ca (A.-M.M.-M.)

[2] Institute of Biomedical Engineering Polytechnique Montréal, Montreal, QC H3T 1J4, Canada

[3] Department of Medicine, Université de Montréal, Montreal, QC H3T 1J4, Canada

[4] Department of Engineering Physics, Polytechnique Montréal, Montreal, QC H3T 1J4, Canada

* Correspondence: anne-marie.mes-masson@umontral.ca; Tel:+1-(514)-890-8000 (ext. 25496); thomas.gervais@polymtl.ca; Tel.: +1-(514)-340-4711 (ext. 3752).

4.1 Background information

Published article 1 [17] is presented in this chapter and discusses the difference in *ex vivo* survival between matched tumour explants that vary in terms of size and culture vessel type. This article gives background information about tumour models, with a special focus on tumour explants cultured *ex vivo*. Then, it provides information on the physics of diffusion-dominant transport in tissue explants cultured *ex vivo* and details a methodology for the culture and manipulation of

tumour explants. It also talks about the adaptation of common clinical practices such as histopathology, for use with microfluidic systems. In the results section, the various parameters referring to the *ex vivo* survival of tumour explants (i.e., hypoxia, apoptosis, necrosis, and proliferation) are measured and compared in tumour explants, all pointing to the superior viability of MDTs compared to tumour tissue slices. For the experimental part, three cell lines (two ovarian cancer and one prostate cancer cell line) were used to verify the results in different tissue types. Finally, the discussion section further explains the challenges in working with tumour explants as a tumour model, and practical solutions to overcome them.

My contribution to this article is 80% of the work. I performed numerical simulations for nutrient transport in tissue cultures. I designed and fabricated the microfluidic device for the culture of tissue slices and modified the culture conditions and formalin fixation and paraffin embedding protocol for tissue slices. I performed the tissue preparation and culture experiment and IF staining and image analysis. I wrote the article. K.S. taught me the experimental protocols to work with MDTs and oversaw the experiments at the beginning. L.C. supervised the statistical analysis. J.K.D. helped in the preparation of tumour models and oversaw cell culture works. A.S.R. helped in the preparation of the figures. B.P. and E.C. helped design the study and experiments. A.-M.M.-M. and T.G. provided support and supervised the research. All authors reviewed the article.

The article was submitted on July 5th, 2021 and accepted on August 20th, 2021 in Cancers, volume 13, issue 16 [Special Issue Modeling Cancer in Microfluidic Chips)], pages 4208-4222.

4.2 Abstract

Predicting patient responses to anticancer drugs is a major challenge both at the drug development stage and during cancer treatment. Tumor explant culture platforms (TECPs) preserve the native tissue architecture and are well-suited for drug response assays. However, tissue longevity in these models is relatively low. Several methodologies have been developed to address this issue, although no study has compared their efficacy in a controlled fashion. We investigated the effect of two variables in TECPs, specifically, the tissue size and culture vessel on tissue survival using micro-dissected tumor tissue (MDT) and tissue slices which were cultured in microfluidic chips and plastic well plates. Tumor models were produced from ovarian and prostate cancer cell line

xenografts and were matched in terms of the specimen, total volume of tissue, and respective volume of medium in each culture system. We examined morphology, viability, and hypoxia in the various tumor models. Our observations suggest that the viability and proliferative capacity of MDTs were not affected during the time course of the experiments. In contrast, tissue slices had reduced proliferation and showed increased cell death and hypoxia under both culture conditions. Tissue slices cultured in microfluidic devices had a lower degree of hypoxia compared to those in 96-well plates. Globally, our results show that tissue slices have lower survival rates compared to MDTs due to inherent diffusion limitations, and that microfluidic devices may decrease hypoxia in tumor models.

Keywords: *cancer treatment; drug screening assays; tumor explant culture platform; hypoxia; ex vivo model*

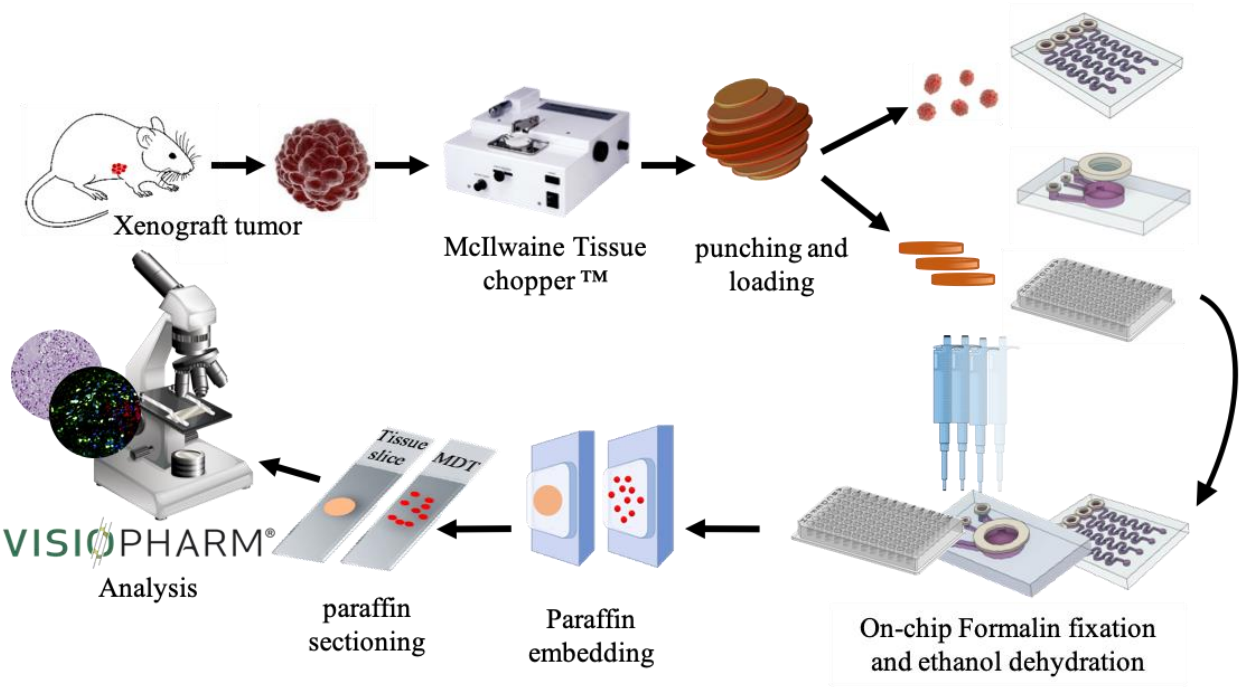

Figure 4-1 Graphical abstract. Workflow of the study

4.3 Introduction

A critical bottleneck in pharmaceutical and clinical oncology is predicting the response of patients to anticancer drugs. Only 3.4% of new cancer drugs reach regulatory approval, despite the fact that oncology accounts for more than 40% of all drug development programs [112]. Cancer progression

is due to an accumulation of multiple genetic and epigenetic alterations, creating intra- and inter-tumoral heterogeneity [113, 114]. This complexity results in the ability of cancer cells to acquire innate and adaptive responses to different drugs, rendering the drug development and clinical decision-making uncertain even when predictive markers exist [115]. To address this variability, researchers have developed multiple preclinical models to evaluate the chemosensitivity profile of patients. In vitro 2D models, such as monolayer cultures of tumor-derived cell lines are simple and high-throughput, but they do not include the tumor architecture or interactions between cancer cells and the tumor microenvironment. This can result in discrepancies in treatment sensitivity compared to the parental tumors. To circumvent these drawbacks, a growing number of 3D models have emerged to incorporate 3D cell interactions and mass transfer limitations, which are more time- and cost-effective. The most commonly used 3D models are tumor spheroids because they are easy to form and have very high viability [7, 36, 37, 65, 116]. However, spheroids also lack the native tumor tissue arrangement and tumor-associated microenvironment. Patient-derived xenografts (PDX) are the current gold standard for in vivo tumor models and incorporate many elements of the primary tumor. However, the engraftment procedure can have an extremely low success rate (<10% for some cancers) and the long time frame for tumor development exceeds a clinically relevant time frame requirement for patient management [66, 117]. A more recent group of 3D models are organotypic tumors, such as patient-derived tumor organoids and ex vivo tumor explants, which offer the possibility to preserve the tumor heterogeneity and the genomic and transcriptomic factors of each tumor [42, 118, 119]. Patient-derived tumor organoids require tumor deconstruction, cell purification, expansion, and tumor reconstruction steps, which destroy the original tumor architecture, and are time-consuming and labour-intensive. In contrast, ex vivo tumor explants do not require such processing and preserve the tumor integrity, including the cell heterogeneity and the specific tumor microenvironment [11, 120, 121].

The use of tumor explants, also known as precision cut or organotypic tissue slices, has steadily increased because they have been shown to replicate characteristics and chemosensitivity profiles of in vivo patient tumors [12]. However, the main challenges faced by tumor explant culture platforms (TECPs) are tissue viability in the absence of an intact vasculature system and the low throughput of drug screening assays due to limited tumor material. In response, several techniques and tools such as fortified culture media [14], shaker incubators [13], porous tissue lifts [122], and

perifusion-based culture systems [15, 84, 123, 124] have been evaluated to improve the short-term tissue viability. Moreover, the integration of a microfluidic infrastructure in TECPs has shown great potential to preserve tumor viability and increase the throughput via the reduced requirement of samples and reagents as well as the parallelization of experiments [125-128]. Our group has introduced a microfluidics-based TECP, known as the micro-dissected tissue (MDT) [16, 51], in which MDTs with sizes similar to large spheroids can be generated rapidly using conventional tissue slicing and punching methods. Their small volume and roughly spherical shape make them easy to manipulate and amenable to high-throughput methods when originating from a primary tumor. This MDT methodology preserves the viability (>70% proliferative and <10% cell death) of tumor fragments for up to 15 days [51].

Despite an increasing number of publications describing tumor explants and their advantages over other 3D tumor models, there does not exist, to the best of our knowledge, any study which compares tumor explant culture strategies with each other on objective, experimental grounds. In this study, we compared the tissue viability of three TECP systems: (1) conventional culture of tissue slices in plastic 96-well plates; (2) the culture of tissue slices in oxygen-permeable microfluidic devices; and (3) the culture of MDTs in microfluidic devices. We investigated the effect of tumor tissue size and culture vessel type on ex vivo tissue survival to identify the limitations of these model systems in a non-perfused setting. Tissue slices (3 mm in diameter) and MDTs (500 µm in diameter) of the same thickness were produced from the same tumor specimen, while keeping the tissue volume and medium volume ratio constant. Samples were cultured for 15 days and examined at various time points for oxygen and glucose consumption, morphology, viability, proliferation, epithelial content, and hypoxia. Our results demonstrate that MDTs preserve higher levels of viability and proliferation than tissue slices over the same culture period. By comparing tissue slices in microfluidic devices and 96-well plates, we show that the oxygen-permeability of the microfluidic devices reduces the extent of hypoxia but does not prevent hypoxic cores from forming within the tissue. Our results identify the strengths and weaknesses of studied models and provide insights to orient the choice of tumor explant models for future studies.

4.4 Materials and methods

4.4.1 Design and Fabrication of the Microfluidic Device

Microfluidic devices were composed of two polydimethylsiloxane (PDMS) layers obtained by moulding on micromachined polymethylmethacrylate (PMMA) or 3D-printed resin moulds. To form both layers, the elastomer base and the curing agent (Sylgard® 184 silicone elastomer kit, Dow Corning, Midland, MI, USA) were mixed at a weight ratio of 10:1, degassed, and cured for 1 h at 80 °C. The MDT chip design has previously been described [51] and is illustrated in Figure 1 a. Briefly, the bottom layer contained four fluidic channels of 0.9 × 1.1 mm rectangular cross-sections, each featuring an inlet and an outlet of 3.2 mm and 1.5 mm, respectively. The bottom layer consisted of a 4 × 8 array of 0.7 mm square cross-section wells that serve as traps for the MDT. The top layer of the tissue slice chip contained two fluidic channels that were 23 mm long with a 0.9 × 1.1 mm rectangular cross-section, each featuring an inlet of 3.2 mm in diameter. The bottom layer consisted of an 18 mm long fluidic channel with a 1.1 mm square cross-section connected to a 7 mm diameter cylinder, which served as the tissue slice chamber on one end and an outlet of 1.5 mm diameter on the other end. The top and bottom layers of both types of microfluidic devices were rendered hydrophilic and bonded using atmospheric plasma treatment to form enclosed channels. To seal the tissue slice chamber, a PDMS plug was designed from a 3D-printed mould (Figure 4-2 a). All microfluidic devices and well plates were sterilized with ethanol and prepped with a triblock copolymer (Pluronic® F-108, Sigma-Aldrich, St. Louis, MO, USA), as previously described [16].

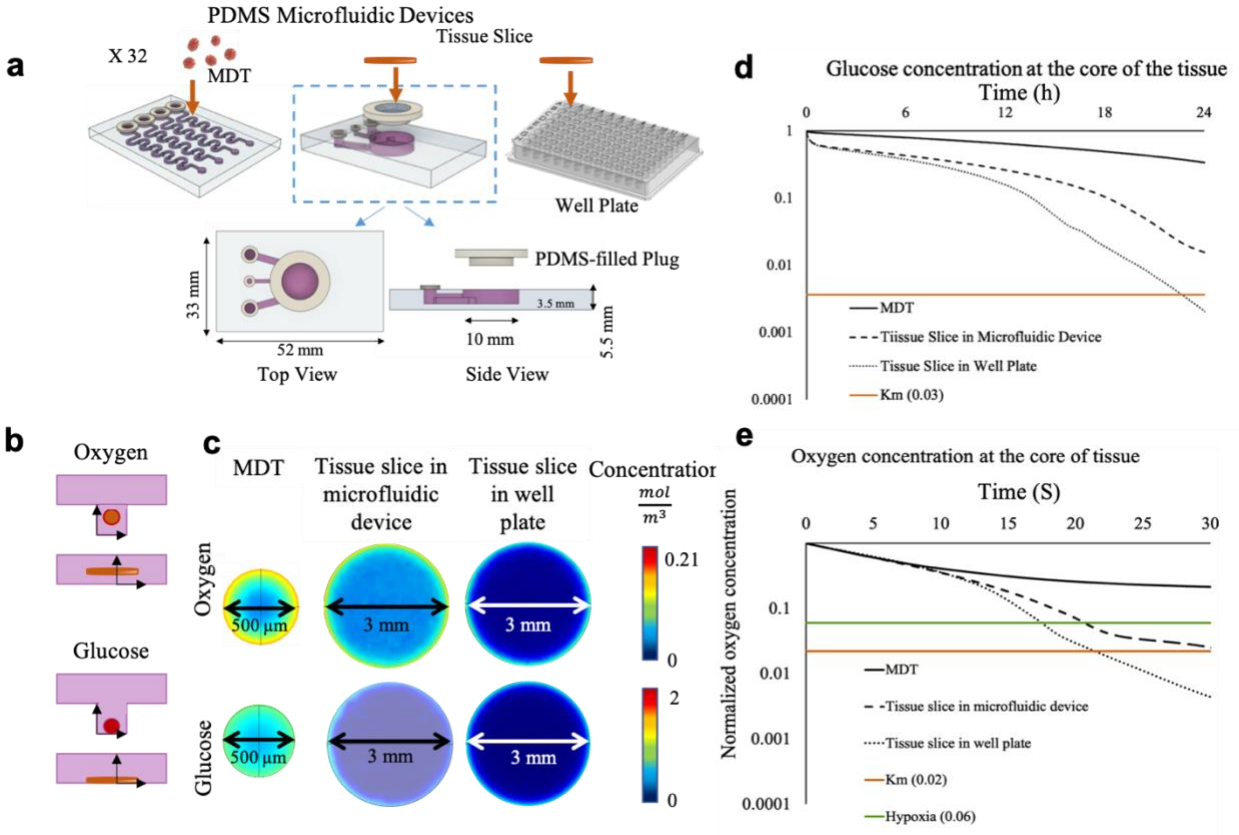

Figure 4-2 Design and operation of the microfluidic devices. (**a**) Schematic representation of the culture vessels. (**b**) Schematic representation of tissue positioning for worst case scenario for oxygen (top) and glucose (bottom). (**c**) Finite element simulation of the concentration distribution of glucose (at 24 h post-culture) and oxygen (at 30 s) in the midplanes of tumor models. Simulated changes in the concentration of glucose (**d**) and oxygen (**e**) in culture.

4.4.2 Finite Element Methodology

We used COMSOL Multiphysics© software v.5.5 (COMSOL Inc, Burlington, ME, USA) to simulate the passive diffusion of oxygen and glucose in the MDTs and tissue slices in between the medium changes. The geometry of the model was drawn using built-in COMSOL drawing tools. The dimensions of the devices can be found in the Supplementary Material, Table 4-1. All simulations were conducted at a constant biological temperature (37 °C). Fick's second law of diffusion was applied using the transport of diluted species physics in COMSOL to model the transport of oxygen and glucose in the culture medium and tissue. We first simulated oxygen transfer through the PDMS layers. As previously reported by Kim et al. [129], our simulations showed rapid oxygen exchange through the thin layers of PDMS at the top and bottom of the device

that were exposed to ambient air. This can also be explained analytically. For instance, the effective diffusion time ($t=x^2/2D$) for oxygen transfer through the 2 mm thick PDMS slab at the bottom of the device was less than 10 s, meaning that oxygen concentration through PDMS stabilizes after a few seconds. For this, we considered a constant oxygen concentration of oxygen at the top and bottom of the devices. However, oxygen transfer through other PDMS walls is not sufficient due to larger PDMS thicknesses and being constrained to medium-filled channels or wells. Hence, we imposed a no-flux (Neumann) boundary conditions at all other PDMS walls as well as plastic walls. All interface boundaries (Air/PDMS, PDMS/Medium and Medium/Tissue) were set with a continuity condition. We used Michaelis–Menten (MM) kinetics to model the glucose and oxygen consumption rates of the cells. The average Michaelis–Menten uptake kinetics found in the literature [30,33,34] imply high consumption rates in the abundance of nutrients and lower consumption rates when nutrients are depleted. The Michaelis–Menten constants served as the concentration thresholds, below which the normal cell metabolism is altered [130, 131]. Furthermore, hypoxia is present in tumors when oxygen partial pressure falls below 10 mmHg (i.e., 13 µM dissolved oxygen in the culture medium) [132, 133]. The design of the previously optimized MDT chip that ensures the high viability of MDTs [51, 54] was adapted for tissue slices. We simulated the worst-case experimental scenario for glucose and oxygen consumption in tissue slices and MDTs: tissue settling on the bottom surface of the well, far from the medium-filled channels for glucose; and tissue floating in the middle of the well, far from the oxygen permeable PDMS walls for oxygen Figure 4-2 b. Oxygen in microfluidic devices is replenished continuously and reaches steady state after a few seconds (30 s or less) in culture. In contrast, in plastic 96-well plates, it is a finite source and is depleted at the tissue core within seconds. Glucose is a finite source in all devices and is supplied through medium refreshment every 24 h. Tissue uptake and diffusion parameters are provided in the Supplementary Material, Table 4-2.

4.4.3 Ovarian and Prostate Cancer Cell Lines for Xenograft Production

Human carcinoma cell lines derived from ovarian cancer tumors, TOV112D (RRID:CVCL_3612) and TOV21G (RRID:CVCL_3613), and one metastatic prostate cancer tumor, DU145 (RRID:CVCL_0105), were used to produce mouse xenografts. Ovarian cancer cells were grown as monolayers (2D culture) in OSE medium (316-030-CL, Wisent Inc., Saint-Bruno-de-

Montarville, Canada) supplemented with 10% fetal bovine serum (FBS; Gibco™, Thermo Fisher Scientific, Waltham, MA, USA), 55 mg/L gentamicin (Gibco™, Thermo Fisher Scientific) and 0.6 mg/L amphotericin B (Gibco™, Thermo Fisher Scientific). Prostate cancer cells were grown in RPMI medium (Thermo Fisher Scientific) supplemented with 10% fetal bovine serum (FBS; Gibco™, Thermo Fisher Scientific), 55 mg/L gentamicin (Gibco™, Thermo Fisher Scientific) and 0.6 mg/L amphotericin B (Gibco™, Thermo Fisher Scientific). After reaching confluency, cell suspensions (1,000,000 cells) were mixed with Matrigel (BD Biosciences, Franklin Lakes, NJ, USA) at a 1:1 ratio and subcutaneously injected into the flank of immunodeficient NOD.Cg-Rag1tm1Mom Il2rgtm1Wjl/SzJ female or male mice (Charles River Development, Wilmington, MA, USA), depending on the cancer type. Xenograft tumors were harvested once they reached a volume between 1500 and 2000 mm^3. All animal procedures were performed in accordance with the Guidelines for the Care and Use of Laboratory Animals of the CRCHUM and approved by the Animal Ethics Committee (the Comité Institutionnel de Protection des Animaux).

4.4.4 MDT and Tissue Slice Production from Cell Line Xenograft Tumors

We adapted our previously published method [51] for the production of MDTs to prepare tissue slices. Briefly, a tissue chopper (McIlwain, Ted Pella©, Redding, CA, USA) was used to cut the xenograft into 350 µm thick tissue slices. Tissue slices were kept in Hank's Balanced Saline Solution (HBSS, 311-516-CL, Wisent Inc., Saint-Jean-Baptiste, QC, Canada) supplemented with 10% FBS, 55 mg/L gentamicin and 0.6 mg L^{-1} amphotericin B. Tissue slices were further punched into MDTs using a 500 µm diameter tissue punch, and into standard tissue slices using a 3 mm diameter tissue punch (Zivic Instruments, Pittsburgh, PA, USA) and kept with the antibiotic and antifungal.

4.4.5 Tissue Loading, Trapping, and Culture of Tissue

The loading, trapping, and culturing of MDTs was performed as previously described [51]. For tissue slices, the device plug was removed, and one tissue slice was placed in the HBSS-filled tissue chamber using tweezers under sterile conditions. The plug was then put back in place to seal the device. One tissue slice per well was transferred to 96-well plates. Culture media were changed right after tissue loading and every 24 h for tissue slices and MDTs.

4.4.6 Formalin Fixation and Paraffin Embedding Protocol and Tissue Staining

We followed our previously published on-chip paraffin embedding lithography (PEL) protocol to produce MDTMA blocks for MDTs and standard paraffin blocks for tissue slices [51]. Each paraffin block was sliced into 4 μm thick sections using a microtome. Each paraffin slice was placed on a TOMO® hydrophilic adhesion slide (Matsunami, Bellingham, WA, USA). Paraffin sections underwent hematoxylin and eosin (H&E) staining as well as immunofluorescence (IF) staining to assess the presence of tumoral cells (cytokeratin 8/18 (CK8/18) and human-specific mitochondria), proliferation (Ki-67), cellular death (cleaved caspase-3, CC3), and the presence of hypoxia (carbonic anhydrase 9, CA-IX) in the tumor models. IF staining was performed using the BenchMark XT automated stainer (Ventana Medical System Inc., Tucson, AZ). Antigen retrieval was carried out with Cell Conditioning 1 (Ventana Medical System Inc; #950-123) for 90 min for all primary antibodies. Rabbit anti-CA-IX (1:1000) antibody (ab15086, Abcam, Cambridge, United Kingdom), mouse anti-CK8/18 (1:200) antibody (IR09461-2, Agilent, CA, USA), mouse anti-mitochondria (1:2500) antibody (ab92824, Abcam), mouse anti-Ki67 (1:500) antibody (9449, Cell Signaling Technology, Massachusetts, USA), and rabbit anti-cleaved caspase-3 (1:200) antibody (9661, Cell Signaling Technology) were automatically dispensed. The slides were incubated at 37 °C for 60 min and secondary antibodies were incubated at room temperature on the bench. All sections were scanned with a 20× 0.75 NA objective with a resolution of 0.3225 μm (bx61vs, Olympus, Toronto, ON, Ontario).

4.4.7 Quantification of Immunofluorescent Staining

To quantify protein expressions using IF, we used VisiomorphDP software (VisioPharm, Hørsholm, Denmark) [134, 135]. Briefly, the tissue core surface area was detected through the Dapi channel. The surface area of CK8/18 and human mitochondria positive cells was labeled and quantified in the tissue core to differentiate human epithelial tumor cells from murine and stromal cells. Proliferation was quantified by dividing the surface area of Ki67-positive tumor cell by the total surface area of the tumoral cells. CC3 staining was observed both in the nuclei and in the cytoplasm. CC3 and CA-IX cytoplasmic staining were quantified by dividing the surface area of positively stained cells by the surface area of the epithelial cells.

4.4.8 Statistical Analysis

Statistical analyses were performed in GraphPad Prism© version 8.0 using the non-parametric one-way ANOVA Kruskal–Wallis test and post hoc Dunn's test, because the data were not normally distributed according to the D'Agostino and Pearson omnibus normality test, and the sample size for tissue slices was small. For each experiment, a minimum of 15 MDTs or 3 tissue slices were analyzed at each time point for each condition. All experiments were repeated at least three times (N = 3). All data are reported as the mean ± SEM unless otherwise stated. The reported *p*-values were generated using a post hoc test (Dunn's test).

4.5 Results

4.5.1 Numerical Simulation Predicts Sufficient Oxygen and Glucose in MDTs and Deficiency in Tissue Slices

Our group has previously designed a microfluidic platform that sustained the viability of 32 MDTs over 15 days [51]. Similar to our MDT model system, a microfluidic device was designed that holds a single tissue slice with a volume equivalent to 32 MDTs (Figure 1 a). Thus, a total tissue volume of 2.4 µL surrounded by 250 µL of medium volume was considered for all three models for both simulations and experiments. Glucose uptake simulations were then conducted to gain insight on glucose depletion in tissue models during the 24 h medium change intervals. Simulations suggested that the concentration of glucose available in tissue slices fell below the Michaelis–Menten threshold, indicating glucose deprivation, regardless of the culture platform (Figure 1 c,d). In contrast, MDTs had sufficient glucose (Figure 4-2 c,d) after 24 h of culture. Simulation results for oxygen depletion in tissue models revealed that complete tissue anoxia (C = 0.5 µM) was present in the core of tissue slices cultivated in 96-well plates (Figure 4-2 c,e). In the oxygen-permeable microfluidic devices, slices fared better but still suffered hypoxia in the core (C = 1.2 µM) (Figure 4-2 c,e). In MDTs, a mild oxygen depletion was calculated, resulting in a final concentration of 34.4 µM oxygen in the core, which was about eight times greater than the hypoxic threshold (C = 4.6 µM) at its core (Figure 4-2 c,e). Overall, our simulations predicted that MDTs had sufficient glucose and oxygen availability, and that tissue slices would experience both oxygen and glucose deficiencies.

4.5.2 Tumor Models Preserve the Characteristics of the Primary Xenograft Tumor

To verify whether specific features of the primary xenograft tumor were captured in our tumor models, a fraction of the harvested specimen was instantly fixed in formalin and the remaining tumor tissue was used to produce the MDT and tissue slice tumor models. We performed histological and protein expression analyses to compare the primary xenograft tumor with the two tissue sizes (i.e., MDTs and tissue slices) on the day of harvest (day 0). H&E staining showed that the architecture of the primary xenograft tumor, including the varying cell-packing densities, tumoral structures and their spatial relation with stromal components, were preserved (Figure 4-3 a). Furthermore, IF scoring of the tumor cells (i.e., CK8/18 combined with human mitochondria), proliferation (Ki67), and cell death (CC3) showed that the tumor models mirror the epithelial cellularity and viability of the corresponding primary xenograft tissue (Figure 4-3 b–d). These results were consistent for the three different cell lines and suggest that, despite their differences in size, our tumor models represent the characteristics of the primary xenograft tumor, and that the tissue dissection procedure did not significantly alter tissue viability.

4.5.3 Viability and Proliferation Activity in MDTs Are Higher than Tissue Slices over the Culture Period

Changes in cell viability or tissue structure that occur over time in tumor explants may affect the interpretation of chemosensitivity analysis. Therefore, we examined the effect of culture conditions within the tumor models, specifically, variations in the cancer cell compartmentalization, and measured the fraction of intact nuclei (DAPI), apoptotic cells (CC3), and proliferative cells (Ki67) within the tumoral component after 0, 2, 5, 10, and 15 days in culture. H&E staining and tumor-cell-specific biomarkers (i.e., CK8/18 and mito) confirmed that the architecture of the primary tumor and the tumoral components were preserved in the tumor models for up to 15 days in culture (Figure 4-4 a,b and Supplementary Figure 4-6 a). Our observations suggest that MDTs and tissue slices have comparable proliferative activity in culture for a maximum of 5 days; however, tissue slices under both culture conditions had significantly lower proliferation compared to MDTs later in the culture period (Figure 4-4 c). Moreover, we observed that a large number of nuclei were lost in tissue slices that were in culture for 10 days or more, which was also a sign of cellular death by

various pathways [136, 137]. We quantified the number of intact nuclei in the tumoral compartment of the tissue. IF scoring suggested that the area of cells with intact nuclei in the tumoral compartment in MDTs was significantly higher than tissue slices after 10 days in culture (Figure 4-4 d). Furthermore, tumor cell proliferation and viability were generally lower in tissue slices cultured in 96-well plates compared to matched tissue slices in microfluidic devices. Analysis of the apoptotic marker CC3 showed no significant difference between the tumor models that had been in culture for 5 days or more (Figure 4-4 e). The loss of CC3 signal could be due a high level of necrosis in tissue slices. These results are consistent for all the three cell lines used in this study (Figure 4-6). Taken together, our findings suggest that MDTs maintained higher viability and proliferation activity compared to the tissue slices over the culture period.

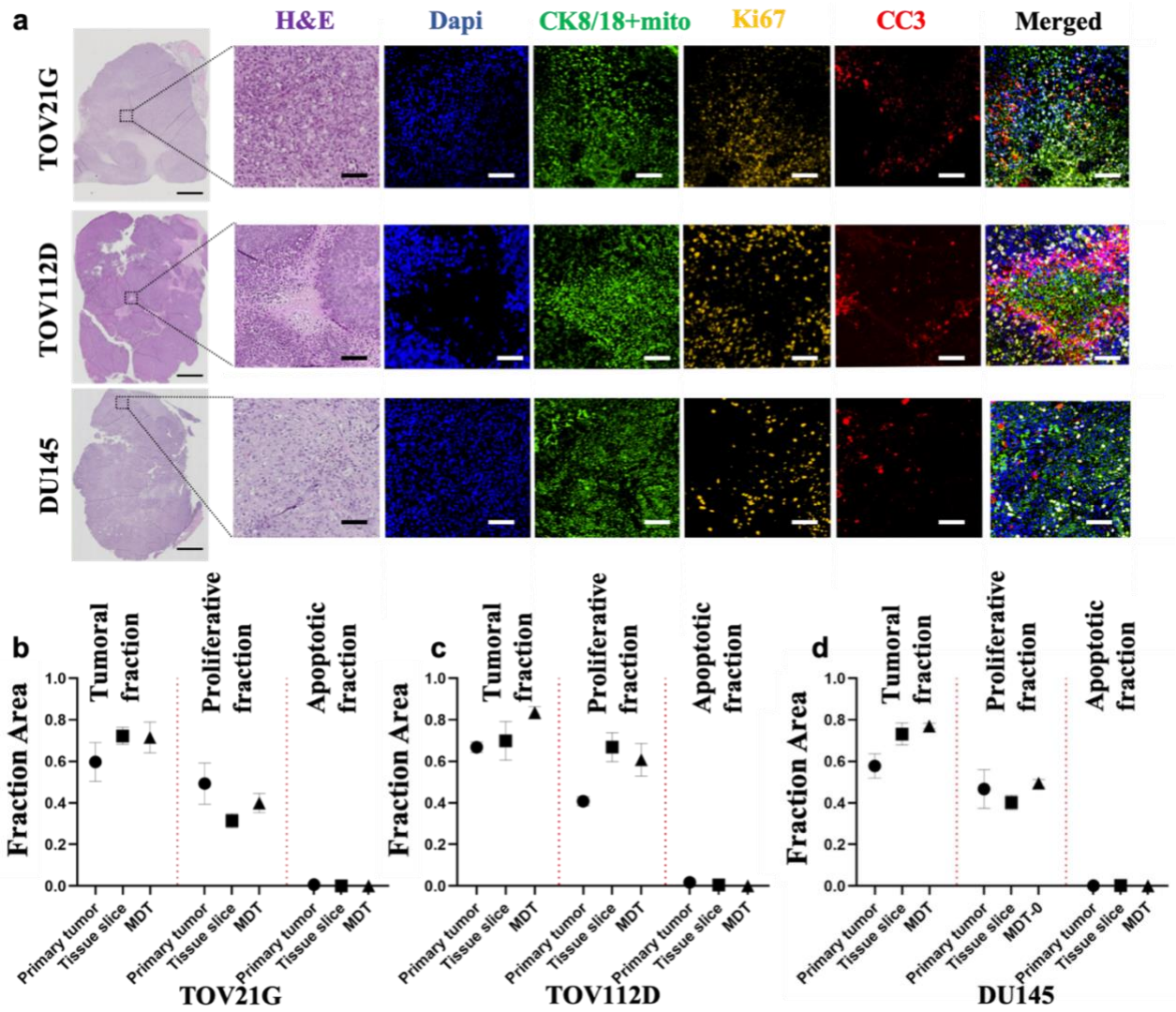

Figure 4-3 Characteristics of primary xenografts and tumor models of ovarian and prostate cancers. (a) Cross sections and staining of the entire primary xenograft tissues of ovarian cancer cell line (TOV21G and TOV112D) and prostate cancer cell line (DU145). Magnified tissue areas stained with H&E, tumor cell marker (CK8/18 + mito), proliferation marker (Ki67), and apoptosis marker (CC3). (b–d) IF scoring of primary xenograft and tumor models of TOV112D (b), TOV21G (c) and DU145 (d). All experiments were performed on the same xenograft as the starting material. Scale bars = 1 mm in whole tissue images and 100 μm in magnified images. Error bars = ±SEM.

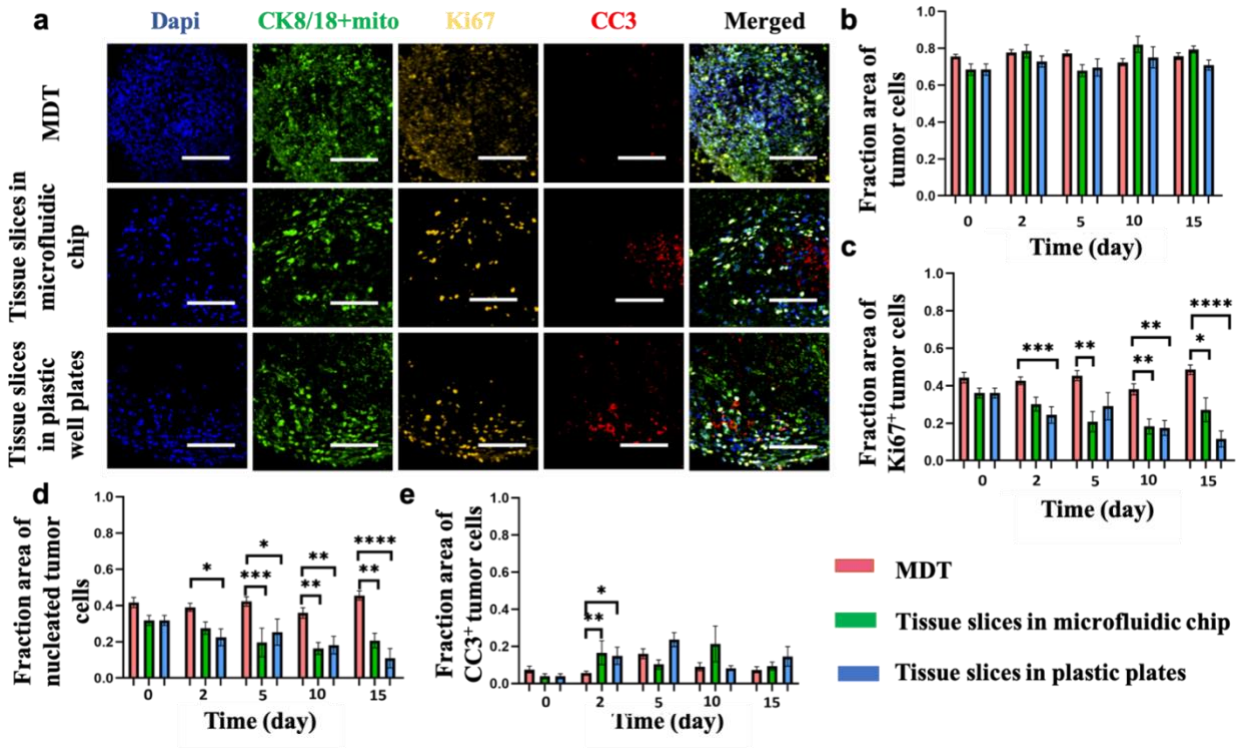

Figure 4-4 Tumor model viability over a 15-day culture period represented by ovarian cancer cell line xenografts (TOV21G). (a) Representative images of tumor models after 10 days in culture stained for nuclei (Dapi), human tumor cells (CK8/18+mito), cell proliferation (Ki67), and cell apoptosis (CC3). (b) IF scoring of tumor models showing stable expression of tumor-cell-specific marker (CK8/18+mito) over the 15-day period. (c-e) IF scoring of tumor models showing higher proliferation (c), larger nucleated area (d), and lower apoptotic cell death (e) in MDTs compared to tissue slices. Scale bars = 100 μm. Error bars = ± SEM. * $p < 0.05$; ** $p < 0.01$; *** $p < 0.0001$; **** $p < 0.00001$.

4.5.4 Elevated Levels of Hypoxia Are Found in Tissue Slices but Not in MDTs under Normoxic Culture Conditions

Ex vivo tissues develop hypoxic cores and subsequent necrosis in a non-perfused TECP, which may alter the drug screening analyses [37]. To date, no study has compared the extent of hypoxia and the hypoxia-associated cell death that occurs in different ex vivo tissue-derived models. To address this, we examined the incidence of hypoxia through carbonic anhydrase-IX (CA-IX) expression, a downstream target of the hypoxia-inducible factor 1-alpha (HIF1A) known to be up-regulated under hypoxic conditions [138-140]. We observed that tissue slices and MDTs had a comparable fraction of hypoxic cells at day 0. The expression level of CA-IX in MDTs was stable and generally lower than in tissue slices at different time points (Figure 4-5 b–d). However, tissue

slices under both culture conditions gained increasing and higher-than-MDT levels of hypoxia for up to 10 days in culture compared to their baseline hypoxic fractions (Figure 4-5 b–d). In particular, higher levels of CA-IX expression were observed in tissue slices cultured in 96-well plates at all the time points. The reduction in CA-IX signal after 10 days in culture may be due to increased cell death at later time points (as shown in Figure 4-5 b-d), resulting in the loss of signal. To further validate the loss of CA-IX signal after 10 days in culture, the H&E and IF staining of CA-IX (Figure 4-5 a) were superimposed for pathological review and revealed that a large proportion of tissue slices in culture for 10 days or more had undergone coagulative necrosis, a form of necrosis mainly caused by hypoxia [137]. Furthermore, even though tissue slices produced from all the three cell lines showed higher levels of hypoxia and necrosis compared to their counterpart MDTs, the difference started earlier on and was more significant in ovarian cancer cell lines (i.e., TOV112D and TOV21G) compared to the prostate cancer cell line (DU145) (Figure 4-5 b–d). This difference may be caused by the different metabolic profiles of cancer cell lines [141]. Furthermore, even though CA IX has been shown to be an excellent endogenous marker [142], it is reported to be less sensitive to prompt changes in the level of oxygenation (i.e., acute hypoxia or reoxygenation) compared to exogenous markers such as Pimonidazole [143, 144]. Responses to exogeneous markers remain to be assessed. However, our transport model seems to match the CA IX results in all circumstances.

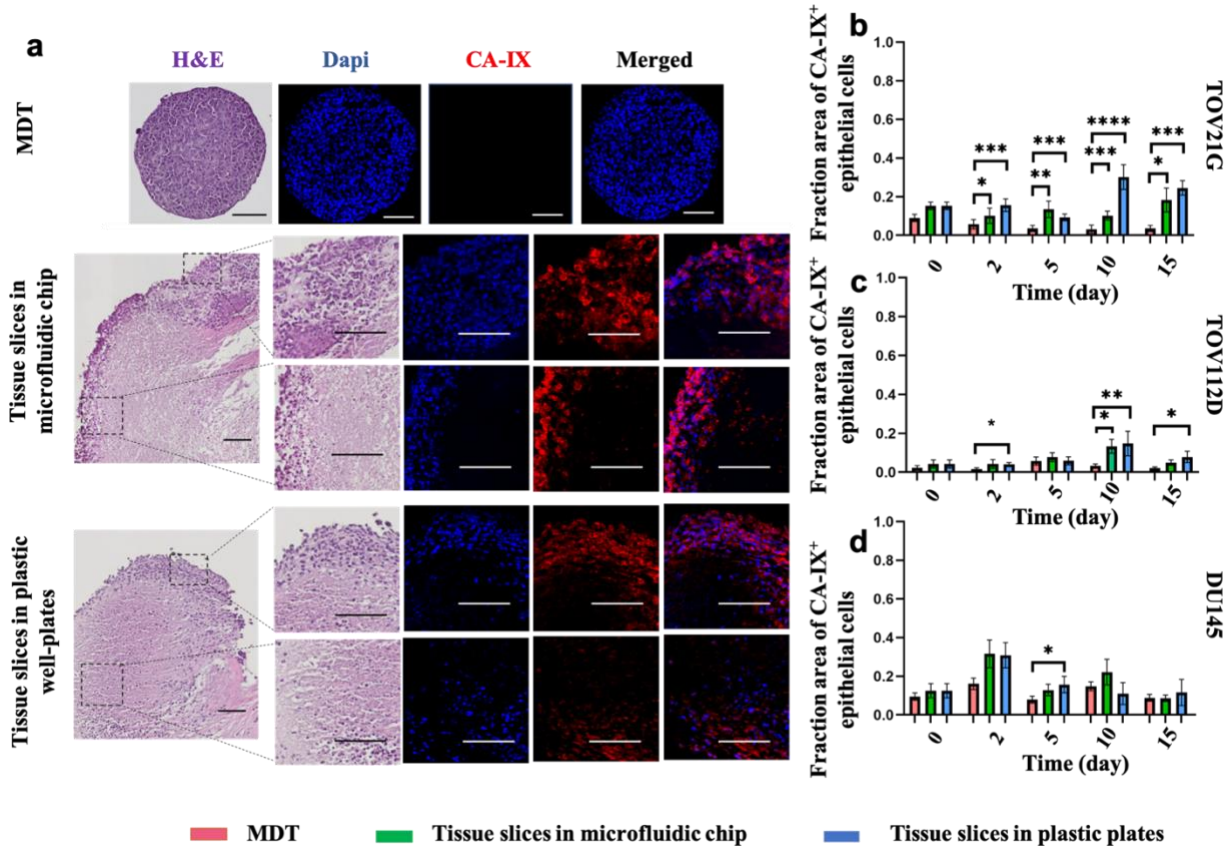

Figure 4-5 Incidence of hypoxia and necrosis in tumor models over a 15-day culture period using ovarian (TOV21G and TOC112D) and prostate (DU145) cancer cell line xenografts. (a) Representative images of tumor models produced from TOV21G after 10 days in culture stained with H&E or following IF with Dapi and CA-IX. H&E staining showed high levels of necrosis in tissue slices. b, c, and d IF scoring of tumor models of showed higher CA-IX expression over the 15-day period in tissue slices compared to MDTs. Results show increasing CA-IX expression until day 10 of culture in tissue slices for TOV21G (b), TOV112D (c), and DU145 (d) xenograft tumor models. Scale bars = 100 µm. Error bars = ± SEM. * $p < 0.05$; ** $p < 0.01$; *** $p < 0.0001$; **** $p < 0.00001$.

4.6 Discussion

The strong drive to improve the predictive power of model systems to maximize the chances of success in the clinic has made TECPs, be they tissue chunks, precision-cut tissue slices, or microdissected tissue, attractive in preclinical settings [19,29,30,51,52]. TECPs are the only model which preserve the native cellular diversity, tumor-stroma compartmentalization, and immune components found in primary animal and human tumors [145]. In addition to the biological aspects [146], there are time and cost gains in choosing TECPs over in vivo animal models. The use of

primary patient tissue requires informed consent from patients, whereas patient tumor specimens are often readily available from surgery or biopsies with minimal or no additional risk for the patient [147]. Moreover, TECPs require fewer resources than in vivo models because many ex vivo tissue samples can be derived from a single specimen to test many drug conditions [5, 148]. Of the two tumor formats and three culture conditions tested, microdissected tissue revealed themselves as the model of choice to maximize viability, throughput, multiplexing of treatment conditions, and overall process efficiency per unit tumor volume. Compared to tissue slices which showed clear signs of necrosis after 3–5 days, MDTs preserved high viability for a period of 15 days, which renders them useful for longer-term drug screening assays. We also found hypoxia, and consequently, hypoxia-induced cell death, to be significantly lower in microdissected tissue compared to tissue slices. Physically, this can be readily explained by the fact that there is a much greater surface-to-volume ratio in a sphere of a certain diameter than in a slice of the same diameter in thickness; thus, oxygen transport is enhanced in spheres [149].

Notably, however, tissue slices preserve larger tissue features in comparison to randomly selected MDTs from a tumor. Cutting tissue to small dimensions limits the use of tumor morphology and phenotypic evolution in treatment response prognoses. However, we have previously assessed the minimum number of MDTs that are required to represent a primary xenografted tumor by a Monte-Carlo simulation, which demonstrated that incorporating 15 or more MDTs in the study would address the question of heterogeneity [51]. Furthermore, randomly selected MDTs may even predict the heterogenous chemotherapeutic responses better than single tissue slices. Regarding hypoxia and oxygen gradients, one could argue that it plays a key role in tumor sensitivity and resistance to treatments [150, 151] and must be present in a preclinical model. In this scenario tissue slice, being severely hypoxic and displaying sharp oxygen gradients may provide better prediction provided they can be kept from dying early in culture. However, the survival of tissues remains a problem which has not been resolved by device perfusion due to the very low tissue porosity and permeability [152, 153], and perfusion techniques only increase the survival marginally [154, 155]. Finally, microdissected tissue, although exhibiting little or no oxygen depletion, could always be used inside hypoxic chambers to test the treatment response as a function of oxygen availability. They form, as such, an interesting alternative to tissue slices [37,

80]. However, the varying and fluctuating levels of oxygenation seen *in vivo* and the subsequent cell responses to such fluctuations cannot be modeled using these *in vitro* assays.

4.7 Conclusions

In this study, we investigated the effect of the tumor tissue size and culture vessel type on *ex vivo* survival by comparing micro-dissected tumor tissue with tissue slices cultured in PDMS-based microfluidic or plastic vessels. We observed that the viability and proliferative capacity of MDTs remained higher than those of tissue slices during the time course of the experiments. Moreover, oxygen-permeable microfluidic devices may improve the survival of tissue slices to some extent, but do not ultimately prevent the nutrient deficiency and cell death commonly associated with tissues of this size. We have shown that necrosis and hypoxia is preventable in MDTs but occurs in tissue slices under both culture conditions. However, tissue slices cultured in oxygen-permeable microfluidic devices have a lower degree of hypoxia compared to those in 96-well plates. Our results provide evidence that the model geometry and culture vessel play an important role in tissue survival and must be carefully selected in designing chemosensitivity assays.

4.8 Supplementary Materials

The following are available online at www.mdpi.com/xxx/s1, Figure S1: Tumor model viability over a 15-day culture period represented by ovarian (TOV112D) and prostate (DU145) cancer cell line xenograft models. Tables S1: Dimensions of devices; Table S2: Tissue uptake parameters and diffusion properties.

Supplementary materials are also provided here.

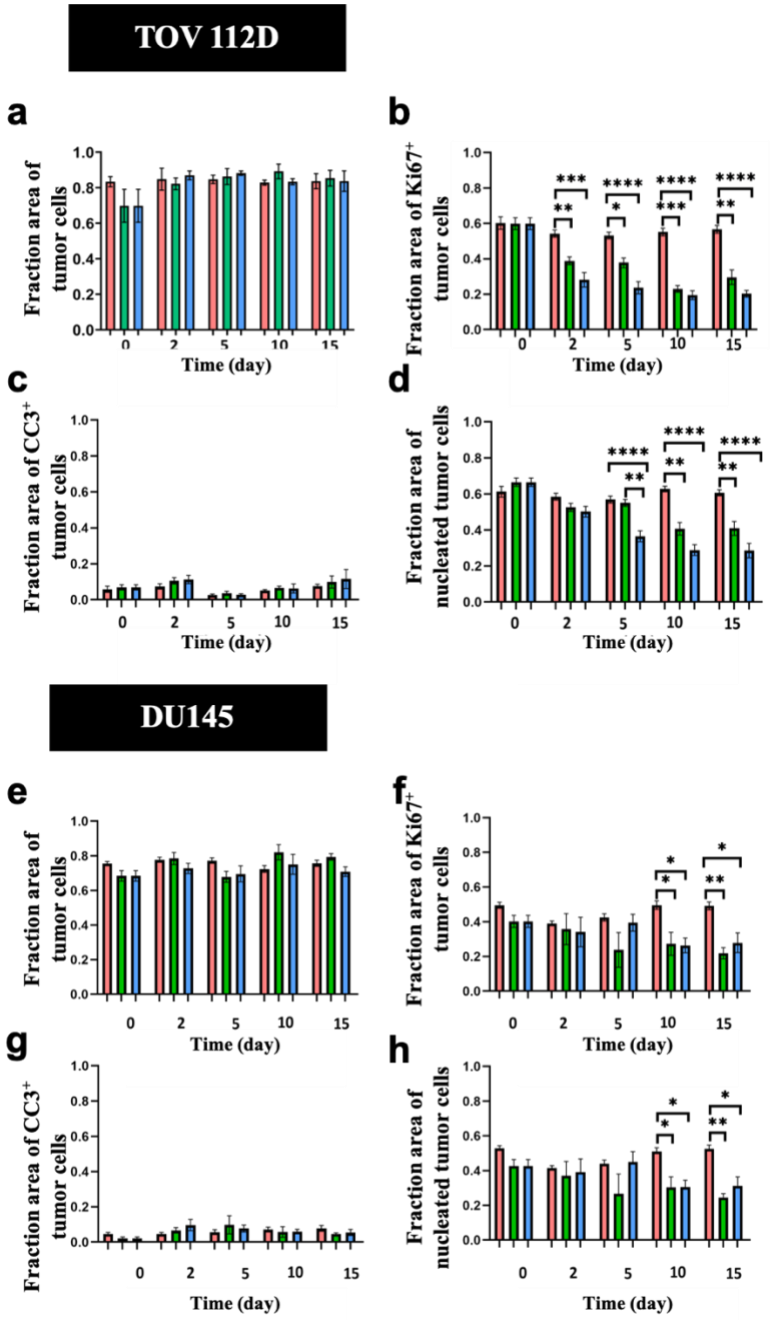

Figure 4-6 IF scoring of tumor model viability over a 15-day culture period represented by ovarian (TOV21G) and prostate (DU145) cancer cell line xenografts. tumor models showing comparable tumor cell compartment (a, e), higher proliferation (b, f), larger nucleated area (d, h), and varying apoptotic cell death (c, g) in MDTs compared to tissue slices. Scale bars = 100 μm. Error bars = ± SEM. *p<0.05; **p<0.01; ***p < 0.0001; ****p < 0.00001

Table 4-1 dimensions of devices

Parameter	value		
Channel height (mm)	MDT chip	0.9	
	Tissue slice chip	Top	0.9
		Bottom	1.1
Channel width (mm)	MDT chip	1.1	
	Tissue slice chip	Top	1.1
		Bottom	1.1
Channel length (mm)	MDT chip	6	
	Tissue slice chip	Top	23
		Bottom	18
Tissue diameter (mm)	MDT	0.5	
	Tissue slice	3	
Tissue thickness (mm)	0.35		
Tissue chamber dimension (mm)	MDT well (cubical)	0.7	
	Tissue slice (cylindrical)	Diameter	7
		Height	2.5
	96 well-plate (Corning ®-cylindrical)	Diameter	6.4
		Height	17

Table 4-2 tissue uptake parameters and diffusion properties

Parameter	**value**		
Diffusion constant of glucose (cm^2/s)	Tissue	$2.7x10^{-6}$	
	Medium	$9.27x10^{-5}$	
Diffusion constant of oxygen (cm^2/s)	Tissue	$1.8x10^{-5}$	
	Medium	$2.6x10^{-5}$	
	PDMS	$3.4x10^{-5}$	
Saturation concentration (mM)	Oxygen	Tissue	1.02
		medium	0.21
		PDMS	1.43
	Glucose	11	
Partition coefficient	PDMS-Medium	0.15	
	Medium-Tissue	4.8	
Maximum cellular uptake rate (mM/S)	Oxygen	2.07	
	Glucose	1.09	
Michaelis-Menten constant (mM)	Oxygen	$4.63x10^{-3}$	
	Glucose	$4x10^{-2}$	

4.9 Author Contributions

Conceptualization: D.D., B.P., E.C., A.-M.M.-M. and T.G.; Data curation, D.D., K.S. and L.C.; Formal analysis, D.D. and L.C.; Funding acquisition, A.-M.M.-M. and T.G.; Investigation, D.D., A.-M.M.-M. and T.G.; Methodology, D.D., K.S., J.K.-D., B.P., E.C., A.-M.M.-M. and T.G.; Project administration, A.-M.M.-M. and T.G.; Resources: A.-M.M.-M. and T.G.; Supervision, A.-M.M.-M. and T.G.; Validation, D.D., K.S., L.C., A.S.R., B.P., E.C., A.-M.M.-M. and T.G.; Visualization, D.D., and A.S.R.; Writing—original draft, D.D., K.S. and T.G.; Writing—review and editing, L.C., J.K.-D., A.S.R., B.P., E.C., A.-M.M.-M. and T.G. All authors have read and agreed to the published version of the manuscript.

4.10 Funding

D.D. and K.S. received bursaries from the Canderel fund of the Institut du cancer de Montréal. A.-M.M.-M and T.G. are researchers of CRCHUM, which receives support from the Fond de recherche Québec—Santé (FRQS). This research was conducted as part of the TransMedTech Institute's activities and thanks, in part, to funding from the Canada First Research Excellence Fund. The research was supported with grants from the Canadian Cancer Society Research Institute (CCSRI), the Cancer Research Society (CRS) partnered with Ovarian Cancer Canada (OCC), the Prostate Cancer Canada (PCC), the Canadian Urological Oncology Group (CUOG), and the National Science and Engineering Research Council of Canada (NSERC). The ovarian cancer cell lines used in this study were provided by the CRCHUM ovarian tumor bank, which is supported by OCC and by the Banque de tissus et de données of the Réseau de recherche sur le cancer of the FRQS, affiliated with the Canadian Tumor Repository Network (CTRNet).

4.11 Institutional Review Board Statement

All animal procedures were performed in accordance with the Guidelines for the Care and Use of Laboratory Animals of the Canadian Council of Animal Care (CCAC) and approved by the Institutional Animal care and ethics Committee, i.e., the Comité Institutionnel de Protection des Animaux (CIPA) (protocol code C18010AMMs and date of approval 2018-03-29, 3rd renewal approved 2021-03-25).

4.12 Informed Consent Statement

Not applicable.

4.13 Data Availability Statement

The data associated with the raw experimental data have been deposited in the Scholar Portal Dataverse: Microdissected tissue vs. tissue slices—A comparative study of two tumor explant models cultured on-chip and off-chip. (https://doi.org/10.5683/SP2/KNRWND, uploaded on 05/08/2021). All other data are contained in the article and supplementary material.

4.14 Acknowledgments

We acknowledge Kim Leclerc-Desaulniers for technical assistance. We thank the Microfluidic Core Facility of the CRCHUM for performing tissue dissection. We thank Liliane Meunier and Véronique Barrès of the Molecular Pathology core facility of the CRCHUM for performing the paraffin block sectioning and slide scanning. We thank Dominique Trudel and Feryel Azzi for pathological evaluation of samples. We acknowledge Jacqueline Chung for manuscript editing. T.G. acknowledges CMC Microsystems.

4.15 Conflicts of Interest

T.G. is the co-founder and Chief Technological Officer of MISO Chip Inc., a company operating in the field of ex vivo tissue culture.

CHAPTER 5 ARTICLE 2: PIXELATED MICROFLUIDICS FOR DRUG SCREENING ON TUMOUR SPHEROIDS AND EX VIVO MICRODISSECTED PRIMARY TISSUE

Dina Dorrigiv [1,2], Pierre Alexandre Goyette [2,4], Amélie St-Georges-Robillard [1,4], Anne-Marie Mes-Masson [1,3,*] and Thomas Gervais [1,2,4,*]

[1] Centre de recherche du Centre hospitalier de l'Université de Montréal, (CRCHUM) and Institut du cancer de Montréal, Montreal, QC H2X 0A9, Canada; dina.dorrigiv@polymtl.ca (D.D.); pierre.alexandre.goyette@gmail.com (P.-A.G.); amelie.st-georges-robillard@polymtl.ca (A.S.R.); anne-marie.mes-masson@umontreal.ca (A.-M.M.-M.); thomas.gervais@polymtl.ca (T.G.);

[2] Institute of Biomedical Engineering Polytechnique Montréal, Montreal, QC H3T 1J4, Canada

[3] Department of Medicine, Université de Montréal, Montreal, QC H3T 1J4, Canada

[4] Department of Engineering Physics, Polytechnique Montréal, Montreal, QC H3T 1J4, Canada

* Correspondence: anne-marie.mes-masson@umontral.ca; Tel:+1-(514)-890-8000 (ext. 25496); thomas.gervais@polymtl.ca; Tel.: +1-(514)-340-4711 (ext. 3752).

5.1 Background information

Submitted article 2 is presented in this chapter and introduces an open-space microfluidic system for high throughput drug screening on 3D tumour models, specifically, spheroids and primary tumour tissue explants. This article gives background information about tumour models, with a special focus on 3D tumour model systems. Then, it provides information on open-space microfluidics and details a methodology for localized reagent delivery to tumour models using a microfluidic device, the PCD. In the results section, multiple preliminary experiments to provide proof of concept for applications of the PCD are explained.

My contribution to this article is 65% of the work. I performed numerical simulations for transport of species in and around MDTs. I performed troubleshooting of the hardware parts. I developed the experimental workflow. I performed the tissue preparation and staining experiments, established the OCT embedding protocol, and conducted the image analysis. I wrote the article. P.-A.G. designed, fabricated, and modified the hardware parts (PCDs, manifolds, microwell arrays)

for the PCD drug screening platform. P.-A.G. developed the PID controller code and oversaw the experiments at the beginning. A.S.R. oversaw the experiments, supervised the microscopy and mage J image analysis, and helped in the preparation of the figures. A.-M.M.-M. and T.G. provided support and supervised the research. All authors reviewed the article. The article was submitted to *biorxiv.org* on October 7th 2022 and will be submitted to *Lab on a Chip* soon after.

5.2 Abstract

Anti-cancer drugs have the lowest success rate of approval in drug development programs. Thus, preclinical assays that closely predict the clinical responses to drugs are of utmost importance in both clinical oncology and pharmaceutical research. 3D tumour models preserve the tumoural architecture and are cost-, labour-, and time-efficient. However, the short-term longevity, limited throughput, and limitations to live imaging of these models have so far driven researchers towards simpler, less realistic tumour models such as monolayer cell cultures. Here, we present a static open-space microfluidic drug screening platform that enables the formation, culture, and multiplexed delivery of several reagents to various 3D tumour models, namely cancer cell line spheroids and ex vivo primary tumour fragments. Our platform utilizes an open-space microfluidic technology, a pixelated chemical display, which creates fluidic "pixels" of biochemical reagents that stream over tumour models in a contact-free fashion. Up to 9 different treatment conditions can be tested over 144 samples in a single experiment. We provide a proof-of-concept application by staining fixed and live tumour models with multiple cellular dyes. Furthermore, we demonstrate that the various responses of the tumour models to biological stimuli can be assessed using the proposed drug screening platform. The platform is amenable to various 3D tumour models, such as tumour organoids. Upscaling the microfluidic platform to larger areas can lead to higher throughputs, and thus will have a significant impact on developing treatments for cancer.

5.3 Introduction

A major impediment to cancer treatment is predicting the response of patients to anti-cancer drugs as they have an extremely low clinical approval rate in drug development programs. [4, 156] Improving preclinical models to predict the response of patients to treatments can improve drug precision and effectiveness, spare patients from exposure to unnecessary toxicities, accelerate the

drug development process, and ultimately reduce healthcare costs. [5],[6] Various predictive preclinical tumour models are available to researchers. Preclinical tumour models include 2D monolayer cultures of cancer cells, 3D tumour models such as cancer cell line spheroids, tumour organoids, ex vivo cultured tumour fragments, and in vivo models, from the simplest to the most complex, respectively. Monolayer cell cultures are easy to replicate but lack the 3D tumour structure and the interactions between the cancer cells and the tumour microenvironment. [157] In vivo models are the gold standard of preclinical models, but their production is time-consuming and labour intensive. They may also fail to predict the clinical efficacy of drugs due to species differences. [63] 3D tumour models can bridge the gap between 2D and in vivo models: unlike 2D monolayers, 3D tumour models mimic the tumoral architecture and are human-derived and easier to work with than in vivo models. [7, 12, 42, 65, 111, 118] Three main groups of 3D tumour models exist. In order of increasing complexity and in vivo relevance, they are cell line spheroids, tumour organoids, and ex vivo cultured tumour explants. They can be selected according to the purpose and requirements of a given study. [65] [158] Drawbacks of the various 3D tumour models include limitations of live imaging and interfacing with histopathology, and the generally low throughput and low viability of tissue, especially for ex vivo tumour explants. The most advanced live imaging methods, such as confocal and multiphoton microscopy, are well known to have severe limitations in 3D biology, notably their limited light penetration depth in live tissue and cost. [159] In addition, the universally recognized standard for primary tissue-based clinical decision-making is histopathology [i.e., the practice of preserving tumour tissues in paraffin or a freezing medium and dissecting them into thin (5-10 µm) slices]. [160] To overcome the limitation of live imaging and increase clinical relevance, in particular taking into account routine clinical pathology, it would be advantageous for 3D tumour models to be compatible with standard histopathology practice. Various techniques have been developed for culture and drug screening on 3D tumour models and preparing them for histopathological analyses. The most conventional technique is culturing tumour models in plastic well plates. Samples are subjected to reagents manually or using robotic liquid handlers in wells. Sample manipulation using pipettes, whether manually or using pipetting robots, imposes risks such as aspirating or shearing the sample while changing the medium. In addition, removing the samples out of the wells for further histopathology processing is tedious. Moreover, plastic well plates are not optimal for preserving the viability and metabolic activity of

fragile 3D tumour models, such as ex vivo tumour explants. Our group has previously studied the ex vivo survival of tumour tissue explants and has shown that tumour tissue slices cultured in non-perfused well plates start to die in two days due to insufficient oxygen supply. [17] Microfluidics can palliate this problem by introducing chips for high throughput processing of micron-sized tumour models. [51, 157] The drawback of most microfluidic chips is that they require sample entrapment in closed microchannels, and are not amenable to surface-based work environments such as Petri dishes. [95] Perifusion-based microfluidic devices have been developed to preserve the viability of larger tissue explants over a longer time. [15, 83] It is important to differentiate between perfusion and perifusion. [124] Tumour tissues are dense structures with permeabilities that are orders of magnitude below the permeability of flow channels. [161, 162] Creating convective flow inside tumour models (i.e., perfusion) is not feasible unless flow around them is prevented. In most cases, when samples are small (< 1 mm), perifusion is sufficient to avoid any form of starvation, anoxia and necrosis in tissue. [54] Perifusion-based devices, while presenting a technical breakthrough, have extremely limited throughputs. [163, 164]

New culture platforms that can improve survival and high throughput drug screening on 3D tumour models, while remaining fully compatible with gold standard tissue analysis, are promising avenues to improve pre-clinical drug testing. In this article, we present a platform that bridges the concepts behind well plates and perifusion-based microfluidics. The platform uses open-space microfluidic laminar flow confinement to stream reagents within self-contained fluidic pixels in which a large number of various 3D tumour models can be placed. The pixels reagent content can be modulated over time with specific frequencies. Open-space microfluidic systems are channel-free and contact-free fluidic processors that deliver reagents directly over the sample. [19] Pioneering open-space microfluidic systems have been used for various purposes including single cell analysis, [165-167] perifusion-based culture of brain slices, [168] localized immunohistochemistry, [169] and imaging mass spectrometry. [170] The open-space microfluidics system here, which we call the Pixelated Chemical Display (PCD), has been used for various processes over flat 2D surfaces, such as immunoassays. [98] Here, for the first time, we have utilized the PCD for multiplexed reagent screening over 3D tumour models. To this end, we investigated the stability of the PCD when working over a large number of 3D biological samples deposited in a custom-built microwells array. To provide proof of concept evidence for the

applicability of the platform across a whole spectrum of 3D tumour models, we first worked with the simplest 3D tumour models, spheroids, and later with the most complex 3D models, ex vivo tumour explants. Using sequences of cellular dyes, we performed crosstalk-free tissue staining on both 3D tumour models. We have also adapted our previously published paraffin-embedding lithography to transfer all samples simultaneously to a paraffin or optimal cutting temperature (OCT) compound block while preserving their spatial orientation. Finally, we investigate the feasibility of using this method to study signalling pathways and cell fate in microdissected tumour tissues. The opportunities and challenges of the method are discussed with respect to competing methodologies such as robotic liquid handlers and closed microfluidic chips.

5.4 Results and discussion

5.4.1 Design and fabrication of the pixelated chemical display drug screening platform

The PCD operates based on the hydrodynamic confinement of a stream of fluid in another miscible fluid through recirculation. [18, 95] It comprises a blunt tip with multiple apertures and is installed in close vicinity of an immersed substrate. The PCD and the immersed substrate form a Hele-Shaw cell, a quasi-2D flow that can be precisely computed using potential flow theory. [101, 171] During its operation over the substrate, fluid streams are expelled through the injection apertures and re-collected through the aspiration apertures. As a result of the convective recirculation, fluid streams leaving the PCD form well-defined patterns over the substrate without mixing. [100] Fluidic "pixels" are created when a fluid stream injected above the surface is confined by neighbouring identical fluid streams, forming a repeating flow unit with translational symmetries. [20] By modulating the design of the PCDs and the injection and aspiration flow rates, different sizes, numbers, and patterns of fluidic pixels can be achieved. Our group has previously demonstrated theoretically and experimentally the operation of up to 144 fluidic pixels (12 x 12) and demonstrated that the number of active pixels and their reagent content can be modulated without altering the stability of the system. [18],[20] Based on our previous findings, we adapted a 9-pixel PCD for tissue culture and drug screening. Each pixel is 36 mm2 (6 x 6 mm2) such that the resulting array fits within a paraffin cassette for later embedding (Figure 5-1 a,b). For this work,

each group of 3 pixels was connected to the same reagent flask to create experimental triplicates. Three different conditions were tested in each experiment. We designed and micromachined a microwell array to keep the tumour models in place at the PCD interface during the experiment. The microwell array features 9 groups of 16 microwells for a total of 144 microwells on a polymethylmethacrylate (PMMA) slab (Figure 5-1 b). Each microwell group is covered by an independent fluidic pixel when the PCD is aligned over the microwell array. The PMMA slab also features a flat surface on the side of the microwell array to safely install the PCD and test its operation prior to biological experiments over tumour models (Figure 5-1 b). 3D printed holder assembly parts (Figure 5-1 c) were fabricated to securely hold the PCD and the PMMA slab together, to stabilize the PCD, and ensure its alignment over the microwell array (Figure 5-1 d).

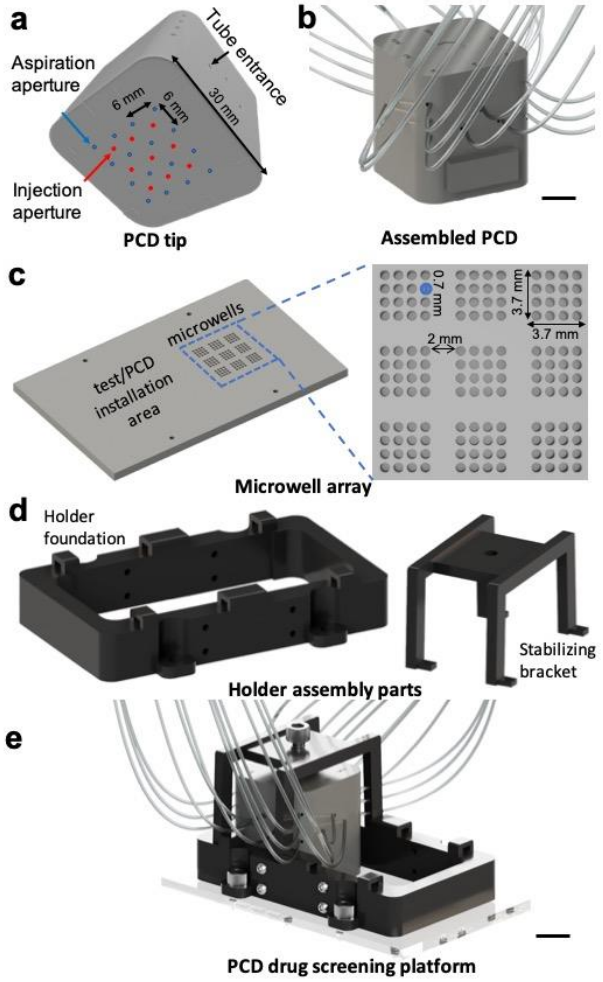

Figure 5-1 PCD components. a) PCD tip and b) tubes connected to the PCD, c) micromachined microwell array featuring 144 microwells, d) holder assembly parts: holder foundation (left) and a bracket to stabilize the PCD once installed over the microwells (right), and e) schematic of the fully assembled PCD drug screening platform Scale bar= 1 cm

5.4.2 Pressure pump operated fluidic lines

Syringe pumps were previously used to operate PCDs [20, 98] as they offer precise and simple control, and are commonly used in microfluidic systems. [172] However, syringe pumps, even high precision ones, have relatively high minimum working flow rates, and require frequent recharging of reagents in syringes. [173] To avoid these limitations, we used pressure pumps in this work. Pressure pumps enable pressurizing of a wide range of flask sizes (from microliters to litres capacity) and thus allow for longer-run experiments. More importantly, a single pressure pump can

be used to pressurize several reagent flasks, whereas each syringe pump is dedicated to a single syringe. Different flow rates can be achieved in different fluidic lines pressurized by one pump by controlling the hydraulic resistance of the tubes (i.e., by using different sizes of tubing). In this work, two pressure pumps were used to operate the PCD: one for the injection groups and one for the aspiration. Similar to our previous works, we used 3D-printed manifolds to deliver fluids from one pump into all the pixels sharing the same reagents. [20] Tubes connecting the manifolds to the PCD were used as precision hydraulic resistors to match the flow rate from all apertures. Four precision flowmeters were installed on the fluidic lines to measure the flow rate for the four injection and aspiration groups. A closed-loop control system with a feedback loop control (a.k.a., proportional–integral–derivative [PID] controller) was developed to control the pressure-driven flows. The PID controller estimates the deviation between the target and the measured injection flow rates and regulates the pressure to reduce deviations in real-time. Moreover, we added medical three-way stopcock valves on the fluidic lines to enable on-demand reagent switching between the various reagent flasks (e.g., priming reagents such as ethanol and isopropanol, culture medium, biochemicals, and cellular dyes). Switch valves enable us to add or remove reagent flasks without interrupting the system (Figure 5-7). We refer to the PCD, microwell array, pumps, and fluidic lines complex as the PCD drug screening platform.

5.4.3 Finite element simulations

Our group has previously studied the mass transport, stability, and reconfigurability of PCDs using 2D convection-diffusion finite-element methods and has demonstrated that stochastic errors such as minor pressure, flowrate changes, or clogging of one aperture do not impact the PCD's operation. [20] Here, we conducted numerical simulations to gain insight into the quality, crosstalk, and stability of fluidic pixels when the PCD is working over 3D structures, such as tumour models. We added a secondary set of simulations to predict the convective-diffusive transport of diluted species in microwells and inside tumour models. We used experimental geometrical and operational parameters: flow rates were selected based on the minimum flow rate that we could achieve with the pressure pumps to have sharp and stable pixels while minimizing reagent consumption. To visualize the pixel formation and crosstalk, we modelled a PCD that functioned in a chequerboard pattern: five injection apertures inject a concentrated solution, and four injection

apertures inject a zero-concentration solution (Figure 5-2 a). Simulation results suggest that the presence of microwells and tumour models does not disturb the pixel shapes, similar to working over flat impermeable surfaces [(Figure 5-2 a(i)]: stable crosstalk-free pixels are formed over the microwell array [(Figure 5-2 a(ii)]. Moreover, we investigated the impact of the tumour model positioning in microwells on fluidic pixels. We modelled a scenario in which random tumour models were partially sticking out of the wells and touched the PCD. We observed that regardless of the tumour model positioning in the well, the pixels are stable ((Figure 5-2 b). We then evaluated the shear stress induced on the cells by the flow and observed that the maximum shear stress imposed by the PCD is 0.0021 Pa, which is 500 times less than the physiologically safe shear stress regime for sensitive cells (~1 Pa). [174] By visualizing velocity fields, we observed that there is no convective flow inside the tumour models [(Figure 5-2 c], showing the diffusion dominant transfer of species inside tumour models. Next, we measured the amount of time required to reach a constant concentration of injected species inside the tumour models with zero initial concentration. Simulation results predict that the system reaches a steady state in less than 20 minutes. The time to reach this state was set as the transition time in the experiments; upon the change of a reagent flask, reagents were streamed for 20 minutes before starting the experiment countdown. Overall, our simulations predict that the PCD provides excellent control over the fluidic pixels, and locally perifuses the tumour models. Finally, to model the spheroid formation assay (i.e., the static culture of 500 µm-tumour models in the microwell array), we used passive diffusion and Michaelis-Menten kinetics parameters for oxygen and glucose consumption by cancer cell lines. [54] The numerical model predicts that spheroids have access to sufficient levels of oxygen and glucose over 24 hours (i.e., the typical medium refreshment interval) ((Figure 5-2 d).

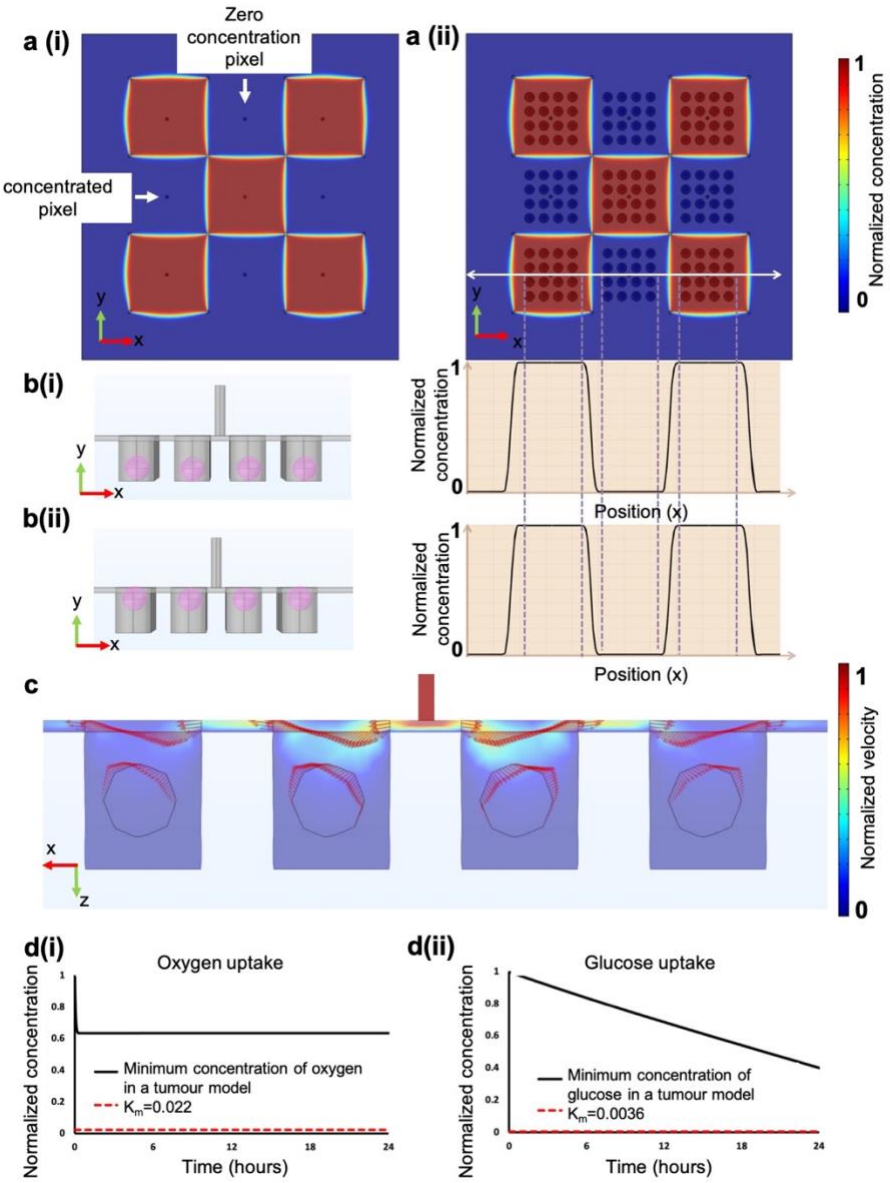

Figure 5-2 Numerical simulations of the PCD operation over tumour models. Figures are simulation data and produced using COMSOL Multiphysics. a) Fluidic pixels formed over a flat surface a(i) are comparable to those formed over the microwell array a(ii); b) The positioning of the MDTs or spheroids in the microwells does not impact the operation of the PCD; c arrow plots to visualize the distribution of velocity field in the numerical model suggest the lack of free flow inside tumour models; d(i) Oxygen and d(ii) glucose consumption profile in tumour models cultured in the microwell array without perifusion. Tissues of up to 500 µm in diameter can survive in microwells for over 24 hours, as the oxygen and glucose concentration stays above typical Km values for cancer cells. Concentrations of oxygen and glucose in sub-figure (d) are normalized by the saturation concentration of oxygen (0.21 mM) and glucose (11 mM) in tumour models.

5.4.4 High-throughput formation of cancer cell line spheroids is possible in the microwell array

Cancer cell line spheroids are self-formed spherical cell aggregates formed from one or more cancer cell lines. [36] Spheroids are the simplest and most often used 3D tumour models. The commonly used technique to form spheroids is to seed a high-density suspension of cells on a non-adherent surface. Spheroids will form if the cell-cell adhesion forces are greater than the cell-surface adhesion forces. [175] To meet our claim about the amenability of PCD to work with different tumour models, we optimized the surface modification technique and cell seeding densities based on previous findings to form spheroids directly in the microwell array. [176-178] We further formed spheroids from squamous cell carcinoma and colorectal cancer cell lines to test the practicality of the approach. Figure 5-3 shows that we can form uniform spheroids in the microwell array in 48 hours. Spheroids were later subjected to the PCD for dynamic cellular staining.

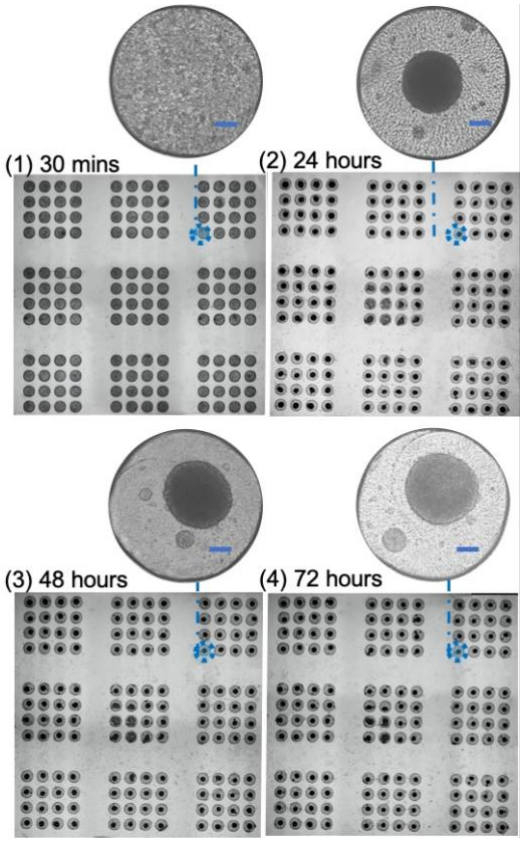

Figure 5-3 Formation of uniform and compact spheroids of colon cancer cell line HCT-116 in the microwell array over time. Scale bar = 100 µm

5.4.5 PCD creates distinct, crosstalk-free fluidic pixels over the tumour models

To test the performance, stability, and precision of the drug screening platform, we used it to stain spheroids formed in the microwell array. Two phases of reagent streaming over spheroids were used to test the stability of the PCD over subsequent changes of reagents, and to verify its potential for dynamic reagent screening. The PCD streamed culture medium for 20 minutes over the microwell array containing spheroids. Subsequently and without interrupting the system, the culture medium was replaced by three cellular dyes that were streamed in the 9 pixels of the PCD for 2 hours. We then switched the reagent flasks, subjecting spheroids to a second dye. The second part of reagent streaming went on for 3 hours, and cellular dyes were swapped with PBS 1X to purge the dyes (Figure 5-4 a). Spheroids were imaged using fluorescence microscopy. The results show crosstalk-free staining of spheroids with the colours of interest (Figure 5-4 b). We further assessed the fluorescent intensity (FI) per unit area of spheroids for different channels and demonstrated that spheroids subjected to a dye for 3 hours have a higher FI than spheroids subjected to the same dye for 2 hours (Figure 5-4 c).

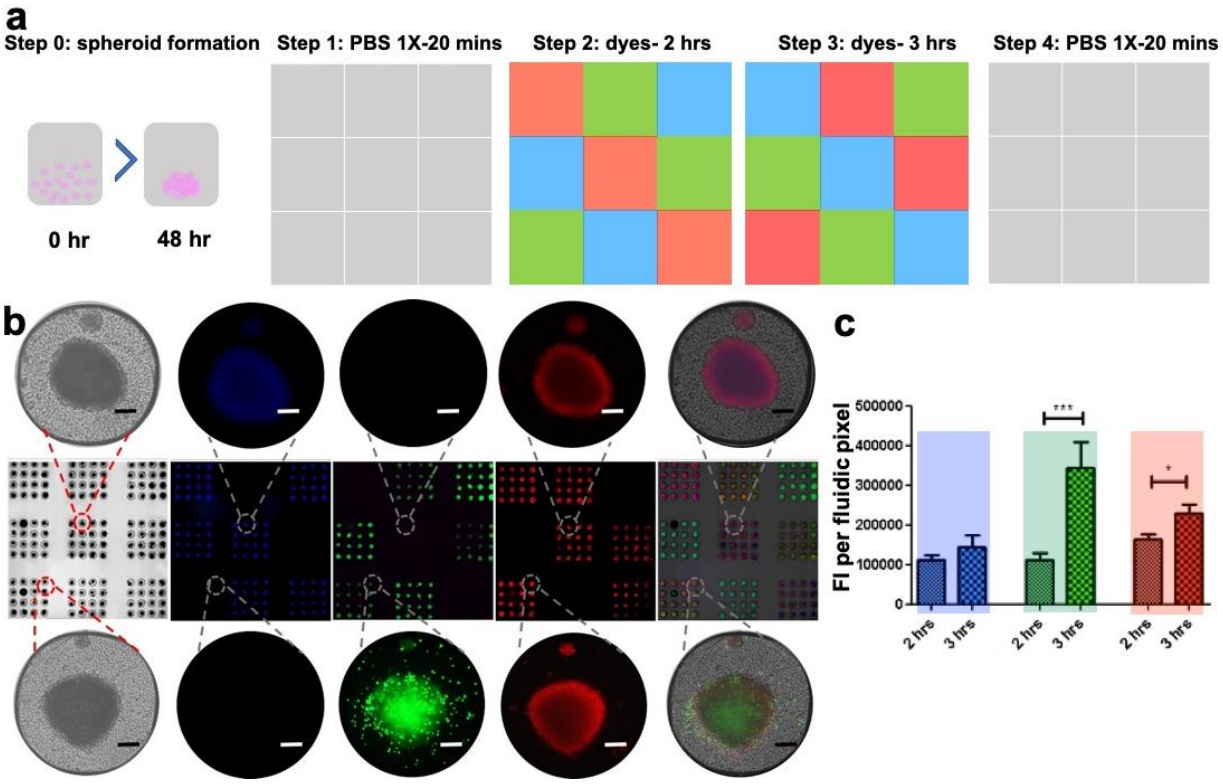

Figure 5-4 Crosstalk-free multiplexed staining of tumour models using the PCD. The PCD is used to stain HCT-116 spheroids 48 hours after cell seeding. Spheroids are exposed spheroids are subjected to 3 different cellular dyes streaming at the 9 pixels of the PCD for two hours. Then, the reagents were switched so that a different dye was streamed at each pixel for 3 hours. Spheroids were imaged after rinsing out the dyes using an inverted fluorescent microscope. The staining protocol (A), micrograph of stained spheroids (b), and quantification of Fluorescent Intensity (FI) of spheroids for each channel. Longer incubation with fluorophores results in higher fluorescent emission of spheroids. Blue: Hoechst, green: Celltracker™ Green, red: Celltracker™ Red. Scale bar = 100 µm.

5.4.6 Tumour tissue microarray

Fluorescence microscopy captured the mean fluorescence emission of tumour model structures but did not allow us to examine the distribution of reagents throughout the tumour models. To demonstrate this capability in our system, we developed a methodology to take tumour models out of the microwells and directly embed them in a freezing medium or paraffin. It is also essential to keep the arrangement and orientation of tumour models as they were in the microwells to be able to correlate them with the treatment conditions (in each fluidic pixel) that they have been exposed to. For this, we adapted a technique previously described by Jones and Calabresi [179] to first embed the tumour models in a hydrogel in their microwells. Then, the hydrogel block containing the tumour models is de-moulded from the microwell array and re-embedded in the OCT compound. The OCT blocks were then sectioned into 5 µm-thick slices, and slices were used for further histopathological staining and analysis (Figure 5-5). It is noteworthy that this protocol makes the PCD drug screening platform compatible with standard histopathology practice. Figure 5-8 shows cryosections of MDTs that were stained using the PCD for different duration and underwent the agarose and OCT embedding protocol.

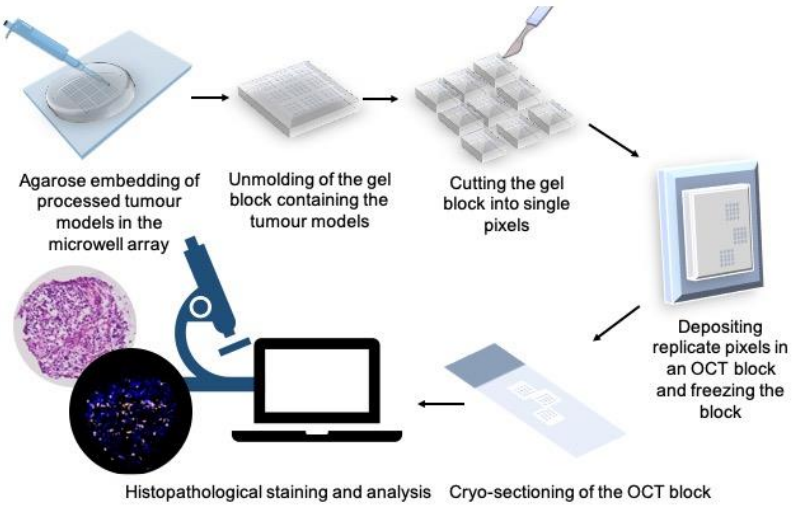

Figure 5-5 The protocol developed to remove the tumour models from microwells while preserving their address for further histopathology analyses. Tumour models are embedded in agarose and removed from the microwell array. Microwell groups exposed to different fluidic pixels are separated, and tumour models that have been subjected to the same treatment condition are regrouped in an OCT block. OCT blocks are sectioned to 5 µm sections to visualize the tissue core and for further immunostaining.

5.4.7 The PCD drug screening platform enables the tracking of biological responses in tumour models

After demonstrating that the PCD platform is capable of forming crosstalk-free fluidic pixels over various tumour models, we sought to examine the ability of the technology to follow various biological responses in tumour models. For this, we assessed the response of Nuclear factor kappa B (NF-κB) transcription factors in MDTs to a cytokine (tumour necrosis factor [TNF]) stimulation. The NF-κB transcription factor is reported to play a role in tumour angiogenesis and invasiveness and is a possible target to improve the clinical diagnosis and prognosis. [180] NF-κB resides in the cytoplasm of every cell and is translocated to the nucleus when activated by various stimuli such as cytokines, viruses, and free radicals. [181] TNF is a proinflammatory cytokine that is known to activate NF-κB. [182] Real-time monitoring of nuclear translocation of Nf-κB proteins in previous studies revealed a rapid increase in the nuclear signal of sub-units of NF-κB that peaks a few minutes after the exposure, followed by a decline in the nuclear signal of proteins. [183, 184] With this in mind, we used the PCD to expose MDTs produced from cell line xenografts to TNF for 0, 30 minutes, or 240 minutes by progressively switching on TNF delivery in certain pixels by replacing neutral culture medium with a TNF solution. We evaluated the nuclear signal of p65, an NF-κB subunit, by immunofluorescence (IF) staining. As expected, the quantification of the IF staining showed an increase in the nuclear signal of p65 in MDTs that have been subjected to TNF stimulus for 30 minutes compared to the control group. The p65 nuclear signal dropped in the MDTs that were treated for 240 minutes (Figure 5-6). This is also expected since p65 translocation is known to be reversible. [182] To further validate the results, we performed parallel experiments on MDTs produced from the same xenograft that were cultured on chips. The on-chip MDT treatment experiment is a repeat of a protocol previously published by our laboratory for other cell line xenograft MDTs. [51] Similar responses were also observed in MDTs on chips (Figure 5-6). 2D cell cultures of the same cell line treated with TNF showed similar results (Figure 5-9), substantiating the results seen in MDTs. It is noteworthy that we expected to see a more significant difference between the control and treatment groups. This can be due to the high baseline levels of nuclear p65 in the cell line selected. [185] We are also aware that the serum factors such as growth factors, cytokines, soluble cytokine receptors and macroglobulin present in the serum-supplemented medium that we used may influence the TNF-α assessment. [186] It is also reported

that the TNF-induced gene expression oscillates in time, [187] hence the treatment durations might need to be individualized for each cell line and TNF-a assessment should be a subject of future investigation. Nevertheless, our results showcase that the PCD drug screening platform can reproduce the on-chip responses of tumour samples to biological stimuli.

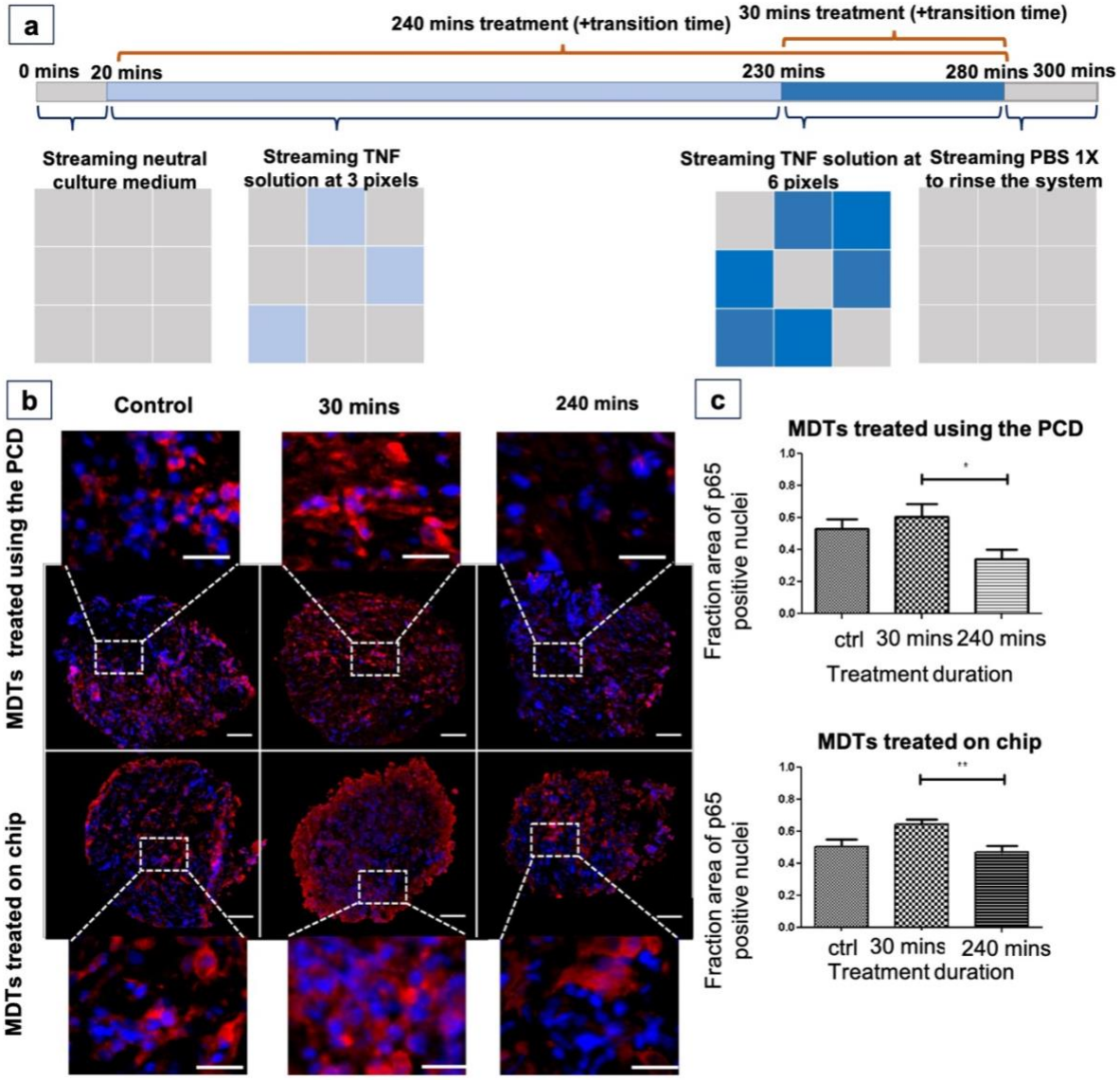

Figure 5-6 The PCD drug screening platform can recreate the on-chip response of tumour models to a cytokine. Xenograft cell line MDTs (TOV 21G) were treated with a TNF solution for different durations using the PCD and on-chip, and the change in the nuclear translocation of p65 was quantified. Red: p65 and blue: DAPI. Scale bar = 20 µm for zoomed-in MDTs, and 100 µm for whole MDTs. N=3

5.5 Material and methods

5.5.1 Design and fabrication of parts

We followed our previously published methodology to design and fabricate PCDs, manifolds, and holder assembly. [20] Briefly, all parts except PCDs and manifolds were designed in Fusion 360 (Autodesk Inc., CA, USA) software. PCDs and manifolds were designed using script-assisted CAD in Catia V5 (Dassault Systèmes, France) previously developed by our group. [98] The parts were 3D printed using a stereolithography 3D printer (PICO2 HD, Asiga, Australia). The resin used was Pro3dure GR-1 black (P3GR1BLK-1L, Pro3dure medical GmbH, Iserlohn, Germany). After the printing, the excess resin was cleaned by sonication of the parts in an isopropanol bath, then post-cured by UV exposure (Flash UV Curing Chamber, Asiga). To assemble the PCD, 1/16" (RK-06419-01, Masterflex Tygon, Cole-Parmer, Quebec, Canada) and 1/32" (RK-06420-01, Masterflex Tygon, Cole-Parmer) tubing was plugged and glued using a UV-sensitive resin. Polycarbonate three-way stopcock valves (RK-30600-02, Cole-Parmer) were installed on the fluidic lines. Glue and screws were used to assemble the parts of the holder assembly. The microwell array was micromachined using an MDX-40A milling machine (Roland DGA, Irvine, CA, USA) on a 1/8" PMMA slab (8560K239, McMaster-Carr, Elmhurst, IL, USA). The holder assembly was fixed over the PMMA slab. Polydimethylsiloxane (PDMS; Sylgard® 184 silicone elastomer kit, Dow Corning, Midland, MI, USA) was used to seal the holder assembly-PMMA slab interface and form a liquid-tight environment inside the holder assembly. Flow rates were controlled using AF1 microfluidic pressure pumps and MFS4 microfluidic flow sensors (Elveflow, Paris, France). Microfluidic chips for drug testing on MDTs were fabricated using our previously published protocol. [188]

5.5.2 System operation

The operation of the system was controlled using custom Python (Python software foundation) and LabView codes (National Instrument, Austin, TX, USA). A flow rate of 0.5 µl/s per aperture was used for all reagent streaming over live tissue. The aspiration to injection flow rate ratio was kept at 1.4. To prepare the system, isopropanol was first streamed at 1 µL/s per aperture in all of the injection and aspiration tubes for at least 15 minutes to wet, prime, and sterilize the fluidic lines.

The system was further infused for 5 minutes with PBS 1X (PBS 10X; 3072318, Wisent Inc., Saint-Bruno-de-Montarville, Canada) in all lines to purge isopropanol. Next, without pausing the pumps, the PCD was installed in the holder assembly over the immersed flat surface beside the microwell array. The experimental flow rates for injection and aspiration were administered, and the PCD was gently slid over the microwell array. PBS 1X for formalin-fixed tissue, or neutral culture medium for live tissue, was administered for 20 minutes to rinse the microwells. Next, the reagents of interest were put in place. For formalin-fixed tissue staining experiments, Sytox™ Green (S7020, Thermo Fisher Scientific, Waltham, MA, USA), Nuclear Mask Red (H10326, Thermo Fisher Scientific), and DAPI (D1306, Thermo Fisher Scientific) were used. 10 mM solution of DAPI in PBS 1X was prepared and aliquoted. Dye solutions were diluted at a 1:500 ratio in PBS 1X. For live tissue staining experiments, Celltracker™ Green (CMFDA; C2925, Thermo Fisher Scientific), Celltracker™ Red (CMRA; C34551, Thermo Fisher Scientific), and Hoechst (Hoechst 33342, H3570, Thermo Fisher Scientific) were used. Dye solutions were diluted at a 1:500 ratio in the culture medium. At the end of the experiment, PBS 1X was injected for at least 10 minutes to rinse the fluidic lines and tumour models from the reagents. Experiments were performed on a microscope stage and at room temperature. Injection reagent flasks were put in a water bath at 40 ˚C. Heating the reagent helps to prevent bubble formation in the fluidic lines and over the microwell array.

5.5.3 Finite Element Methodology

We used COMSOL Multiphysics© software v.5.6 (COMSOL Inc, Burlington, MA, USA) to simulate the convection and diffusion of species under the PCD and within tissue models. Passive diffusion of oxygen and glucose in the static culture of tumour models in between the medium changes was also modelled for the spheroid formation assay. The geometry of the model was drawn using built-in COMSOL drawing tools. The dimensions of the model can be found in Table 5-1. All simulations were conducted at a constant biological temperature (37 °C). We used a time-dependent solver to model the PCD tumour model system and the spheroid formation assay. For the PCD tumour model system, Fick's second law of diffusion and Navier-Stokes equation for laminar flow were applied using the "transport of diluted species in porous medium" module. The injection apertures were considered as inflows (i.e., source), injecting species with two

interchangeably varying concentrations (i.e., concentrated or zero concentration solutions): starting from the top right side of the PCD tip, every other pixel received the concentrated solution, resulting in 5 pixels streaming the concentrated solution and 4 pixels streaming the zero-concentration solution. The aspiration apertures were considered as outflows (i.e., sink). The aspiration to injection flow rate ratio was optimized to yield sharp pixels at the experimental flow rates and was kept constant throughout the simulation. The operational parameters of the model can be found in Table 5-2. All the liquid compartments of the model had the physical properties (i.e., density and viscosity) of water at 37 ˚C. The porosity and hydraulic permeability are extremely low for the tumour model compartment. [161, 162] With this in mind, we assumed the tumour models non-porous and used the diffusion coefficient of glucose in water to model the transport of concentrated solution in the tissue models. For the spheroid formation assay, the transport of diluted species module was used to model the passive uptake of glucose and oxygen by tumour models. We first simulated oxygen transfer within the tumour models in the spheroid formation assay. We considered a constant oxygen concentration at the medium-air interface over the microwell array. PMMA is not gas-permeable, thus we imposed no-flux (Neumann) boundary conditions at the bottom and walls of the microwells. For glucose, we assumed continuity boundary conditions at the medium-tumour model interface. We used Michaelis–Menten (MM) kinetics to model cancer cells' glucose and oxygen consumption rates in the spheroid formation assay. The average Michaelis–Menten uptake kinetics found in the literature [16, 54, 189] imply high consumption rates in the abundance of nutrients and decreased consumption rates when nutrients are depleted. The Michaelis–Menten constants refer to concentration thresholds, below which the normal cell metabolism is impacted. [130] We evaluated the minimum concentration of oxygen and glucose in the core of tissues of 500 μm in diameter. Tissue uptake and diffusion parameters are provided in Table 5-2.

5.5.4 Cancer Cell Lines Xenograft Production

A human carcinoma cell line derived from an ovarian cancer tumour TOV21G (RRID:CVCL_3613) was used to produce mouse xenografts. Ovarian cancer cells were grown as monolayers (2D culture) in OSE medium (316-030-CL, Wisent Inc.) supplemented with 10% fetal bovine serum (FBS; Gibco™, Thermo Fisher Scientific), 55 mg/L gentamicin (Gibco™, Thermo

Fisher Scientific) and 0.6 mg/L amphotericin B (Gibco™, Thermo Fisher Scientific). After reaching confluency, cells were detached with 0.25% trypsin-EDTA solution (Life Technologies, California, USA), and cell suspensions (1 000 000 cells) were mixed with Matrigel (BD Biosciences, Franklin Lakes, NJ, USA) at a 1:1 ratio and subcutaneously injected into the flank of immunodeficient NOD.Cg-Rag1tm1Mom Il2rgtm1Wjl/SzJ female (Charles River, Wilmington, MA, USA). Xenograft tumours were harvested once they reached a volume between 1 500 and 2000 mm3. All animal procedures were performed in accordance with the Guidelines for the Care and Use of Laboratory Animals of the CRCHUM and approved by the Animal Ethics Committee (the Comité Institutionnel de Protection des Animaux).

5.5.5 MDT Production from Cell Line Xenograft Tumours

We used our previously published method [51, 188] for the production of MDTs. Briefly, a tissue chopper (McIlwain, Ted Pella, Redding, CA, USA) was used to cut the xenograft into 350 µm-thick tissue slices. Tissue slices were kept in Hank's Balanced Saline Solution (HBSS, 311-516-CL, Wisent Inc.) supplemented with serum and antibiotics. Tissue slices were further punched into MDTs using a 500 µm diameter tissue punch (Zivic Instruments, Pittsburgh, PA, USA) and kept in HBSS supplemented with antibiotics.

5.5.6 Microwell prepping and MDT loading in the microwell array

Similar to PDMS devices [16], the microwell arrays were wetted and rendered hydrophilic by plasma treatment and rinsed with 100% ethanol. They were then sterilized by soaking in 70 % ethanol for 15 minutes and prepared by incubation with a triblock copolymer (Pluronic® F-108, Sigma-Aldrich, St. Louis, MO, USA) overnight (at least 16 hours) at 37 °C in a 5% CO2 incubator. The microwell arrays were then rinsed with PBS 1X three times to purge the Pluronic® F-108 solution. We adapted the previously published method of our laboratory to load the MDTs in the microwells. [51, 188] Briefly, the overlay liquid over the microwells was removed. 16 MDTs were picked using a 20 µL pipette and emptied over a microwell group. MDTs were diverted towards empty microwells using the pipette tip where they would fall in the microwells. In the case of more than one MDT falling in a microwell, the extra MDTs were pipetted out of the well and transferred to empty wells. This process was repeated for all 9 microwell groups.

5.5.7 Spheroid formation assay

We used a human squamous cell carcinoma FaDu (RRID: CVCL_1218) and a human colon cancer cell line HCT-116 (RRID: CVCL_0291) for spheroid formation experiments. Cells were grown as monolayers (2D culture) in Dulbecco's Modified Eagle Medium (DMEM; 11965118, Gibco™, Thermo Fisher Scientific) supplemented with serum and antibiotics. After reaching confluency, cells were detached and cell suspensions of 2 000 000 cells in 1 ml of culture medium were prepared. 400 µL of cell suspension was seeded over each microwell array, and the cell suspension was replenished three times to exchange the liquid in the microwells with the cell suspension. 15 minutes after the cell seeding, the cell suspension over the microwell array was removed by drawing 400 µL of the cell suspension and adding 400 µL of medium to remove the floating cells over the microwell array. The medium was changed every 24 hours by adding 400 µL of fresh medium near one corner of the microwell array, removing 400 µL from the opposite corner, and repeating the process three times.

5.5.8 OCT Embedding Protocol

Following fresh tissue experiments, some tumour models underwent formalin fixation in the microwell arrays. 400 µL of formalin was added near one corner of the microwell array and removed from the opposite corner and repeated three times. The tumour models were incubated in formalin for 40 minutes and formalin was rinsed by three washes with PBS 1X. For agarose embedding, an 8% solution of agarose (Ultrapure™ Low Melting Point Agarose; 16520100, Thermo Fisher Scientific) in PBS 1% was prepared by dissolving 8 g of agarose in 100 ml PBS 1X and microwaving the solution for 80 seconds (4 cycles of 20 seconds) or until agarose powder was completely dissolved. The agarose in PBS solution was then cooled down to 62 ˚C. 400 µL of agarose solution was discharged and removed three times over the microwell array using a positive displacement pipette. The microwell array was placed in an oven at 60 ˚C for 30 minutes to ensure agarose permeates in the microwells and tissues. The microwell arrays were further cooled at 4 ˚C for 30 minutes, and the agarose layer was peeled off gently. If tumour models were left in the microwells after the removal of the agarose, a needle was used to remove the tumour models from the wells and add them to the agarose tissue array. The agarose block was cut to separate the microwell groups, and microwells subjected to the same treatment condition were placed in the

same plastic mold, ensuring that tissues were touching the bottom of the plastic mold. OCT was poured gently over the agarose block to prevent bubble formation. Plastic molds were placed on a flat and levelled surface in dry ice and cooled down for 20 minutes for OCT to solidify. Each OCT block was sliced into 5 µm-thick sections using a cryostat, and each section was placed on a TOMO® hydrophilic adhesion slide (Matsunami, Bellingham, WA, USA).

5.5.9 Histopathological staining

OCT sections underwent hematoxylin and eosin (H&E) staining as well as IF staining to assess the expression of p65 protein (Anti-NFkB p65 protein; SC-8008, Santa Cruz, Texas, USA) and DAPI in the tumour models. IF staining was performed using the BenchMark XT automated stainer (Ventana Medical System Inc., Tucson, AZ). Antigen retrieval was carried out with Cell Conditioning 1 (#950-123, Ventana Medical System Inc) for 90 minutes for all primary antibodies. Mouse anti-p65 (1:200) antibody was automatically dispensed. The slides were incubated at 37 °C for 60 minutes and secondary antibodies were incubated at room temperature on the bench. We used our laboratory's protocol to quantify the TNF response in 2D culture. [190] Briefly, cells were seeded onto coverslips at 20 000 cells/well in 24-well plates. After 24 h, cells were incubated with TNF solution for 5 minutes or 2 hours. Cells were fixed with formalin for 15 minutes at room temperature, washed using PBS 1X, permeabilized with 0.25% Triton (Triton™ X-100 solution; 93443, Sigma-Aldrich), and incubated with mouse anti-p65 (1:400) overnight. The primary antibody was detected by incubation with a secondary antibody for 60 minutes. Coverslips were mounted onto slides using Prolong Gold® anti-fade reagent with DAPI (14209 S, Life Technologies Inc.). All sections were scanned with a 20x/0.75 NA objective with a resolution of 0.3225 µm (bx61vs, Olympus, Toronto, Ontario.

5.5.10 Tumour model treatment with TNF

For cytokine stimulation experiments, MDTs were exposed to a neutral culture medium or to 20 ng/ml of TNF solution (Recombinant TNF alpha human; 300-01A, PeproTech, Thermo Fisher Scientific) in culture medium for either 30 minutes or 240 minutes. The TNF treatment using the PCD lasted 300 minutes. First, the PCD streamed neutral culture medium at every pixel for 20 minutes. Then, we streamed TNF in one group (3 pixels) while the two remaining groups (6 pixels)

received a neutral culture medium. At 230 minutes, TNF streaming was started in a second group. For the next 50 minutes, TNF was streaming at 6 pixels, all the while the control group on the same 3 pixels received culture medium. At 280 minutes, we swapped all reagent flasks for PBS 1X, and PBS 1X was streamed for 20 minutes to rinse the tumour models. The PCD was then removed, and the immersion liquid over the microwell array was withdrawn. Tumour models underwent OCT embedding for further histopathology processes. We followed our group's protocol for MDT treatment on-chip. [51]

5.5.11 Quantification of Immunofluorescent Staining

To measure the FI of tumour models stained using the PCD, an open-source image processing software (Fiji) was used. [191] At least 3 spheroids were randomly selected in each fluidic pixel, and the corrected FI per area (subtracting the background FI from tissue FI) was calculated for each fluorescent channel. The average corrected FI per area of the 3 pixels subjected to the same treatment was compared between the 2- and 3-hour incubation time for each channel. To quantify protein expressions using immunofluorescent staining, we used VisiomorphDP software (VisioPharm, Hørsholm, Denmark) [40,41]. Briefly, the tissue core surface area was detected through the DAPI channel. The nuclear signal of p65 was quantified by dividing the surface area of p65-positive nuclei by the total surface area of the nuclei. We used a similar approach for quantifying p65 translocation in 2D culture of the cells.

5.5.12 Statistical Analysis

Statistical analyses were performed in GraphPad Prism version 8.0 (San Diego, CA, USA) using the non-parametric one-way ANOVA Kruskal–Wallis test and post hoc Dunn's test, because the data were not normally distributed according to the D'Agostino and Pearson omnibus normality test. For the TNF treatment experiment, a minimum of 15 MDTs were analyzed for each condition, and experiments were repeated three times ($N = 3$). All data are reported as the mean ± standard error of the mean (SEM) unless otherwise stated. The reported p-values were generated using a post hoc test (Dunn's test).

5.6 Conclusions

The need to improve the predictive power of in vitro and ex vivo model systems to maximize the chances of success in clinical trials has made 3D tumour models, such as microdissected tissue and cancer cell line spheroids, attractive in preclinical settings. [146, 192] Thus, it is essential to implement tools and techniques to automate drug screening on 3D tumour model systems and make them compatible with clinical practices. To address this, we introduced a drug screening platform for automated simultaneous streaming of up to 9 reagents on 144 tumour models. We used human cancer cell line xenograft and spheroid models to validate the potential of the PCD drug screening platform for multiplexed and dynamic streaming of biochemicals over tumour models. Microtissues processed in the drug screening platform can directly be transferred to an embedding medium and undergo various endpoint measurements (i.e., immunohistochemistry, immunofluorescence, and H&E). These measurements are standard protocols in clinical and pharmaceutical practices and allow the monitoring of multiple biological pathways. Furthermore, because the platform is amenable to different 3D tumour models, it allows the co-culture of spheroids, organoids, and ex vivo tumour tissue explants. In turn, this enables comparing treatment efficacy on various tumour models. The main drawback of the PCD arises from the continuous streaming of reagents. Even though flow rates are extremely low, streaming over several hours consumes a considerable amount of reagents, and thus limits applications in cases where reagents are extremely expensive (e.g., recombinant protein drugs). However, a highly parallel drug screening assay using the PCD would probably even be worthwhile despite the high reagent consumption. We have reported a low number of large pixels (9×6 mm^2) in this article. However, PCDs of up to 144×1 mm^2 pixels have been produced routinely in our laboratory with successive reagent changes as fast as 1 change per 30 s. This makes the PCD drug screening platform appealing for highly parallel and dynamic assays. The reconfigurable sizes and numbers of pixels along with the fast reagent change will speed up the throughput.

Compared to traditional well plate-based approaches [193] and their downsized microfluidic counterparts such as InSphero GravityTRAP™, [194] idenTx™, [195] and Organoplate® [196], our platform does not require the manual delivery of reagents to microtissues or the use of robotic liquid handlers. This should greatly reduce the time and cost required to perform the experiments. Moreover, the possibility of the direct transfer of tumour models to an embedding medium reduces

the potential tissue damage and makes our platform more efficient compared to previous approaches where each individual sample is transferred from well plates to an embedding medium.

5.7 Supplementary Materials

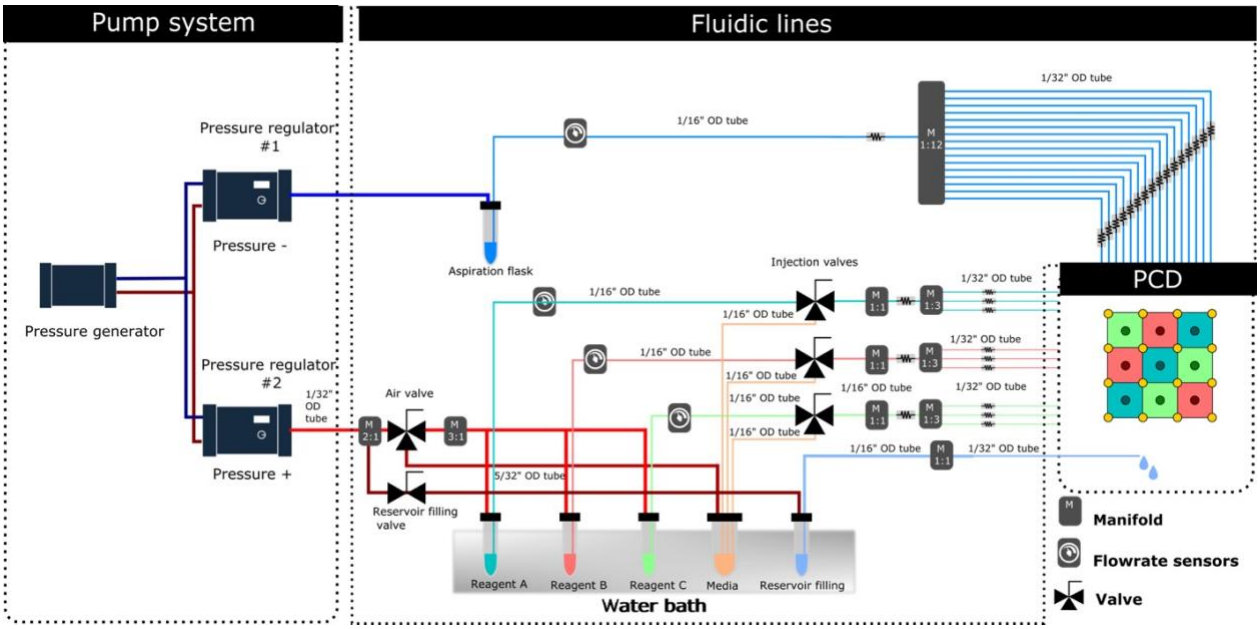

Figure 5-7 Fluidic connections in the PCD drug screening platform. The use of valves allows for switching between the streaming of various reagents and the flowrate sensors allow for control and validation that the platform is working correctly. OD; outside diameter

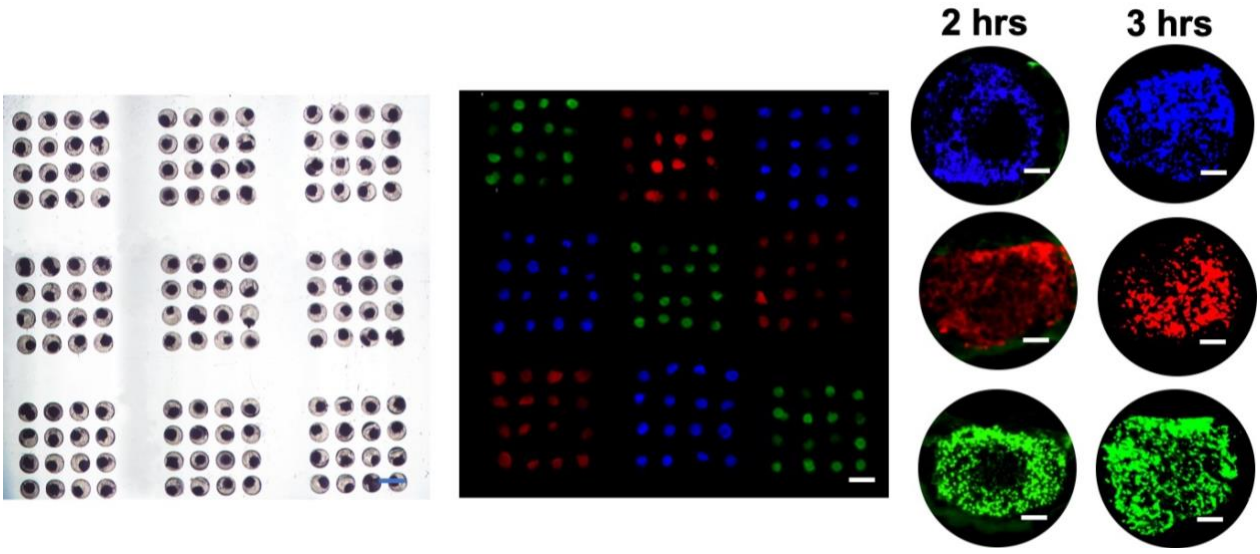

Figure 5-8 Micrographs of MDTs stained with various cellular dyes using the PCD. Images taken from the tumour model cores that have been treated with cellular dyes for different amounts of time show that core cells are not stained in the shorter treatment durations.

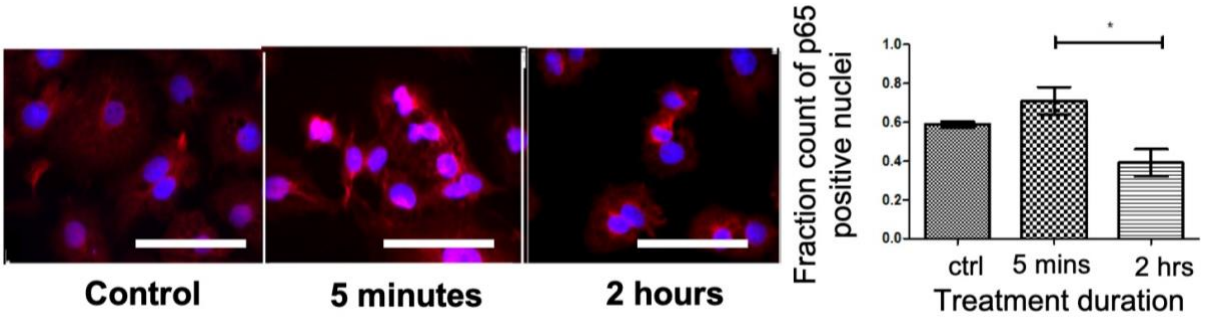

Figure 5-9 time-dependent treatment of 2D culture of TOV21G cells with TNF shows a response similar to MDTs treated on-chip or using the PCD. This further validates the potential of the PCD drug screening platform to predict the response of 3D tumour models to stimuli.

Table 5-1 dimensions

Parameter	**Value (µm)**
Microwell array	
well height	900
well width	700
well length	700
Distance between microwells	1000
PCD	
Gap between the PCD and the microwell array	100
Aperture diameter	200
Distance between apertures (i.e., pixel size)	5000
Number of aspiration apertures	16
Number of injection apertures	9
Tissue	
Tissue diameter	450

Table 5-2 tissue uptake parameters, diffusion properties, the PCD working condition

Parameter	**value**		
Diffusion/Reaction Parameters			
Diffusion constant of glucose (cm^2/s)	Tissue	$2.7x10^{-6}$ [54, 197]	
	Medium	$9.27x10^{-5}$ [54]	
	Agar 5%	Same as water [8, 198]	
Diffusion constant of oxygen (cm^2/s)	Tissue	$1.8x10^{-5}$	
	Medium	$2.6x10^{-5}$	
	Agar 5%	$2x10^{-5}$ [8]	
	PDMS	$3.4x10^{-5}$ [199, 200]	
Diffusion constant of Carboplatin/Paclitaxel (cm^2/s)	Could we use glucose properties? [201, 202]		
Saturation concentration (mM)	Oxygen	Tissue	1.02
		medium	0.21
		Agar 5%	0.21colagen[203]
		PDMS	1.43
	Glucose	11	
Oxygen partition coefficient (relative solubility of oxygen)	PDMS-Medium	0.15	

	Medium-Tissue	4.8
Maximum cellular uptake rate (mM/S)	Oxygen	2.07
	Glucose	1.09
Michaelis-Menten constant (mM)	Oxygen	$4.63x10^{-3}$
	Glucose	$4x10^{-2}$
PCD working conditions		
Injection pressure (Pa)	4	
Aspiration pressure (Pa)	4	
Injection/Aspiration flowrate (nL/s)	100	

5.8 Author Contributions

Conceptualization: D.D., P.-A.G., A.-M.M.-M. and T.G.; Data curation, D.D.; Formal analysis, D.D.; Funding acquisition, A.-M.M.-M. and T.G.; Investigation, D.D., A.-M.M.-M. and T.G.; Methodology, D.D., P.-A.G., A.S.R., A.-M.M.-M. and T.G.; Project administration, A.-M.M.-M. and T.G.; Resources: A.-M.M.-M. and T.G.; Supervision, A.-M.M.-M. and T.G.; Validation, D.D., A.S.R., P.-A.G., A.-M.M.-M. and T.G.; Visualization, D.D., and A.S.R.; Writing—original draft, D.D. and T.G.; Writing—review and editing, A.S.R., and T.G. All authors have read and agreed to the published version of the manuscript.

5.9 Conflicts of interest

T.G. is the co-founder and Chief Technological Officer of MISO Chip Inc., a company operating in the field of *ex vivo* tissue culture.

5.10 Acknowledgements

We acknowledge Kim Leclerc-Desaulniers for technical assistance with the animal work. We thank the CRCHUM Microfluidics Core Facility supported by the TransMedTech Institute and its main financial partner, the Canada First Research Excellence Fund and namely Jennifer Kendall-Dupont and Benjamin Péant for performing tissue dissection and useful scientific and technical discussions. We thank Liliane Meunier and Véronique Barrès of the CRCHUM Molecular Pathology core facility for performing the OCT block sectioning and slide scanning. We acknowledge Jacqueline Chung for manuscript editing. T.G. acknowledges CMC Microsystems.

CHAPTER 6 GENERAL DISCUSSION

The main goal of this project was to investigate, characterize, and improve drug screening assays on 3D tumour model systems, and more specifically, *ex vivo* cultured tumour explants. This was ultimately achieved by developing a multiplexed and high throughput open space microfluidic platform for drug screening on micron-sized 3D tumour models. This chapter first discusses the role of diffusive-convective transport in primary tissue culture and how it shaped the research objectives in this thesis work. It also details important observations that diverted the project into new directions. Finally, the limitations of this research project and the limitations of *ex vivo* cultured tumour explants as a predictive preclinical model are discussed.

6.1 Understanding the role of diffusive-convective transport in primary tissue culture

6.1.1 Characterization of the impact of tissue size and culture vessel type on the *ex vivo* survival of tumour tissue explants

The fact that MDTs will survive longer than tissue slices in a non-perfused culture setting can be easily explained theoretically. It can be shown by Fick's second law of diffusion that there is a maximum diameter (R_{max}) for a spherical tissue structure deposited in an infinite pool of culture medium to survive without anoxia. In non-perfused conditions and without convection, oxygen transfer within and around the tissue happens only by diffusion. Also, cells consume oxygen. The following equation describes mass transfer of oxygen in *ex vivo* tumour explants:

6-1

$$\frac{\partial C}{\partial t} = D\nabla^2 \mathrm{C} - \mathrm{q}$$

Where C is the concentration of oxygen, t is the time, D is the diffusion constant of oxygen and q is the volumetric oxygen consumption rate by cells. The equation can be solved for tissue and medium subdomains separately, linking the two by defining a continuity boundary condition at the medium-tissue interface. The other boundary conditions can be defined as 1) zero concentration at the centre of the tissue (C (r = 0) =0) to prevent anoxia, and 2) maximum dissolution concentration of oxygen in the medium at infinity (C ($r \rightarrow \infty$ = C_{max})). In the medium, the oxygen consumption term q is zero. Assuming steady state ($\partial C/\partial t = 0$) and solving the differential equations for tissue

and medium separately, for a spherical tissue (polar coordinates) the following expression of the non-perfused R_{max} is found:

6-2

$$R_{max} = \sqrt{\frac{6D_T D_M C_{max}}{q(2D_T + D_M)}}$$

Where D_T and D_M are the diffusion coefficients of oxygen in tissue and medium respectively. [16] Substituting the values found in the literature for tumour cells and assuming zero-order uptake kinetics gives 425 µm as the maximum diameter of tissue to prevent anoxic cores in non-perfused culture. However, as reported by our group [51] and others [78] slightly larger tissues survive the non-perfused culture without facing necrosis or hypoxia. This can be explained by the fact that the worst-case scenario assumption (e.g., compact tumour tissue, zero-order maximum consumption rates) are made to calculate the 425 µm threshold. Therefore, it can be predicted that the experimental diameter threshold is greater than 425 µm. Nevertheless, before the publication of the first article of this project, there was no direct experimental comparison between survival rates of tissue explants with different sizes and spatial geometries. To address this, *ex vivo* survival rates of two tissue sizes 1) MDTs as quasi-spherical structures with diameters very close to theoretical threshold to prevent anoxia, and 2) tumour tissue slices, the most commonly used approach in the *ex vivo* explant realm, were compared. The choice of the models was to comply with common practices used in the *ex vivo* culture of tumours, and new microfluidic systems that are becoming more and more popular. For both models, MDTs and tissue slices, numerical simulations were used to estimate oxygen and glucose depletion in tumour models. Moreover, with the numerical model, it is possible to apply a Michaelis Menten kinetics for nutrient uptake, which is more realistic than the zero-order kinetic used in the analytical solution. The details of the numerical model including kinetics and boundary conditions are explained in section 4.4.2. Numerical simulations also showed consistently that tumour tissue slices will face oxygen and glucose deficiency and MDTs will not. For experiments, since it is very challenging to measure glucose and oxygen concentrations in tumour tissues directly, indirect measures of cell survival (i.e., cell proliferation, cell death, and hypoxia) were studied using appropriate biomarkers. To measure cell survival, immunostaining on formalin-fixed and paraffin-embedded tissues was performed. This technique offers the advantage of showing exactly where a given protein is located within the tissue and

colocalizing the proteins expressed. As an advantage, multiple paraffin sections are produced from the tumour models, which can be stored over a long time and undergo various histopathological analyses. To compare the survival of tumour tissue explants, the expression levels of biomarkers were quantified using the image analysis method described in appendix C. The viability of freshly produced tumour models was also compared to the primary tumours they were produced from to understand the effect of the tumour model production procedure on cells. To circumvent the possible effect of tumour heterogeneity on *ex vivo* tissue survival, three cell lines of two different cancers (ovarian and prostate) were used in the study. The experimental results also confirmed that tissue slices face hypoxia and necrosis, a sign of anoxia and glucose depletion, while MDTs maintain the baseline levels of viability. We also observed that there was no significant damage to the cells in tumour models compared to primary tumour tissues, which shows that the tumour model production procedure is safe for the tumour tissue. The results provided evidence that the model size and geometry and the culture vessel play a key role in *ex vivo* survival and should be carefully considered in designing drug screening assays. This objective and the finding from it, while not introducing novel tools, are fundamental for researchers working in the tumour tissue explant field and provide important criteria for designing drug screening assays using tumour explants.

6.1.2 Evaluation of the operation of the PCD over tissue explants and prepare the system for culture and drug screening on MDTs.

The first article demonstrated that tissue slices will die in a non-perfused culture setting and MDTs will maintain their viability. To mitigate this limitation, as explained in section 2.5.1, previous works have used perfusion to improve the *ex vivo* survival of tumour tissue slices. However, the throughput of perfusion-based culture assays is usually limited to one or two tissue slices per device. To address this, the original plan for the second objective was to develop high throughput perfusion tools that enable increased *ex vivo* viability of tumour tissue slices while accommodating drug screening. Initially, analytical and numerical models were developed to estimate oxygen and glucose accessibility in perfused versus non-perfused tumour tissue explants. Adding the convection term changes equation 6-1 into:

6-3

$$\frac{\partial C}{\partial t} = D\nabla^2 \mathrm{C} + \mathrm{u}\nabla \mathrm{C} - \mathrm{q}$$

Where u is the velocity of flow. The determining factors in a perfusion model are convection in the medium (i.e., the rate at which the medium is refreshed around the tissue) and the hydraulic conductivity and permeability of the tumour tissue (i.e., the ease with which a fluid can move through the tissue). The former can be addressed by controlling the experimental conditions while the latter depends on the characteristic of tumour tissues and vary from one tumour to another, and even within one tumour due to tissue heterogeneity. The flow of fluid through a porous medium (e.g., tumour tissue) can also be described by Darcy's law:

6-4

$$q = \frac{-k}{\mu L}\Delta p$$

where q ($\frac{m}{s}$) is the flux of fluid (hydraulic conductivity), k (m^2) is the permeability, μ ($Pa.s$) is the dynamic viscosity, L (m) is the sample length, and Δp (Pa) is the pressure drop. It is obvious from the equation that low permeability will result in lower hydraulic conductivity, which means fluid will pass through with difficulty. The parameters found in the literature show that the hydraulic permeabilities of most tumour tissues are very low, in the range of 10^{-18} to 10^{-14} m^2. [52, 162, 204] As a simple example to emphasize the point, the permeability of a bed of gravel is 10^{-9} m^2, and the permeability of a bed of clay is 10^{-16} m^2. [205] A one-meter layer of water travels through a 1-meter-long bed of gravel in 2 minutes, mostly through convection, while the same amount of water deposited over the same height of clay takes 2 days to pass through, mostly through diffusion. Based on this analogy, and the extremely low permeability of tumour tissue, the theoretical model for tissue perfusion here assumes that there is no convection inside the tissue (an infinitesimal permeability and hydraulic conductivity), and the medium is continuously refreshed, maintaining a constant concentration of species at the tissue-medium interface. The continuous refreshment of the medium surrounding the tissue while the transfer of species in tissue mostly happens by diffusion and is referred to as "perifusion". [124] Applying the new assumptions simplifies equation 6-2 into:

6-5

$$R_{max} = \sqrt{\frac{6D_T C_{max}}{q}}$$

Substituting the values gives 700 µm as the maximum diameter of a spherical tissue explant that survives without anoxia in a perifused culture condition. I developed a numerical model in COMSOL Multiphysics for the transport of oxygen in perifused and non-perifused tumour tissue explants. The diffusion and uptake parameters and the geometry of the system and tissue explants match the parameters given in Table 4-2. For perfusion, a constant concentration of oxygen is assumed at all tissue-medium interfaces in MDTs and tissue slices cultured in PDMS microfluidic devices. For tissue slices cultured in plastic well plates, no flux boundary condition is applied at the tissue-well plate interface, and a constant concentration of oxygen is assumed on tissue-medium interfaces. Simulations show that perifusion improves the accessibility of oxygen to tissue models to different extents. Perifused tissue slices cultured in plastic well plates are estimated to face hypoxia and anoxia. Perifused tissue slices cultured in PDMS devices are expected to survive without hypoxia or anoxia. Numerical simulations predict that the concentration of oxygen in MDTs will remain constantly at a high level, well above hypoxia and anoxia thresholds, and higher than oxygen level in tissue slices (Figure 6-1).

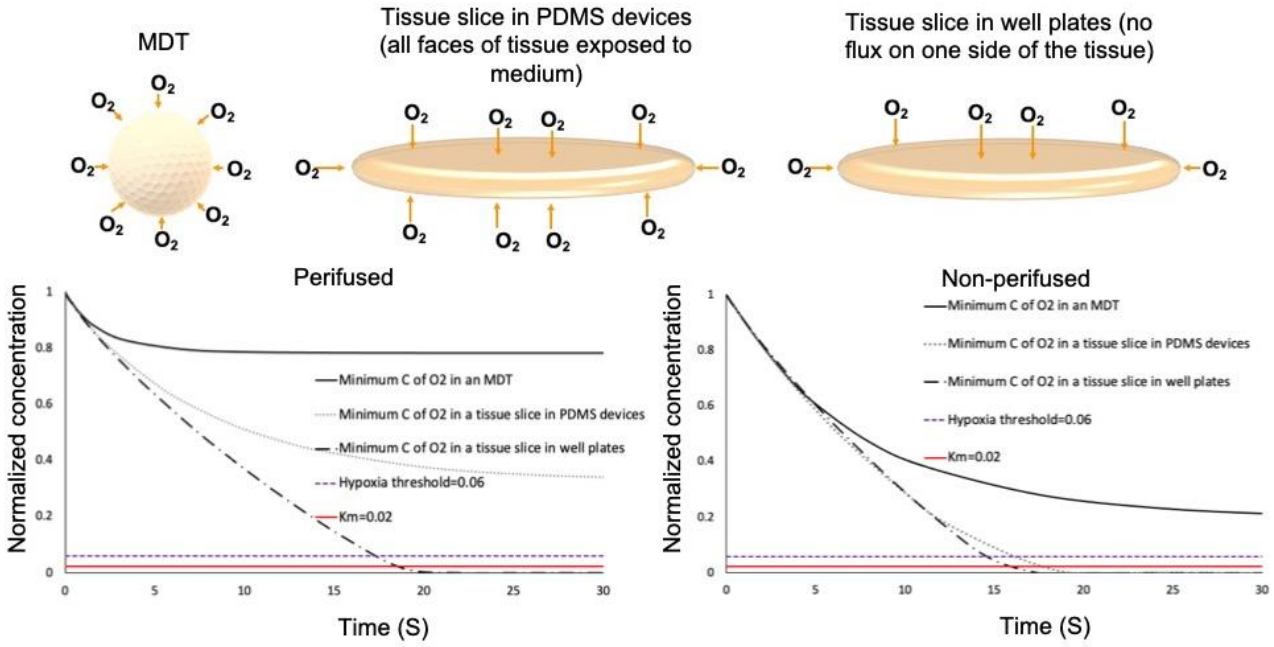

Figure 6-1 Numerical modelling of oxygen accessibility in tumour tissue explants under perifusion and static culture conditions predict higher oxygen concentration in MDTs compared

to tumour tissue slices. The plotted parameter is minimum concentration (C) of oxygen (O_2) in tumour tissue explants.

With this information, I planned to adapt the PCD for drug screening on tumour tissue slices placed on PDMS surfaces. A few preliminary experiments focused on treating tumour tissue slices and agarose slices similar to tissue in terms of permeability with cellular dyes showed that the PCD cannot form fluidic pixels over and inside tissue slices. This mainly arises from the lack of convection inside the tumour: reagents injected at different fluidic pixels can only diffuse throughout the tissue (no free flow inside the tissue), and travel through the tissue at different rates, which causes the loss of the precision of fluidic pixels created by the PCD in deeper layers of tissue (Figure 6-2).

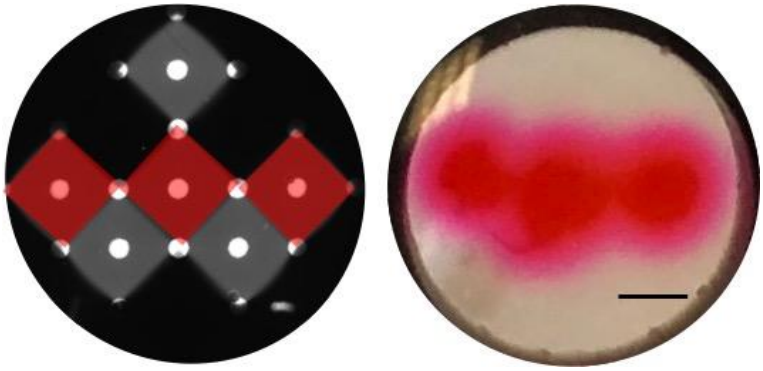

Figure 6-2 A 350 µm-thick agarose slab stained with Phloxine B using the PCD shows that the precision of fluidic pixels is lost. Micrograph of fluidic pixels of various concentrations of fluorescein created over a glass slide (left). Phloxine B injected at 3 pixels of the PCD while the other pixels inject a colourless solution (water). Red pixels on the micrograph are highlighted to match the pixels on agarose. Scale bar= 1 mm

Possible solutions to preserve the precision of fluidic pixels over and inside tissue were to cut tissue explants into very thin (<100 µm-thick) tissue slices or dissect them into MDTs. Slicing tumour slices thinner than 300 µm-thick is not feasible for some tumour tissues, as they are destroyed under the heavy shear stresses imposed. Besides, the stickiness, poor and uneven surface qualities, and buoyancy of fat-rich tumour tissue slices made it very difficult to align the PCD over tumour tissue slices. These observations and considerations were not published but are important since they give insights relevant to the tumour tissue slice drug screening platform. Moreover, these trials and errors rerouted the project towards using MDTs. Eventually, the PCD was adapted to deliver biochemical reagents over the MDTs. A larger PCD with larger pixels would allow for manipulating a larger number of MDTs. The largest dimension possible to print with the 3D printer

available in our laboratory is 52 mm. This limit allowed for a PCD that has nine 6 mm* 6 mm pixels. It is also important to hold the MDTs still and in place for the duration of the experiment which resulted in the design of the microwell array that groups MDTs corresponding to fluidic pixels. After designing the PCD and microwell array, the operation of the PCD over an array of 3D tumour models was modeled using COMSOL Multiphysics as explained in section 5.4.3, which further proved the robustness of the PCD.

For the experimental part of operating the PCD over MDTs, similar to many people working with microfluidics, my first go-to material to make the microwell array was PDMS. However, after a few failed attempts, PDMS was replaced with PMMA. The flexibility of PDMS which is often considered a perk, caused it to easily deform under the PCD. This further moved the problem away from Hele-Shaw flow considerations (i.e., stokes flow between parallel flat surfaces). The gas-permeability property of PDMS, one of the most important reasons that make PDMS interesting for cell and tissue culture, increased bubble formation when coupled with the continuous aspiration of the PCD. As a biocompatible, microfluidic-friendly replacement for PDMS, PMMA was selected, which resolved the issues of working with PDMS (Figure 6-3). The other perk of working with PMMA is the simple fabrication en-masse using micromachining. In addition, PMMA is more durable than PDMS making it reusable.

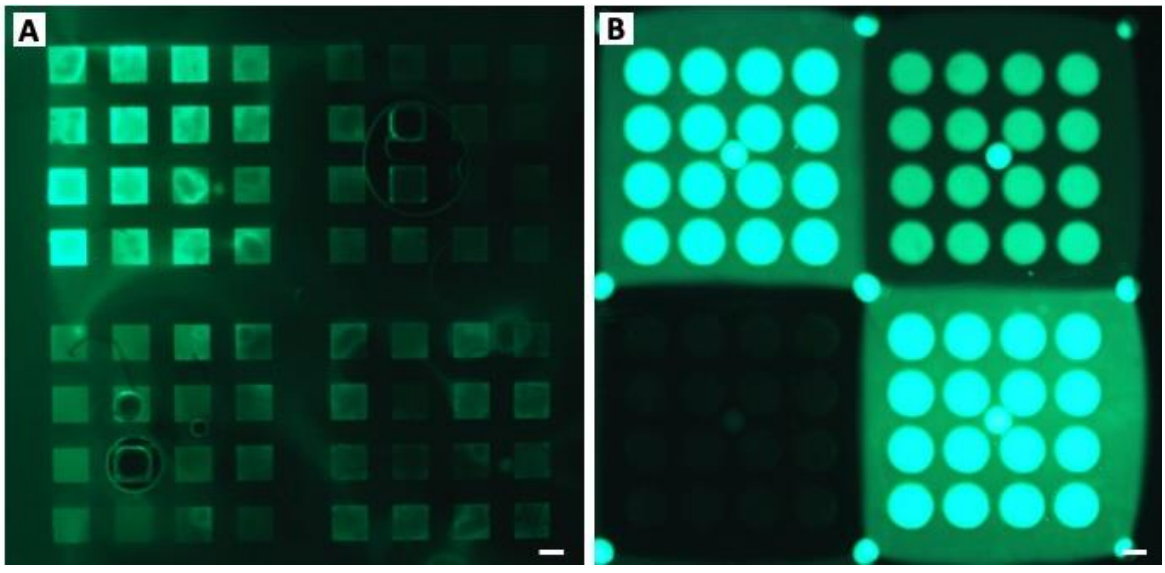

Figure 6-3 microwell array made with PDMS (A) and with PMMA (B). PCD alignment over PDMS is challenging, and PDMS increases the risk of bubble formation. Scale bar= 500 µm

Once the microwell array and the PCD were in place, the next obstacle was to precisely align the PCD over the microwell array. For this, additional parts were designed, and 3D printed to hold the PCD in place as explained in section 5.4.1. With these, the PCD drug screening platform produced was amenable to laboratory experimentation.

6.1.3 Validation of the potential of the PCD as a drug screening tool for 3D tumour models.

The first experiments with the PCD drug screening platform were staining formalin-fixed MDTs with cellular dyes as explained in section 5.4.5. To frequently monitor the operation of the PCD though microscopy, experiments were performed on a microscope stage. Formalin-fixed tissue was selected over fresh tissue because formalin-fixed MDTs appear to sediment more easily and move less in wells, making preliminary experiments less challenging. Also, for the first experiments, serial concentrations of fluorescein were injected over the microwells to test the placement and operation of the PCD before administrating cellular dyes, which would not have been possible with fresh tumour tissue. A protocol to take the MDTs out of the well without losing their orientation in microwells was also developed as explained in section 5.4.6. Even though I pursued OCT embedding of MDTs throughout this work, paraffin embedding is also an option. However, paraffin embedding makes the process more tedious and requires more tissue manipulation due to the following reasons: 1) removing dehydrated MDTs from microwells is difficult. To prevent this, formalin-fixed MDTs must be taken out of the well and dehydrated *ex situ*. 2) Paraffin does not infuse in agarose. For this, another gel such as HistoGel™ must be used for MDT embedding in microwells. HistoGel™ is not as consistent as 8% agarose and breaks more easily, making the process more labour-intensive.

The next step to test the operation of the PCD was to use it over fresh MDTs. Long-term fresh tissue experiments require a CO_2 incubation chamber, and a microscope incubation chamber large enough to fit the PCD platform was not available at the laboratory. For this, short-term (less than 5 hours) tissue staining and treatment response assessment experiments (see sections 5.4.5 and 5.4.7) were performed to provide proof of concept applications for the PCD. These experiments provided evidence that the PCD is capable of forming 9 well-defined and crosstalk free fluidic pixels over 144 MDTs.

As a final test and to showcase that the PCD drug screening platform can process a wide spectrum of 3D tumour models, spheroid formation and staining were performed in the platform. Spheroids from two different cell lines were directly formed in the microwell array and subjected to the PCD. The PCD streamed solutions of cellular dyes in culture medium over the PCD. The details of the experiments demonstrating the ability of PCD to perform dynamic reagent screening is explained in section 5.4.4.

The PCD drug screening platform functions flawlessly in short-term experiments. Longer term experiments varying from 1 to 4 days to verify the operation of PCD were performed. In some experiments, the PCD crashed due to various reasons including bubble formation in microwells, fluctuations in injections flow rate, and bubbles clogging the aspiration tubes. The first issue is addressable by placing the injection flask at a higher temperature than the microwell array. The solubility of gases in liquids increases with decreasing temperature. Therefore, lower temperatures in the microwells will prevent bubble formation. Also, the length of tubing connecting reagent flasks to the PCD was minimized. [206] Controlling bubble formation also reduces the chances of the blocked aspiration tubes but does not fully prevent it. To address this and to combat flow rate fluctuations, flow sensors were purchased and a PID controller was developed to measure the flow rates of injection and aspiration of the PCD. These sensors and the PID controller served to diagnose unexpected flow rate fluctuations and prevent the system rupture by reversing them. Although the new additions resolved the issues partly, no further experiments were done in this project.

6.2 Limitations of this thesis work and *ex vivo* tumour explants as a preclinical model

6.2.1 Limitations of this thesis work

The goal of this project was to develop a high throughput drug screening assay for 3D tumour models, which was achieved by adapting the PCD for drug screening over MDTs. However, there were certain constraints and some aspects of the system need further improvements. This section points out the shortcomings of the system that should be addressed to prepare the system for preclinical and clinical applications. The first group of limitations are in regard to the 3D tissue

models used in this project. Firstly, the PCD drug screening system is adapted for applications over microtissues and is not able to manipulate tumour tissue slices. In spite of the poor *ex vivo* survival, tissue slices have several advantages over MDTs. To name a few, tissue slices preserve more spatial information, and their production and manipulation are less labour-intensive than the procedures required to produce MDTs. Also, due to the small size of the tissue, manipulation of MDTs in well plates and Petri dishes is cumbersome and requires custom microfluidic devices. The production process and on-chip manipulation may render the model system less favourable for clinical applications by general technicians. Therefore, developing user-friendly tools to preserve the viability of tumour tissue slices is essential. Secondly, this thesis work focuses only on cell line xenograft tumours and spheroids. I anticipate that MDTs produced from human specimens will pose more challenges. Human tumour tissues are more heterogeneous, and it is expected that their processing and stability in the microwell array would be more delicate than xenografted tumours.

The second group of limitations deals with the PCD system and its operation. Firstly, PCDs are vulnerable to air bubbles since they are comprised of an intricate system of tubes. Bubbles can block a tube or form in or over a microwell. Both cases affect the quality of fluidic pixels and can impact MDTs negatively. Although bubble formation can be reduced to some extent, it is an inherent challenge in working with microfluidic systems and can never be fully rid of. Besides, extra caution must be taken in longer-term experiments since a system is more prone to bubble formation in a longer experiment. The next issue, which to me is the most important limitation of the PCD, is its high reagent consumption. The minimum injection flow rate enough to sustain the precision of fluidic pixels is 500 nL/sec per pixel. This means a 9-pixels PCD injects about 400 mL of reagents per 24 hours. While this amount might not be a problem for a culture medium and non-expensive reagents, it makes the system unsuitable for expensive reagents such as small molecule inhibitors and targeted therapies. Also, since the aspiration rate is higher than the injection rate (more than 500 mL over 24 hours of liquid assuming an aspiration to injection flowrate ratio of 1.4) waste management of the system is complicated, especially when working with cytotoxic reagents. These limitations can be circumvented by using smaller PCDs that require slower flow rates. However, the flow rates cannot be infinitesimal because the Péclet number should remain large (i.e., convection should be bigger than diffusion) for precise pixel formation.

6.2.2 Limitation of the use of *ex vivo* tumour explants for drug screening

Ex vivo tumour explants are one of the most fascinating, yet most delicate and challenging models to work with. The benefits and importance of this group of tumour models are listed in the previous chapters of this dissertation. This section touches on the limitations of *ex vivo* tumour explants as drug screening tools. The first major limitation is the impossibility to totally reproduce tumour specimens. Accordingly, the throughput of the system depends largely on the size of the specimen. Models such as MDTs in which even a small sample can be dissected into several microtissues somewhat bypass the throughput issue. However, in case of a problem such as sample contamination, it is not possible to retrieve or replicate the sample. The second major limitation is that the long-term storage of tumour specimens is not feasible. Cells lines and organoids can be bio-banked and replicated or reused at a later time. Bio-banking is still evolving and has yet to define experimental conditions for intact tumour tissue long-term cryo-preservation. This is a key problem since if the experimental setup or the team is not available to receive the sample on the day of the surgery, the sample cannot be preserved and processed at another time. The lack of reproducibility and storage of intact patient tissues also makes experiments with *ex vivo* tumour explants unrepeatable. The other limitation of the model is that the sampling is random and prone to sampling issues related to tissue heterogeneity. Fresh tissue explants must be processed and cultured rapidly to prevent cell death. It is almost impossible to know until the end of the experiment if slices or MDTs are cut from a region with many cancer cells, or in contrast, from a fibrous or fatty part of the tissue where cancer cells are sparse. Working with *ex vivo* tumour explants also requires close communication between the operating room staff and the research lab where tissue explants are used. It happened more than once over the course of my work with patient MDTs that there was a change in the staff at the hospital, and we would not receive an appropriate portion of the tumour or we were forgotten during tissue processing in the pathology laboratory. Moreover, modelling the pharmacokinetics and pharmacodynamics (PK/PD) of treatments using *ex vivo* tumour explants is still not practical. The culture of tumour explants of multiple organs on-chip has been done, [84] paving the way for modelling drug distribution and multi-organ communication using *ex vivo* tissue models. However, the field is still not ready for PK/PD studies on tumour explants. Last but not the least, there is still limited though encouraging data to suggest that *ex vivo* platforms are a true reflection of responses seen in patients.

CHAPTER 7 CONCLUSION AND RECOMMENDATIONS

The aim of this project was to provide a versatile and high-throughput platform for drug screening on 3D tumour models. An open-space microfluidics tool, the PCD was used for this purpose. This is the first time that the PCD has been applied for processing 3D tumour tissues, and while initial proof of concept for the potential of the PCD as a drug screening tool is demonstrated, more work is required to prepare it for use in a clinical or industrial setting. This chapter gives recommendations on how to improve the PCD drug screening platform.

7.1 Recommendations

The first recommendation is regarding the size and number of fluidic pixels. The size and resolution of current PCDs are limited by the 3D printer in our laboratory, and while the throughput of the drug screening system is higher than chip-based systems, there is still room for improvement. A larger printer frame allows for a larger number of pixels, rendering the system even higher throughput. Making changes in the design of the PCD (e.g., size and number of the pixels) was largely facilitated by the previous work of Pierre-Alexandre Goyette on developing library components of script-assisted CAD designs for PCDs. The second recommendation for a future project is to determine the range of sizes and number of pixels that the PCD can create over tumour models without substantial changes in the system operation. In this thesis work, constant pixel size and number were used, and I did not determine the range of pixel size that can be created over 3D tumour models.

The next suggestion is to purchase a microscope with an incubation stage. The next big step in working with the PCD is to operate it over longer terms and in a biologically relevant environment. Once the microscope with the incubation stage is available, days-long experiments can be performed inside the CO_2 incubator. Longer-term experiments will require a more robust system, and better spillage control and waste management, especially when working with biohazards and

cytotoxic agents. Once the system is functional in a CO_2 incubator and over longer times, testing more biologically relevant drugs on MDTs are highly recommended. System automation needs some modifications too. Several modifications were made in this work to make the PCD drug screening platform more user-friendly, such as incorporating switch valves which enabled the rotation between reagents without the need to interrupt the system. PID controller and flow meters were also added. However, the long-term operation of the system is not optimized and needs further validation.

Regarding the tissue model, improvements are needed in the micro-dissection method. The dissection, while based on a previously established method, is tedious when hundreds of MDTs are needed. Automating the dissection method is an interesting, yet challenging future project.

Lastly, biobanking of tissue explants is vital to make working with *ex vivo* tumour explants more versatile. This is an ongoing project at the microfluidic core facility of the CRCHUM. Being able to conserve tissue explants over a long time, thaw, and re-culture them is an essential missing step in working with tumour tissue explants *ex vivo*.

7.2 Outlook

As *ex vivo* cultured tumour explants gain more and more attention as models for drug response assessment and personalized medicine, the need to develop drug screening tools for these tumour models becomes a high priority in cancer research. During this project, I worked with various modalities of *ex vivo* tumour culture, found the one that offers the longest *ex vivo* tissue survival (i.e., MDTs), and developed a functional system to manipulate these tumour models. My work involved designing and fabricating some of the microfluidic systems, analytical and numerical analysis of the survival of tumour tissues in culture, the experimental part of *ex vivo* tumour tissue culture, histopathology, image analysis, verification of the PCD and the diagnosis of parameters needed to adapt it for 3D tissue processes, and trial and error with the PCD system to prepare it for drug screening over MDTs. The results showing the superior *ex vivo* viability of MDTs generated great interest and further trust in the model system in our collaborators' laboratories at the CRCHUM and the University of Manitoba. Researchers are now using the chip-based MDT model system for experiments on various cancers, and different therapies including immunotherapy (Dr John Stagg, CRCHUM), oncolytic viruses (Dr Marie-Claude Bourgeois-Daigneault, CRCHUM),

and small molecules targeted therapy (Dr Mark Nachtigal, University of Manitoba). A spin-off company, MISO Chip Inc., is investigating the feasibility of their use in companion diagnostics test to improve treatments selection for cancer patients.

Once modifications to the PCD drug screening system are made to increase its robustness and user-friendliness, the system will be ready for higher throughput and more automated tests on MDTs and other 3D model systems. Multiple applications can be thought of, such as using the PCD drug screening platform for combinational drug screening to determine the synergistic effect of treatments. In conclusion, MDTs and the PCD system have been shown to form a potent drug screening assay that can follow the response of more than a hundred microtissues to treatments, in a multiplexed and dynamic manner. Because of the versatility of the PCD platform to process both MDTs and spheroids, I believe that the PCD drug screening platform can benefit and accelerate 3D tumour model research.

REFERENCES

[1] C. C. Society, "Canadian Cancer Society's Advisory Committe on Cancer Statistics," *Canadian Cancer Statistics 2021,* 2021.

[2] A. Chatterjee, S. Chilukuri, E. Fleming, A. Knepp, S. Rathore, and J. Zabinski, "Real-world evidence: Driving a new drug development paradigm in oncology," *Toronto, ON: McKinsey and Company,* 2018.

[3] N. L. Henry and D. F. Hayes, "Cancer biomarkers," *Molecular oncology,* vol. 6, no. 2, pp. 140-146, 2012.

[4] M. Hay, D. W. Thomas, J. L. Craighead, C. Economides, and J. Rosenthal, "Clinical development success rates for investigational drugs," *Nature biotechnology,* vol. 32, no. 1, pp. 40-51, 2014.

[5] M. Ibarrola-Villava, A. Cervantes, and A. Bardelli, "Preclinical models for precision oncology," *Biochimica et Biophysica Acta (BBA)-Reviews on Cancer,* vol. 1870, no. 2, pp. 239-246, 2018.

[6] S. Misra *et al.,* "Ex vivo organotypic culture system of precision-cut slices of human pancreatic ductal adenocarcinoma," *Scientific reports,* vol. 9, no. 1, p. 2133, 2019.

[7] Y. Imamura *et al.,* "Comparison of 2D-and 3D-culture models as drug-testing platforms in breast cancer," *Oncology reports,* vol. 33, no. 4, pp. 1837-1843, 2015.

[8] L. Figueiredo *et al.,* "Assessing glucose and oxygen diffusion in hydrogels for the rational design of 3D stem cell scaffolds in regenerative medicine," *Journal of tissue engineering and regenerative medicine,* vol. 12, no. 5, pp. 1238-1246, 2018.

[9] K. Ganesh *et al.,* "A rectal cancer organoid platform to study individual responses to chemoradiation," *Nature medicine,* vol. 25, no. 10, pp. 1607-1614, 2019.

[10] C. Y. Lim *et al.,* "Organotypic slice cultures of pancreatic ductal adenocarcinoma preserve the tumor microenvironment and provide a platform for drug response," *Pancreatology,* vol. 18, no. 8, pp. 913-927, 2018.

[11] V. Vaira *et al.,* "Preclinical model of organotypic culture for pharmacodynamic profiling of human tumors," *Proceedings of the National Academy of Sciences,* vol. 107, no. 18, pp. 8352-8356, 2010.

[12] I. R. Powley *et al.,* "Patient-derived explants (PDEs) as a powerful preclinical platform for anti-cancer drug and biomarker discovery," *British Journal of Cancer,* pp. 1-10, 2020.

[13] H. van der Kuip *et al.,* "Short term culture of breast cancer tissues to study the activity of the anticancer drug taxol in an intact tumor environment," *BMC cancer,* vol. 6, no. 1, p. 86, 2006.

[14] B. Majumder *et al.,* "Predicting clinical response to anticancer drugs using an ex vivo platform that captures tumour heterogeneity," *Nature communications,* vol. 6, no. 1, pp. 1-14, 2015.

[15] S. M. Hattersley, C. E. Dyer, J. Greenman, and S. J. Haswell, "Development of a microfluidic device for the maintenance and interrogation of viable tissue biopsies," *Lab on a Chip*, vol. 8, no. 11, pp. 1842-1846, 2008.

[16] M. Astolfi *et al.*, "Micro-dissected tumor tissues on chip: an ex vivo method for drug testing and personalized therapy," *Lab on a Chip*, vol. 16, no. 2, pp. 312-325, 2016.

[17] D. Dorrigiv *et al.*, "Microdissected Tissue vs. Tissue Slices—A Comparative Study of Tumor Explant Models Cultured On-Chip and Off-Chip," *Cancers*, vol. 13, no. 16, p. 4208, 2021.

[18] P.-A. Goyette, É. Boulais, F. Normandeau, G. Laberge, D. Juncker, and T. Gervais, "Microfluidic multipoles theory and applications," *Nature communications*, vol. 10, no. 1, pp. 1-10, 2019.

[19] G. V. Kaigala, R. D. Lovchik, and E. Delamarche, "Microfluidics in the "open space" for performing localized chemistry on biological interfaces," *Angewandte Chemie International Edition*, vol. 51, no. 45, pp. 11224-11240, 2012.

[20] P.-A. Goyette, É. Boulais, M. Tremblay, and T. Gervais, "Pixel-based open-space microfluidics for versatile surface processing," *Proceedings of the National Academy of Sciences*, vol. 118, no. 2, 2021.

[21] V. T. DeVita Jr and E. Chu, "A history of cancer chemotherapy," *Cancer research*, vol. 68, no. 21, pp. 8643-8653, 2008.

[22] R. Oun, Y. E. Moussa, and N. J. Wheate, "The side effects of platinum-based chemotherapy drugs: a review for chemists," *Dalton transactions*, vol. 47, no. 19, pp. 6645-6653, 2018.

[23] P. M. Carrera, H. M. Kantarjian, and V. S. Blinder, "The financial burden and distress of patients with cancer: understanding and stepping-up action on the financial toxicity of cancer treatment," *CA: a cancer journal for clinicians*, vol. 68, no. 2, pp. 153-165, 2018.

[24] M. Huang, A. Shen, J. Ding, and M. Geng, "Molecularly targeted cancer therapy: some lessons from the past decade," *Trends in pharmacological sciences*, vol. 35, no. 1, pp. 41-50, 2014.

[25] D. Longley and P. Johnston, "Molecular mechanisms of drug resistance," *The Journal of Pathology: A Journal of the Pathological Society of Great Britain and Ireland*, vol. 205, no. 2, pp. 275-292, 2005.

[26] D. Newell, "Getting the right dose in cancer chemotherapy–time to stop using surface area?," *British journal of cancer*, vol. 86, no. 8, pp. 1207-1208, 2002.

[27] I. Vitale, E. Shema, S. Loi, and L. Galluzzi, "Intratumoral heterogeneity in cancer progression and response to immunotherapy," *Nature medicine*, vol. 27, no. 2, pp. 212-224, 2021.

[28] F.-N. B. W. Group, "Susceptibility/Risk Biomarker," in *BEST (Biomarkers, EndpointS, and other Tools) Resource [Internet]*: Food and Drug Administration (US), 2020.

[29] K. Strimbu and J. A. Tavel, "What are biomarkers?," *Current Opinion in HIV and AIDS*, vol. 5, no. 6, p. 463, 2010.

[30] K. K. Jain, *Textbook of personalized medicine*. Springer, 2009.

[31] W. P. Carney, "HER2 status is an important biomarker in guiding personalized HER2 therapy," 2005.

[32] C. Oldenhuis, S. Oosting, J. Gietema, and E. De Vries, "Prognostic versus predictive value of biomarkers in oncology," *European journal of cancer,* vol. 44, no. 7, pp. 946-953, 2008.

[33] E. A. Mansfield, "FDA perspective on companion diagnostics: an evolving paradigm," *Clinical Cancer Research,* vol. 20, no. 6, pp. 1453-1457, 2014.

[34] S. Ahadian *et al.*, "Organ-On-A-Chip Platforms: A Convergence of Advanced Materials, Cells, and Microscale Technologies," *Advanced healthcare materials,* vol. 7, no. 2, p. 1700506, 2018.

[35] M. Ghandi *et al.*, "Next-generation characterization of the cancer cell line encyclopedia," *Nature,* vol. 569, no. 7757, pp. 503-508, 2019.

[36] M. Zanoni *et al.*, "3D tumor spheroid models for in vitro therapeutic screening: a systematic approach to enhance the biological relevance of data obtained," *Scientific reports,* vol. 6, p. 19103, 2016.

[37] T. Anada, J. Fukuda, Y. Sai, and O. Suzuki, "An oxygen-permeable spheroid culture system for the prevention of central hypoxia and necrosis of spheroids," *Biomaterials,* vol. 33, no. 33, pp. 8430-8441, 2012.

[38] S. Eetezadi, J. C. Evans, Y.-T. Shen, R. De Souza, M. Piquette-Miller, and C. Allen, "Ratio-Dependent Synergism of a Doxorubicin and Olaparib Combination in 2D and Spheroid Models of Ovarian Cancer," *Molecular pharmaceutics,* vol. 15, no. 2, pp. 472-485, 2018.

[39] T.-H. Kim, C. W. Mount, W. R. Gombotz, and S. H. Pun, "The delivery of doxorubicin to 3-D multicellular spheroids and tumors in a murine xenograft model using tumor-penetrating triblock polymeric micelles," *Biomaterials,* vol. 31, no. 28, pp. 7386-7397, 2010.

[40] K. J. Lampe, R. G. Mooney, K. B. Bjugstad, and M. J. Mahoney, "Effect of macromer weight percent on neural cell growth in 2D and 3D nondegradable PEG hydrogel culture," *Journal of Biomedical Materials Research Part A,* vol. 94, no. 4, pp. 1162-1171, 2010.

[41] S. A. Langhans, "Three-dimensional in vitro cell culture models in drug discovery and drug repositioning," *Frontiers in pharmacology,* vol. 9, p. 6, 2018.

[42] D. Tuveson and H. Clevers, "Cancer modeling meets human organoid technology," *Science,* vol. 364, no. 6444, pp. 952-955, 2019.

[43] H. Fan, U. Demirci, and P. Chen, "Emerging organoid models: leaping forward in cancer research," *Journal of hematology & oncology,* vol. 12, no. 1, pp. 1-10, 2019.

[44] G. Vlachogiannis *et al.*, "Patient-derived organoids model treatment response of metastatic gastrointestinal cancers," *Science,* vol. 359, no. 6378, pp. 920-926, 2018.

[45] O. Kopper *et al.*, "An organoid platform for ovarian cancer captures intra-and interpatient heterogeneity," *Nature medicine,* vol. 25, no. 5, pp. 838-849, 2019.

[46] N. Sachs *et al.*, "A living biobank of breast cancer organoids captures disease heterogeneity," *Cell,* vol. 172, no. 1-2, pp. 373-386. e10, 2018.

[47] M. Kim *et al.*, "Patient-derived lung cancer organoids as in vitro cancer models for therapeutic screening," *Nature communications*, vol. 10, no. 1, pp. 1-15, 2019.

[48] E. Driehuis, K. Kretzschmar, and H. Clevers, "Establishment of patient-derived cancer organoids for drug-screening applications," *Nature protocols*, vol. 15, no. 10, pp. 3380-3409, 2020.

[49] K. K. Dijkstra *et al.*, "Challenges in establishing pure lung cancer organoids limit their utility for personalized medicine," *Cell reports*, vol. 31, no. 5, p. 107588, 2020.

[50] W. Kim, Y. Gwon, S. Park, H. Kim, and J. Kim, "Therapeutic strategies of three-dimensional stem cell spheroids and organoids for tissue repair and regeneration," *Bioactive Materials*, vol. 19, pp. 50-74, 2023.

[51] K. Simeone *et al.*, "Paraffin-embedding lithography and micro-dissected tissue micro-arrays: tools for biological and pharmacological analysis of ex vivo solid tumors," *Lab on a Chip*, vol. 19, no. 4, pp. 693-705, 2019.

[52] R. K. Jain, "Transport of molecules in the tumor interstitium: a review," *Cancer research*, vol. 47, no. 12, pp. 3039-3051, 1987.

[53] M. Gerlach *et al.*, "Slice cultures from head and neck squamous cell carcinoma: a novel test system for drug susceptibility and mechanisms of resistance," *British journal of cancer*, vol. 110, no. 2, p. 479, 2014.

[54] N. Rousset, F. Monet, and T. Gervais, "Simulation-assisted design of microfluidic sample traps for optimal trapping and culture of non-adherent single cells, tissues, and spheroids," *Scientific reports*, vol. 7, no. 1, p. 245, 2017.

[55] K. A. Naipal *et al.*, "Tumor slice culture system to assess drug response of primary breast cancer," *BMC cancer*, vol. 16, no. 1, pp. 1-13, 2016.

[56] I. E. Carranza-Torres *et al.*, "Organotypic culture of breast tumor explants as a multicellular system for the screening of natural compounds with antineoplastic potential," *BioMed research international*, vol. 2015, 2015.

[57] E. J. Davies *et al.*, "Capturing complex tumour biology in vitro: histological and molecular characterisation of precision cut slices," *Scientific reports*, vol. 5, no. 1, pp. 1-17, 2015.

[58] J. Koerfer *et al.*, "Organotypic slice cultures of human gastric and esophagogastric junction cancer," *Cancer medicine*, vol. 5, no. 7, pp. 1444-1453, 2016.

[59] D. Behrens, W. Walther, and I. Fichtner, "Pancreatic cancer models for translational research," *Pharmacology & therapeutics*, vol. 173, pp. 146-158, 2017.

[60] J. J. Morton, G. Bird, Y. Refaeli, and A. Jimeno, "Humanized Mouse Xenograft Models: Narrowing the Tumor–Microenvironment GapHumanized Mouse Xenograft Models," *Cancer research*, vol. 76, no. 21, pp. 6153-6158, 2016.

[61] N. E. Sharpless and R. A. DePinho, "The mighty mouse: genetically engineered mouse models in cancer drug development," *Nature reviews Drug discovery*, vol. 5, no. 9, pp. 741-754, 2006.

[62] M. Simeoni *et al.*, "Predictive pharmacokinetic-pharmacodynamic modeling of tumor growth kinetics in xenograft models after administration of anticancer agents," *Cancer research*, vol. 64, no. 3, pp. 1094-1101, 2004.

[63] L. A. Kunz-Schughart, J. P. Freyer, F. Hofstaedter, and R. Ebner, "The use of 3-D cultures for high-throughput screening: the multicellular spheroid model," *Journal of biomolecular screening*, vol. 9, no. 4, pp. 273-285, 2004.

[64] A. Buqué and L. Galluzzi, "Modeling tumor immunology and immunotherapy in mice," *Trends in Cancer*, vol. 4, no. 9, pp. 599-601, 2018.

[65] A. Nyga, U. Cheema, and M. Loizidou, "3D tumour models: novel in vitro approaches to cancer studies," *Journal of cell communication and signaling*, vol. 5, no. 3, p. 239, 2011.

[66] C. L. Scott, H. J. Mackay, and P. Haluska Jr, "Patient-derived xenograft models in gynecologic malignancies," *American Society of Clinical Oncology Educational Book*, vol. 34, no. 1, pp. e258-e266, 2014.

[67] FDA, "List of Cleared or Approved Companion Diagnostic Devices (In Vitro and Imaging Tools)," *US Food & Drug administration (FDA)*, 2022. [Online]. Available: https://www.fda.gov/medical-devices/in-vitro-diagnostics/list-cleared-or-approved-companion-diagnostic-devices-in-vitro-and-imaging-tools.

[68] A. D. Puranik, H. R. Kulkarni, and R. P. Baum, "Companion diagnostics and molecular imaging," *The Cancer Journal*, vol. 21, no. 3, pp. 213-217, 2015.

[69] S. N. Bhatia and D. E. Ingber, "Microfluidic organs-on-chips," *Nature biotechnology*, vol. 32, no. 8, p. 760, 2014.

[70] D. An, K. Kim, and J. Kim, "Microfluidic system based high throughput drug screening system for curcumin/TRAIL combinational chemotherapy in human prostate cancer PC3 cells," *Biomolecules & therapeutics*, vol. 22, no. 4, p. 355, 2014.

[71] C. W. McAleer *et al.*, "Multi-organ system for the evaluation of efficacy and off-target toxicity of anticancer therapeutics," *Science translational medicine*, vol. 11, no. 497, p. eaav1386, 2019.

[72] K. Moshksayan *et al.*, "Spheroids-on-a-chip: Recent advances and design considerations in microfluidic platforms for spheroid formation and culture," *Sensors and Actuators B: Chemical*, vol. 263, pp. 151-176, 2018.

[73] B. Patra, C.-C. Peng, W.-H. Liao, C.-H. Lee, and Y.-C. Tung, "Drug testing and flow cytometry analysis on a large number of uniform sized tumor spheroids using a microfluidic device," *Scientific reports*, vol. 6, p. 21061, 2016.

[74] M. Bavoux *et al.*, "X-ray on chip: Quantifying therapeutic synergies between radiotherapy and anticancer drugs using soft tissue sarcoma tumor spheroids," *Radiotherapy and Oncology*, vol. 157, pp. 175-181, 2021.

[75] H. Lu, L. Noorani, Y. Jiang, A. W. Du, and M. H. Stenzel, "Penetration and drug delivery of albumin nanoparticles into pancreatic multicellular tumor spheroids," *Journal of Materials Chemistry B*, vol. 5, no. 48, pp. 9591-9599, 2017.

[76] M. Marimuthu *et al.*, "Multi-size spheroid formation using microfluidic funnels," *Lab on a Chip*, vol. 18, no. 2, pp. 304-314, 2018.

[77] E. Refet-Mollof *et al.*, "Hypoxic Jumbo Spheroids On-A-Chip (HOnAChip): Insights into Treatment Efficacy," *Cancers,* vol. 13, no. 16, p. 4046, 2021.

[78] L. F. Horowitz *et al.*, "Microdissected “cuboids” for microfluidic drug testing of intact tissues," *Lab on a Chip,* vol. 21, no. 1, pp. 122-142, 2021.

[79] Y.-C. Chen, X. Lou, Z. Zhang, P. Ingram, and E. Yoon, "High-throughput cancer cell sphere formation for characterizing the efficacy of photo dynamic therapy in 3D cell cultures," *Scientific reports,* vol. 5, p. 12175, 2015.

[80] A. Richardson, L. A. Schwerdtfeger, D. Eaton, I. Mclean, C. S. Henry, and S. A. Tobet, "A microfluidic organotypic device for culture of mammalian intestines ex vivo," *Analytical Methods,* vol. 12, no. 3, pp. 297-303, 2020.

[81] A. Riley *et al.*, "A novel microfluidic device capable of maintaining functional thyroid carcinoma specimens ex vivo provides a new drug screening platform," *BMC cancer,* vol. 19, no. 1, p. 259, 2019.

[82] V. Green *et al.*, "A novel microfluidic device capable of maintaining functional thyroid carcinoma," *BMC cancer,* vol. 19, 2019.

[83] J. H. Hammel, S. R. Cook, M. C. Belanger, J. M. Munson, and R. R. Pompano, "Modeling Immunity In Vitro: Slices, Chips, and Engineered Tissues," *Annual review of biomedical engineering,* vol. 23, pp. 461-491, 2021.

[84] S. Shim, M. C. Belanger, A. R. Harris, J. M. Munson, and R. R. Pompano, "Two-way communication between ex vivo tissues on a microfluidic chip: Application to tumor–lymph node interaction," *Lab on a Chip,* vol. 19, no. 6, pp. 1013-1026, 2019.

[85] S. Takayama, E. Ostuni, P. LeDuc, K. Naruse, D. E. Ingber, and G. M. Whitesides, "Laminar flows: subcellular positioning of small molecules," *Nature,* vol. 411, no. 6841, p. 1016, 2001.

[86] S. Takayama, E. Ostuni, P. LeDuc, K. Naruse, D. E. Ingber, and G. M. Whitesides, "Selective chemical treatment of cellular microdomains using multiple laminar streams," *Chemistry & biology,* vol. 10, no. 2, pp. 123-130, 2003.

[87] C.-H. Hsu, C. Chen, and A. Folch, "“Microcanals” for micropipette access to single cells in microfluidic environments," *Lab on a Chip,* vol. 4, no. 5, pp. 420-424, 2004.

[88] T. C. Chang, A. M. Mikheev, W. Huynh, R. J. Monnat, R. C. Rostomily, and A. Folch, "Parallel microfluidic chemosensitivity testing on individual slice cultures," *Lab on a Chip,* vol. 14, no. 23, pp. 4540-4551, 2014.

[89] L. Ying *et al.*, "The scanned nanopipette: a new tool for high resolution bioimaging and controlled deposition of biomolecules," *Physical chemistry chemical physics,* vol. 7, no. 15, pp. 2859-2866, 2005.

[90] A. Bruckbauer *et al.*, "Writing with DNA and protein using a nanopipet for controlled delivery," *Journal of the American Chemical Society,* vol. 124, no. 30, pp. 8810-8811, 2002.

[91] D. Chen *et al.*, "The chemistrode: a droplet-based microfluidic device for stimulation and recording with high temporal, spatial, and chemical resolution," *Proceedings of the National Academy of Sciences,* vol. 105, no. 44, pp. 16843-16848, 2008.

[92] A. Meister *et al.*, "FluidFM: combining atomic force microscopy and nanofluidics in a universal liquid delivery system for single cell applications and beyond," *Nano letters,* vol. 9, no. 6, pp. 2501-2507, 2009.

[93] P. Dörig *et al.*, "Force-controlled spatial manipulation of viable mammalian cells and micro-organisms by means of FluidFM technology," *Applied Physics Letters,* vol. 97, no. 2, p. 023701, 2010.

[94] O. Guillaume-Gentil, E. Potthoff, D. Ossola, C. M. Franz, T. Zambelli, and J. A. Vorholt, "Force-controlled manipulation of single cells: from AFM to FluidFM," *Trends in biotechnology,* vol. 32, no. 7, pp. 381-388, 2014.

[95] M. A. Qasaimeh, S. G. Ricoult, and D. Juncker, "Microfluidic probes for use in life sciences and medicine," *Lab on a Chip,* vol. 13, no. 1, pp. 40-50, 2013.

[96] D. Juncker, H. Schmid, and E. Delamarche, "Multipurpose microfluidic probe," *Nature materials,* vol. 4, no. 8, p. 622, 2005.

[97] A. Sarkar, S. Kolitz, D. A. Lauffenburger, and J. Han, "Microfluidic probe for single-cell analysis in adherent tissue culture," *Nature communications,* vol. 5, p. 3421, 2014.

[98] A. Brimmo, P.-A. Goyette, R. Alnemari, T. Gervais, and M. A. Qasaimeh, "3D Printed Microfluidic Probes," *Scientific reports,* vol. 8, no. 1, p. 10995, 2018.

[99] É. Boulais and T. Gervais, "Hele-Shaw Flow Theory in the Context of Open Microfluidics: From Dipoles to Quadrupoles," *Open-Space Microfluidics: Concepts, Implementations, Applications,* 2018.

[100] M. A. Qasaimeh, T. Gervais, and D. Juncker, "Microfluidic quadrupole and floating concentration gradient," *Nature communications,* vol. 2, no. 1, pp. 1-8, 2011.

[101] M. Safavieh, M. A. Qasaimeh, A. Vakil, D. Juncker, and T. Gervais, "Two-aperture microfluidic probes as flow dipoles: Theory and applications," *Scientific reports,* vol. 5, no. 1, pp. 1-16, 2015.

[102] G. C. Jayson, E. C. Kohn, H. C. Kitchener, and J. A. Ledermann, "Ovarian cancer," *The Lancet,* vol. 384, no. 9951, pp. 1376-1388, 2014.

[103] L. R. Boyd and F. M. Muggia, "Carboplatin/paclitaxel induction in ovarian cancer: the finer points," *Oncology (08909091),* vol. 32, no. 8, 2018.

[104] A. Du Bois *et al.*, "A randomized clinical trial of cisplatin/paclitaxel versus carboplatin/paclitaxel as first-line treatment of ovarian cancer," *Journal of the National Cancer Institute,* vol. 95, no. 17, pp. 1320-1329, 2003.

[105] V. Samouelian *et al.*, "Chemosensitivity and radiosensitivity profiles of four new human epithelial ovarian cancer cell lines exhibiting genetic alterations in BRCA2, TGFβ-RII, KRAS2, TP53 and/or CDNK2A," *Cancer chemotherapy and pharmacology,* vol. 54, no. 6, pp. 497-504, 2004.

[106] E. Franzese *et al.*, "PARP inhibitors in ovarian cancer," *Cancer treatment reviews,* 2018.

[107] F. Ricci, M. Broggini, and G. Damia, "Revisiting ovarian cancer preclinical models: implications for a better management of the disease," *Cancer treatment reviews,* vol. 39, no. 6, pp. 561-568, 2013.

[108] T. Das *et al.*, "Empirical chemosensitivity testing in a spheroid model of ovarian cancer using a microfluidics-based multiplex platform," *Biomicrofluidics,* vol. 7, no. 1, p. 011805, 2013.

[109] S.-S. Li *et al.*, "Modeling ovarian cancer multicellular spheroid behavior in a dynamic 3D peritoneal microdevice," *JoVE (Journal of Visualized Experiments),* no. 120, p. e55337, 2017.

[110] L. I. Ibrahim, C. Hajal, G. S. Offeddu, M. R. Gillrie, and R. D. Kamm, "Omentum-on-a-chip: A multicellular, vascularized microfluidic model of the human peritoneum for the study of ovarian cancer metastases," *Biomaterials,* vol. 288, p. 121728, 2022.

[111] M. N. Brodeur *et al.*, "Carboplatin response in preclinical models for ovarian cancer: comparison of 2D monolayers, spheroids, ex vivo tumors and in vivo models," *Scientific reports,* vol. 11, no. 1, pp. 1-12, 2021.

[112] C. H. Wong, K. W. Siah, and A. W. Lo, "Estimation of clinical trial success rates and related parameters," *Biostatistics,* vol. 20, no. 2, pp. 273-286, 2019.

[113] A. P. Feinberg and B. Tycko, "The history of cancer epigenetics," *Nature Reviews Cancer,* vol. 4, no. 2, pp. 143-153, 2004.

[114] L. A. Loeb, K. R. Loeb, and J. P. Anderson, "Multiple mutations and cancer," *Proceedings of the National Academy of Sciences,* vol. 100, no. 3, pp. 776-781, 2003.

[115] A. P. Feinberg, R. Ohlsson, and S. Henikoff, "The epigenetic progenitor origin of human cancer," *Nature reviews genetics,* vol. 7, no. 1, pp. 21-33, 2006.

[116] Y.-C. Tung, A. Y. Hsiao, S. G. Allen, Y.-s. Torisawa, M. Ho, and S. Takayama, "High-throughput 3D spheroid culture and drug testing using a 384 hanging drop array," *Analyst,* vol. 136, no. 3, pp. 473-478, 2011.

[117] J. Jung, H. S. Seol, and S. Chang, "The generation and application of patient-derived xenograft model for cancer research," *Cancer research and treatment: official journal of Korean Cancer Association,* vol. 50, no. 1, p. 1, 2018.

[118] H. Clevers, "Modeling development and disease with organoids," *Cell,* vol. 165, no. 7, pp. 1586-1597, 2016.

[119] M. van de Wetering *et al.*, "Prospective derivation of a living organoid biobank of colorectal cancer patients," *Cell,* vol. 161, no. 4, pp. 933-945, 2015.

[120] T. G. Meijer, K. A. Naipal, A. Jager, and D. C. van Gent, "Ex vivo tumor culture systems for functional drug testing and therapy response prediction," *Future science OA,* vol. 3, no. 2, p. FSO190, 2017.

[121] M. C. Belanger *et al.*, "Acute lymph node slices are a functional model system to study immunity ex vivo," *ACS Pharmacology & Translational Science,* vol. 4, no. 1, pp. 128-142, 2021.

[122] L. Vesci *et al.*, "Trastuzumab and docetaxel in a preclinical organotypic breast cancer model using tissue slices from mammary fat pad: Translational relevance Corrigendum in/or/35/1/602," *Oncology reports,* vol. 34, no. 3, pp. 1146-1152, 2015.

[123] P. M. van Midwoud, M. T. Merema, E. Verpoorte, and G. M. Groothuis, "A microfluidic approach for in vitro assessment of interorgan interactions in drug metabolism using intestinal and liver slices," *Lab on a Chip,* vol. 10, no. 20, pp. 2778-2786, 2010.

[124] P. M. Van Midwoud, G. M. Groothuis, M. T. Merema, and E. Verpoorte, "Microfluidic biochip for the perifusion of precision-cut rat liver slices for metabolism and toxicology studies," *Biotechnology and bioengineering,* vol. 105, no. 1, pp. 184-194, 2010.

[125] A. Sontheimer-Phelps, B. A. Hassell, and D. E. Ingber, "Modelling cancer in microfluidic human organs-on-chips," *Nature Reviews Cancer,* vol. 19, no. 2, pp. 65-81, 2019.

[126] A. B. Holton, F. L. Sinatra, J. Kreahling, A. J. Conway, D. A. Landis, and S. Altiok, "Microfluidic biopsy trapping device for the real-time monitoring of tumor microenvironment," *PLoS One,* vol. 12, no. 1, p. e0169797, 2017.

[127] F. Eduati *et al.*, "A microfluidics platform for combinatorial drug screening on cancer biopsies," *Nature communications,* vol. 9, no. 1, pp. 1-13, 2018.

[128] L. F. Horowitz *et al.*, "Multiplexed drug testing of tumor slices using a microfluidic platform," *NPJ Precision Oncology,* vol. 4, no. 1, pp. 1-15, 2020.

[129] M.-C. Kim, R. H. Lam, T. Thorsen, and H. H. Asada, "Mathematical analysis of oxygen transfer through polydimethylsiloxane membrane between double layers of cell culture channel and gas chamber in microfluidic oxygenator," *Microfluidics and Nanofluidics,* vol. 15, no. 3, pp. 285-296, 2013.

[130] R. Sorensen and N. Novak, "The use of Michaelis-Menten kinetics in cell biology and physiology teaching laboratories," *Biochemical Education,* vol. 24, no. 1, pp. 26-28, 1996.

[131] A. Al-Ani, D. Toms, D. Kondro, J. Thundathil, Y. Yu, and M. Ungrin, "Oxygenation in cell culture: Critical parameters for reproducibility are routinely not reported," *PLoS One,* vol. 13, no. 10, p. e0204269, 2018.

[132] R. H. Wenger, V. Kurtcuoglu, C. C. Scholz, H. H. Marti, and D. Hoogewijs, "Frequently asked questions in hypoxia research," *Hypoxia,* vol. 3, p. 35, 2015.

[133] M. Hockel and P. Vaupel, "Tumor hypoxia: definitions and current clinical, biologic, and molecular aspects," *Journal of the National Cancer Institute,* vol. 93, no. 4, pp. 266-276, 2001.

[134] I. Labouba *et al.*, "Potential Cross-Talk between Alternative and Classical NF-κB Pathways in Prostate Cancer Tissues as Measured by a Multi-Staining Immunofluorescence Co-Localization Assay," *PLoS One,* vol. 10, no. 7, p. e0131024, 2015.

[135] M. F. Molina *et al.*, *Visualization, Quantification, and Mapping of Immune Cell Populations in the Tumor Microenvironment*. MyJoVE Corporation, 2016.

[136] R. Adigun, H. Basit, and J. Murray, "Necrosis, cell (liquefactive, coagulative, caseous, fat, fibrinoid, and gangrenous)," *StatPearls [Internet]*, 2019.

[137] R. A. Caruso *et al.*, "Mechanisms of coagulative necrosis in malignant epithelial tumors," *Oncology letters,* vol. 8, no. 4, pp. 1397-1402, 2014.

[138] N. K. Tafreshi *et al.*, "Evaluation of CAIX and CAXII expression in breast cancer at varied O 2 levels: CAIX is the superior surrogate imaging biomarker of tumor hypoxia," *Molecular imaging and biology,* vol. 18, no. 2, pp. 219-231, 2016.

[139] J. Tostain, G. Li, A. Gentil-Perret, and M. Gigante, "Carbonic anhydrase 9 in clear cell renal cell carcinoma: a marker for diagnosis, prognosis and treatment," *European journal of cancer,* vol. 46, no. 18, pp. 3141-3148, 2010.

[140] E. J. Moon, D. M. Brizel, J. T. A. Chi, and M. W. Dewhirst, "The potential role of intrinsic hypoxia markers as prognostic variables in cancer," *Antioxidants & redox signaling,* vol. 9, no. 8, pp. 1237-1294, 2007.

[141] P. A. Schornack and R. J. Gillies, "Contributions of cell metabolism and H+ diffusion to the acidic pH of tumors," *Neoplasia,* vol. 5, no. 2, pp. 135-145, 2003.

[142] S. E. Rademakers, J. Lok, A. J. van der Kogel, J. Bussink, and J. H. Kaanders, "Metabolic markers in relation to hypoxia; staining patterns and colocalization of pimonidazole, HIF-1α, CAIX, LDH-5, GLUT-1, MCT1 and MCT4," *BMC cancer,* vol. 11, no. 1, pp. 1-10, 2011.

[143] K. H. Shin *et al.*, "Detecting changes in tumor hypoxia with carbonic anhydrase IX and pimonidazole," *Cancer biology & therapy,* vol. 6, no. 1, pp. 70-75, 2007.

[144] K. J. Williams, C. A. Parker, and I. J. Stratford, "Exogenous and Endogenous Markers of Tumour Oxygenation Status," *Oxygen Transport to Tissue XXVI,* pp. 285-294, 2005.

[145] W. Wang *et al.*, "Microarray profiling shows distinct differences between primary tumors and commonly used preclinical models in hepatocellular carcinoma," *BMC cancer,* vol. 15, no. 1, pp. 1-10, 2015.

[146] I. W. Mak, N. Evaniew, and M. Ghert, "Lost in translation: animal models and clinical trials in cancer treatment," *American journal of translational research,* vol. 6, no. 2, p. 114, 2014.

[147] C. G. Begley and L. M. Ellis, "Raise standards for preclinical cancer research," *Nature,* vol. 483, no. 7391, pp. 531-533, 2012.

[148] S. E. Gould, M. R. Junttila, and F. J. de Sauvage, "Translational value of mouse models in oncology drug development," *Nature medicine,* vol. 21, no. 5, pp. 431-439, 2015.

[149] D. R. Grimes, A. G. Fletcher, and M. Partridge, "Oxygen consumption dynamics in steady-state tumour models," *Royal Society open science,* vol. 1, no. 1, p. 140080, 2014.

[150] A. M. Shannon, D. J. Bouchier-Hayes, C. M. Condron, and D. Toomey, "Tumour hypoxia, chemotherapeutic resistance and hypoxia-related therapies," *Cancer treatment reviews,* vol. 29, no. 4, pp. 297-307, 2003.

[151] J. M. Brown and W. R. Wilson, "Exploiting tumour hypoxia in cancer treatment," *Nature Reviews Cancer,* vol. 4, no. 6, p. 437, 2004.

[152] A. I. Minchinton and I. F. Tannock, "Drug penetration in solid tumours," *Nature Reviews Cancer,* vol. 6, no. 8, pp. 583-592, 2006.

[153] P. A. Wijeratne and V. Vavourakis, "A quantitative in silico platform for simulating cytotoxic and nanoparticle drug delivery to solid tumours," *Interface focus,* vol. 9, no. 3, p. 20180063, 2019.

[154] A. Riley *et al.*, "A novel microfluidic device capable of maintaining functional thyroid carcinoma specimens ex vivo provides a new drug screening platform," *BMC cancer,* vol. 19, no. 1, pp. 1-13, 2019.

[155] M. G. Muraro *et al.*, "Ex-vivo assessment of drug response on breast cancer primary tissue with preserved microenvironments," *Oncoimmunology,* vol. 6, no. 7, p. e1331798, 2017.

[156] A. Mullard, "Parsing clinical success rates," *Nature Reviews Drug Discovery,* vol. 15, no. 7, pp. 447-448, 2016.

[157] R. Z. Lin and H. Y. Chang, "Recent advances in three-dimensional multicellular spheroid culture for biomedical research," *Biotechnology Journal: Healthcare Nutrition Technology,* vol. 3, no. 9-10, pp. 1172-1184, 2008.

[158] E. T. Verjans, J. Doijen, W. Luyten, B. Landuyt, and L. Schoofs, "Three-dimensional cell culture models for anticancer drug screening: Worth the effort?," *Journal of cellular physiology,* vol. 233, no. 4, pp. 2993-3003, 2018.

[159] F. Helmchen and W. Denk, "Deep tissue two-photon microscopy," *Nature methods,* vol. 2, no. 12, pp. 932-940, 2005.

[160] M. N. Gurcan, L. E. Boucheron, A. Can, A. Madabhushi, N. M. Rajpoot, and B. Yener, "Histopathological image analysis: A review," *IEEE reviews in biomedical engineering,* vol. 2, pp. 147-171, 2009.

[161] S. H. Gehrke, J. P. Fisher, M. Palasis, and M. E. Lund, "Factors determining hydrogel permeability," *Annals of the New York Academy of Sciences,* vol. 831, pp. 179-207, 1997.

[162] S. Ramanujan, A. Pluen, T. D. McKee, E. B. Brown, Y. Boucher, and R. K. Jain, "Diffusion and convection in collagen gels: implications for transport in the tumor interstitium," *Biophysical journal,* vol. 83, no. 3, pp. 1650-1660, 2002.

[163] A. Dawson *et al.*, "A microfluidic chip based model for the study of full thickness human intestinal tissue using dual flow," *Biomicrofluidics,* vol. 10, no. 6, p. 064101, 2016.

[164] L.-T. Cheah *et al.*, "Microfluidic perfusion system for maintaining viable heart tissue with real-time electrochemical monitoring of reactive oxygen species," *Lab on a Chip,* vol. 10, no. 20, pp. 2720-2726, 2010.

[165] A. Sarkar, S. Kolitz, D. A. Lauffenburger, and J. Han, "Microfluidic probe for single-cell analysis in adherent tissue culture," *Nature communications,* vol. 5, no. 1, pp. 1-8, 2014.

[166] A. T. Brimmo, A. Menachery, and M. A. Qasaimeh, "Microelectrofluidic probe for sequential cell separation and patterning," *Lab on a Chip,* vol. 19, no. 24, pp. 4052-4063, 2019.

[167] A. Kashyap, J. Autebert, E. Delamarche, and G. V. Kaigala, "Selective local lysis and sampling of live cells for nucleic acid analysis using a microfluidic probe," *Scientific reports,* vol. 6, no. 1, pp. 1-10, 2016.

[168] A. Queval *et al.*, "Chamber and microfluidic probe for microperfusion of organotypic brain slices," *Lab on a Chip,* vol. 10, no. 3, pp. 326-334, 2010.

[169] R. D. Lovchik, G. V. Kaigala, M. Georgiadis, and E. Delamarche, "Micro-immunohistochemistry using a microfluidic probe," *Lab on a Chip,* vol. 12, no. 6, pp. 1040-1043, 2012.

[170] X. Li *et al.*, "An integrated microfluidic probe for mass spectrometry imaging of biological samples," *Angewandte Chemie,* vol. 132, no. 50, pp. 22574-22577, 2020.

[171] E. Boulais and T. Gervais, "Two-dimensional convection–diffusion in multipolar flows with applications in microfluidics and groundwater flow," *Physics of Fluids,* vol. 32, no. 12, p. 122001, 2020.

[172] K. W. Bong, S. C. Chapin, D. C. Pregibon, D. Baah, T. M. Floyd-Smith, and P. S. Doyle, "Compressed-air flow control system," *Lab on a Chip,* vol. 11, no. 4, pp. 743-747, 2011.

[173] W. Zeng, S. Li, and Z. Wang, "Characterization of syringe-pump-driven versus pressure-driven microfluidic flows," in *2015 International Conference on Fluid Power and Mechatronics (FPM)*, 2015: IEEE, pp. 711-715.

[174] D. Di Carlo, L. Y. Wu, and L. P. Lee, "Dynamic single cell culture array," *Lab on a Chip,* vol. 6, no. 11, pp. 1445-1449, 2006.

[175] B. Kwak, Y. Lee, J. Lee, S. Lee, and J. Lim, "Mass fabrication of uniform sized 3D tumor spheroid using high-throughput microfluidic system," *Journal of controlled release,* vol. 275, pp. 201-207, 2018.

[176] Y. Sakai and K. Nakazawa, "Technique for the control of spheroid diameter using microfabricated chips," *Acta biomaterialia,* vol. 3, no. 6, pp. 1033-1040, 2007.

[177] Y. Wang *et al.*, "Spheroid formation of hepatocarcinoma cells in microwells: experiments and Monte Carlo simulations," *PloS one,* vol. 11, no. 8, p. e0161915, 2016.

[178] N. Azizipour, R. Avazpour, M. Sawan, A. Ajji, and D. H. Rosenzweig, "Surface Optimization and Design Adaptation toward Spheroid Formation On-Chip," *Sensors,* vol. 22, no. 9, p. 3191, 2022.

[179] M. V. Jones and P. A. Calabresi, "Agar-gelatin for embedding tissues prior to paraffin processing," *Biotechniques,* vol. 42, no. 5, pp. 569-570, 2007.

[180] C. M. Annunziata *et al.*, "Nuclear factor κB transcription factors are coexpressed and convey a poor outcome in ovarian cancer," *Cancer,* vol. 116, no. 13, pp. 3276-3284, 2010.

[181] K. S. Ahn and B. B. Aggarwal, "Transcription factor NF-κB: a sensor for smoke and stress signals," *Annals of the new York Academy of Sciences,* vol. 1056, no. 1, pp. 218-233, 2005.

[182] O. Maguire, C. Collins, K. O'Loughlin, J. Miecznikowski, and H. Minderman, "Quantifying nuclear p65 as a parameter for NF-κB activation: Correlation between ImageStream cytometry, microscopy, and Western blot," *Cytometry Part A,* vol. 79, no. 6, pp. 461-469, 2011.

[183] C. E. Badr, J. M. Niers, L.-A. Tjon-Kon-Fat, D. P. Noske, T. Wurdinger, and B. A. Tannous, "Real-time monitoring of nuclear factor κB activity in cultured cells and in animal models," *Molecular imaging,* vol. 8, no. 5, p. 7290.2009. 00026, 2009.

[184] B. Péant *et al.*, "Regulation of IκB kinase ε expression by the androgen receptor and the nuclear factor-κB transcription factor in prostate cancer," *Molecular cancer research,* vol. 5, no. 1, pp. 87-94, 2007.

[185] V. Kocbek, S. Imboden, K. Nirgianakis, M. Mueller, and B. McKinnon, "Dual influence of TNFα on diverse in vitro models of ovarian cancer subtypes," *Heliyon,* vol. 7, no. 2, p. e06099, 2021.

[186] Y. Figenschau, B. Sveinbjörnsson, and K. Bertheussen, "Improvement of a cytokine (TNF-α) bioassay by serum-free target cell (WEHI 164) cultivation," *Cytotechnology,* vol. 29, no. 2, pp. 121-134, 1999.

[187] L. Sun, G. Yang, M. Zaidi, and J. Iqbal, "TNF-induced gene expression oscillates in time," *Biochemical and biophysical research communications,* vol. 371, no. 4, pp. 900-905, 2008.

[188] D. Dorrigiv *et al.*, "Microdissected Tissue vs Tissue Slices—A Comparative Study of Tumor Explant Models Cultured On-Chip and Off-Chip," *Cancers,* vol. 13, no. 16, p. 4208, 2021.

[189] J. J. Casciari, S. V. Sotirchos, and R. M. Sutherland, "Variations in tumor cell growth rates and metabolism with oxygen concentration, glucose concentration, and extracellular pH," *Journal of cellular physiology,* vol. 151, no. 2, pp. 386-394, 1992.

[190] M. Cahuzac, P. Langlois, B. Péant, H. Fleury, A.-M. Mes-Masson, and F. Saad, "Pre-activation of autophagy impacts response to olaparib in prostate cancer cells," *Communications biology,* vol. 5, no. 1, pp. 1-14, 2022.

[191] J. Schindelin *et al.*, "Fiji: an open-source platform for biological-image analysis," *Nature methods,* vol. 9, no. 7, pp. 676-682, 2012.

[192] P. Horvath *et al.*, "Screening out irrelevant cell-based models of disease," *Nature reviews Drug discovery,* vol. 15, no. 11, pp. 751-769, 2016.

[193] K. S. Smalley, N. K. Haass, P. A. Brafford, M. Lioni, K. T. Flaherty, and M. Herlyn, "Multiple signaling pathways must be targeted to overcome drug resistance in cell lines derived from melanoma metastases," *Molecular cancer therapeutics,* vol. 5, no. 5, pp. 1136-1144, 2006.

[194] N. Falkenberg *et al.*, "Three-dimensional microtissues essentially contribute to preclinical validations of therapeutic targets in breast cancer," *Cancer medicine,* vol. 5, no. 4, pp. 703-710, 2016.

[195] J. L. Teh *et al.*, "Rapid spheroid assays in a 3-dimensional cell culture chip," *BMC research notes,* vol. 14, no. 1, pp. 1-6, 2021.

[196] H. L. Lanz *et al.*, "Therapy response testing of breast cancer in a 3D high-throughput perfused microfluidic platform," *BMC cancer,* vol. 17, no. 1, pp. 1-11, 2017.

[197] T. L. Place, F. E. Domann, and A. J. Case, "Limitations of oxygen delivery to cells in culture: An underappreciated problem in basic and translational research," *Free Radical Biology and Medicine,* vol. 113, pp. 311-322, 2017.

[198] O. Ariga, T. Kubo, and Y. Sano, "Effective diffusivity of glucose in PVA hydrogel," *Journal of fermentation and bioengineering,* vol. 78, no. 2, pp. 200-201, 1994.

[199] D. A. Markov, E. M. Lillie, S. P. Garbett, and L. J. McCawley, "Variation in diffusion of gases through PDMS due to plasma surface treatment and storage conditions," *Biomedical microdevices,* vol. 16, no. 1, pp. 91-96, 2014.

[200] S. Chowdhury, V. R. Bhethanabotla, and R. Sen, "Measurement of oxygen diffusivity and permeability in polymers using fluorescence microscopy," *Microscopy and Microanalysis,* vol. 16, no. 6, pp. 725-734, 2010.

[201] K. Hicks, S. Ohms, P. Van Zijl, W. Denny, P. Hunter, and W. Wilson, "An experimental and mathematical model for the extravascular transport of a DNA intercalator in tumours," *British journal of cancer,* vol. 76, no. 7, pp. 894-903, 1997.

[202] F. B. Pruijn, K. Patel, M. P. Hay, W. R. Wilson, and K. O. Hicks, "Prediction of tumour tissue diffusion coefficients of hypoxia-activated prodrugs from physicochemical parameters," *Australian journal of Chemistry,* vol. 61, no. 9, pp. 687-693, 2008.

[203] H. E. Abaci, R. Truitt, S. Tan, and S. Gerecht, "Unforeseen decreases in dissolved oxygen levels affect tube formation kinetics in collagen gels," *American Journal of Physiology-Cell Physiology,* vol. 301, no. 2, pp. C431-C440, 2011.

[204] D. Y. Arifin, K. Y. T. Lee, and C.-H. Wang, "Chemotherapeutic drug transport to brain tumor," *Journal of controlled release,* vol. 137, no. 3, pp. 203-210, 2009.

[205] J. Matschullat, "Basin Analysis. Principles and Applications," *Journal of Soils and Sediments,* vol. 5, no. 3, p. 191, 2005.

[206] I. Pereiro, A. F. Khartchenko, L. Petrini, and G. V. Kaigala, "Nip the bubble in the bud: a guide to avoid gas nucleation in microfluidics," *Lab on a Chip,* vol. 19, no. 14, pp. 2296-2314, 2019.

Appendix A the image analysis methodology

Visiomorph™ image analysis software was used throughout this work to quantify the expression of biomarkers in immunofluorescent staining of tumour tissues. The software provides a user-friendly interface to analyze the IF staining using common methods for digital image analysis, such as image segmentation. Various algorithms can be developed or purchased in the Visiomorph™ environment to quantify biomarkers. It is also possible to produce several readouts of each image, for example, the number or area of cells, or the fluorescent intensity can be measured. In his thesis work, I developed simple algorithms that use thresholding to differentiate fluorophores. I measured cell count, area, and mean fluorescent intensity, but used the area of cells/markers to perform the analysis, since cell count was not possible for some tissues (e.g., where cells are very close), and fluorescent intensities seemed to vary between different batches of IF staining. The stepwise image analysis protocol to quantify Ki67 as an example is presented here.

1) Core detection
    a) Tissue core detection from the background
    b) Measuring the area of the tissue core
2) Tumour-stroma separation
    a) Detection of the epithelial marker by identifying the fluorophore tagged to cytokeratin and human anti-mitochondrial antibody.
    b) 2) Measuring the area, cell count, and fluorescent intensity of the epithelium in tissue core
3) Nuclei detection
    a) Detection of nuclei of tumour cells in the region detected in step 2
    b) Measuring the area, cell count, and fluorescent intensity of the nuclei
4) Ki 67 detection (Ki67 is a nuclear protein)
    a) Detection of Ki67 in nuclei detected in step 3
    b) Measuring the area, cell count, and fluorescent intensity of the Ki67 expressing nuclei

To perform the analysis, the percentage of Ki67 expressing nuclei (4-b) among the total area of cancer cells (2-b) is assessed

A similar protocol can be used for quantification of other markers, based on their expression location. Figure 0-1 summarizes the image analysis protocol.

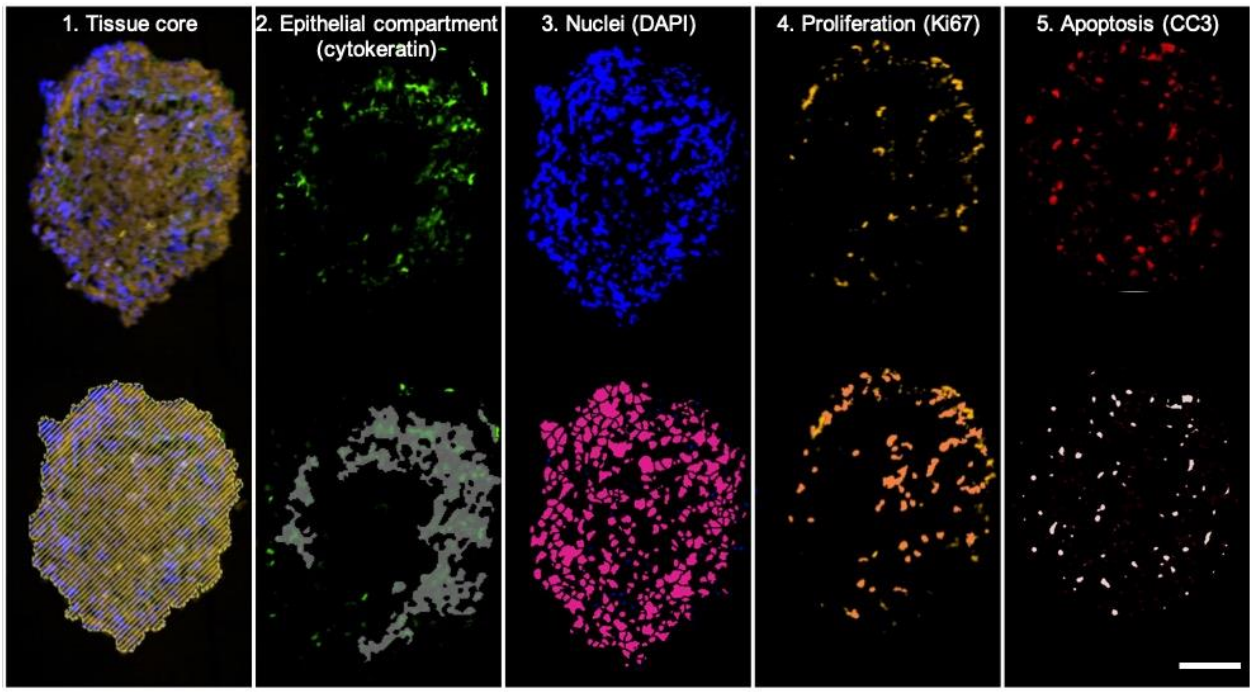

Figure 0-1 Quantification of biomarkers in an immunofluorescent staining of an MDT. Scale bar= 100 µm

Appendix B List of contributions

Articles

1. **Dina Dorrigiv,** Kayla Simeone, Laudine Communal, Jennifer Kendall-Dupont, Amélie St-Georges-Robillard, Benjamin Péant, Euridice Carmona, Anne-Marie Mes-Masson, and Thomas Gervais, "Microdissected Tissue vs. Tissue Slices—A Comparative Study of Tumor Explant Models Cultured On-Chip and Off-Chip," *Cancers*, vol. 13, no. 16, p. 4208, 2021.
2. **Dina Dorrigiv,** Pierre-Alexandre Goyette, Amélie St-Georges-Robillard, Anne-Marie Mes-Masson, and Thomas Gervais, "Cancer drug screening on spheroids and live primary tissue samples," *Lab Chip*, 2022 (in preparation)

Oral and video presentations

1. **Dina Dorrigiv,** Pierre-Alexandre Goyette, Amélie St-Georges-Robillard, Anne-Marie Mes-Masson, and Thomas Gervais, “Towards higher throughput with 3D cancer models: an open-space microfluidic platform for cancer drug screening”, BioNanoTech Montreux, Montreux, Switzerland, 2022
2. **Dina Dorrigiv,** Thomas Gervais, Anne Marie Mes Masson, “Ex vivo tumour model systems for drug screening in cancer”, 23rd CHUM annual congress, online, 2022
3. **Dina Dorrigiv,** Kayla Simeone, Benjamin Péant, Euridice Carmona, Jennifer K. Dupont, Anne-Marie Mes-Masson, and Thomas Gervais, “Slices or spheres? A comparison of tumor explant culture platforms.”, Pharma week conference, online, 2021
4. **Dina Dorrigiv,** Kayla Simeone, Benjamin Péant, Euridice Carmona, Jennifer Kendall-Dupont, Anne-Marie Mes-Masson, and Thomas Gervais, “Comparison of ex vivo tumour models of ovarian cancer”, Canadian cancer research network (RRcancer), online, 2021
5. **Dina Dorrigiv,** Thomas Gervais, Anne Marie Mes Masson, “Characterizion of ex vivo tumour model systems”, 30th ICM scientific day, online, 2021

6. **Dina Dorrigiv,** Kayla Simeone, Benjamin Péant, Euridice Carmona, Jennifer K. Dupont, Anne-Marie Mes-Masson, and Thomas Gervais, "Microdissected tumor tissue has lower hypoxia, apoptosis, and necrosis, and higher proliferation than tumor slices cultured under similar conditions", μTAS, online, 2020

Posters

1. **Dina Dorrigiv**, Pierre Alexandre Goyette, Amélie St-Georges Robillard, Jennifer Kendall-Dupont, Euridice Carmona, Benjamin Péant, Thomas Gervais, Anne Marie Mes Masson, "A high-throughput microfluidic-based organotypic model of ovarian cancer", Canadian Conference on Ovarian Cancer Research (CCOCR), Ottawa, Canada, 2022
2. **Dina Dorrigiv**, Anne-Marie Mes-Masson, and Thomas Gervais, "*Ex vivo* tumors on-chip - a comparative study of microdissected tissue and tissue slices", 31st ICM scientific day, Montreal, 2022
3. **Dina Dorrigiv**, Kayla Simeone, Benjamin Péant, Euridice Carmona, Jennifer K. Dupont, Anne-Marie Mes-Masson, and Thomas Gervais, "*Ex vivo* tumors on-chip - comparison of microdissected tissue and tissue slices", μTAS, Palm Springs, 2021
4. **Dina Dorrigiv**, Kayla Simeone, Benjamin Péant, Euridice Carmona, Jennifer Kendall-Dupont, Anne-Marie Mes-Masson, and Thomas Gervais, "Comparison of *ex vivo* tumour models of ovarian cancer," Canadian Conference on Ovarian Cancer Research (CCOCR), online, 2021